FORCE-SIGNALING COUPLING AT SINGLE FOCAL ADHESIONS

A Dissertation
Presented to
The Academic Faculty

by

Dennis Wei Zhou

In Partial Fulfillment
of the Requirements for the Degree
Doctor of Philosophy in
Bioengineering

Georgia Institute of Technology

May 2019

FORCE-SIGNALING COUPLING AT SINGLE FOCAL ADHESIONS

Approved by:

Dr. Andrés J García, Advisor
George W. Woodruff School of
Mechanical Engineering
Georgia Institute of Technology

Dr. Andrew P. Kowalczyk
Department of Cell Biology
Emory University

Dr. Aránzazu del Campo
Head of Dynamic Biomaterials
Leibniz Institute for New Materials

Dr. Cheng Zhu
Wallace H. Coulter Department
of Biomedical Engineering
Georgia Institute of Technology

Dr. Jennifer E. Curtis
School of Physics
Georgia Institute of Technology

Date Approved: March 5, 2019

To my family, for their never-ending love and support during my endeavors.

ACKNOWLEDGEMENTS

I would first like to thank my parents for their indefinite love and support through the years. Thank you for working so hard to support me and my siblings. Dad, I will always admire your intense passion for your work and dedication to your patients. You are one of my greatest role models, and I hope to emulate your passion for your work once I get older. Mom, you are one of the kindest people I've ever met. I also greatly appreciate your creative sense of humor. Allen/Rose: I'm so grateful to have you both as siblings. Allen – I love your sense of humor and adventure. You are very fun to be around, and I greatly appreciate your love for trying new foods/recipes. You'll be an amazing physician someday. Rose – You are an amazing little sister. I love your blunt attitude and creative sense of humor. I'm confident you'll be amazing computer programmer, and I hope to visit you for free food once you start your dream job at Google! Lastly, I thank my grandparents for helping to raise me during my youth. You taught me humility and kindness and those characteristics have been invaluable to my life so far.

I would like to thank my undergraduate advisor, Dr. Roger Spanswick, at Cornell. Your love for science was inspiring, and I appreciated your enthusiastic support for me during my academic endeavors. I could not have asked for a better undergraduate academic advisor, and I greatly miss you. I'd also like to thank my undergraduate research advisors: John Slater – you are one of the most hilarious people I've ever met, and certainly the funniest scientist I know. Thank you for introducing me to research and putting up with me as I learned basic laboratory skills. Cindy Reinhart-King and John Huynh – Thank you for mentoring me, when I was an undergraduate student at Cornell. You were both amazing

mentors, and I am extremely lucky to work with you both. Dave Clarke – Thank you for mentoring me during my REU at MIT. You taught me to think critically as a scientist and rigorously design my experiments. Jeff Werner and Lars Angenent: Thank you for supporting me during freshman year at Cornell. I learned a lot from you and appreciated your kindness and passionate attitude towards science.

I'd like to thank my thesis committee: Dr. del Campo – Thank you for your supporting my project and your willingness to conference in all the way from Germany. I greatly appreciate your unique chemistry expertise and your willingness to help with our caged RGD experiments. Dr. Curtis – Thank you for your support, knowledge, and eagerness to give feedback on my project. I've greatly enjoyed working with you and your students as well on the spinning disk projects! Dr. Zhu – Thank you for your wisdom and critical analysis of my results – it's certainly improved my ability to think as a scientist and rigorously design and explain my experiments. Dr. Kowalczyk – Thank you for bringing in a cell biology perspective for my project and teaching me the importance of conceptualizing my findings into a model. Lastly, Andrés – Thank you for being an amazing mentor. You've taught me a lot about being a good scientist and the importance of critically evaluating literature and rigorously designing my experiments. I've grown tremendously as a scientist from working in your lab.

To the Garcia lab, thank you for your support over the years. You guys have been a really fun group to hang out with, in addition to being a highly talented group of scientists. Thank you for your support and encouragement through my PhD. In particular, I'd like to thank Rachit Agarwal for your advice and support during my project. You provided valuable insights and advice for my project and helped me mature as a scientist.

Furthermore, I'd like to thank Ted Lee and Dave Dumbauld for mentoring me and training me on the techniques. I'd also like to thank Mark Colasurdo and Elijah Holland for being great mechanobiology teammates and Nick Castro for being a truly outstanding undergraduate. Lastly, I'd like to thank Eric O'Neill for being a truly incredible and amazing laboratory manager. You honestly made my thesis project so much easier. To the IBB staff, thank you for your hard work in keeping everything running in shape. I'd like to especially thank Allen Echols, for your helpfulness and kind attitude. I wish you the very best of luck in your retirement. Laura Paige, you are amazing. Thank you for your kindness, encouragement, and vast knowledge of Georgia Tech and BioE program policies. You've made my PhD experience so much easier and more enjoyable. To the numerous friends that I have made during my time at GT, thank you for the happy hours, YOLO cooking events, Friendsgiving potlucks, and wonderful memories. To GT FCGS (Fellowship of Christian Graduate Students) – Thank you for supporting me through the past several years. You helped me mature in my faith, and provided an invaluable source of support during my PhD. I'd also like to thank the congregation at my church, Ekklesia Atlanta Christian Fellowship, who have encouraged and challenged me to grow toward the character of Jesus Christ. As I complete this document, I consider the massive privileges that I've been given and the source of true happiness and peace in my life. I was graciously born with ability that I did not earn and with supportive family and friends in my life who I did not choose. Therefore, I ultimately acknowledge God who knew all of my days even before I was born and demonstrated his never-ending love for me in the person of Jesus Christ.

TABLE OF CONTENTS

LIST OF TABLES

LIST OF FIGURES

LIST OF SYMBOLS AND ABBREVIATIONS

FA	focal adhesion
CSK	cytoskeleton
FAK	focal adhesion kinase
ECM	extracellular matrix
FN	fibronectin
nN	nano newton
pY397-FAK	FAK phosphorylated at tyrosine 397
mPAD	microfabricated post-array-detector
FRAP	fluorescence recovery after photobleaching
eGFP	enhanced green fluorescent protein
PDMS	polydimethylsiloxane
IF	immunofluorescence

SUMMARY

Integrin-mediated adhesion to extracellular matrices (ECM) provides forces and signals that direct cell processes central to tissue organization, homeostasis, and disease. Recent studies show an important relationship between cell adhesive force generation and focal adhesion (FA) assembly, yet it remains unclear how forces are transduced into adhesive signals. Our work seeks to identify coupling between cell adhesive force generation and signaling at FAs. To measure forces, we used Microfabricated Post-Array-Deflectors (mPADs), which are an array of PDMS ~1.8 μm diameter microposts. Based on the micropost deflections, we can calculate the forces exerted by cells. We previously showed that vinculin regulates force transmission at FAs. Vinculin residence time in FAs correlated with applied force, supporting a mechanosensitive model in which forces stabilize vinculin's active conformation to promote force transfer. We first examined the relationship between traction force and vinculin-paxillin localization to single FAs in the context of substrate stiffness and actomyosin contractility. Substrate stiffness and contractility regulated vinculin localization to FAs, and vinculin auto-inhibition is a crucial regulatory step in this process that overrides the effects of cytoskeletal tension and substrate stiffness. Vinculin and paxillin FA area did not correlate with traction force magnitudes at single FAs, and this was consistent across different ECM stiffness and cytoskeletal tension states. Vinculin residence time at FAs linearly varied with applied force for stiff substrates, but this coupling was disrupted on soft substrates and in the presence of contractility inhibitors. In contrast, paxillin residence time at FAs was independent of force, substrate stiffness, and cytoskeletal contractility. Lastly, substrate stiffness and cytoskeletal

contractility regulated whether vinculin and paxillin turnover dynamics are correlated to each other at single FAs.

We also found that pFAK Y397 levels are linearly coupled to force at single FAs on stiff substrates. On soft substrates, however, this positive relationship is eliminated. We found that talin is required for FAK localization and Y397 phosphorylation at FAs and mediates force-FAK linear coupling at FAs via talin-FAK binding. Furthermore, averaged levels of FAK localization and Y397 phosphorylation at FAs are relatively insensitive to vinculin expression. However, a full-length vinculin molecule that binds talin and actin is required for linear coupling to occur between force-FAK localization and force-FAK Y397 phosphorylation at individual FAs. Lastly, we demonstrate that a full-length vinculin molecule that binds talin and actin is required to promote YAP nuclear accumulation. These findings suggest that force generation and signaling are coupled at FAs and underscore the role of environmental stiffness, talin, and vinculin in regulating force-signaling coupling at FAs. Our results generate new insights into how cell adhesive forces are integrated into biochemical signals. Furthermore, this understanding provides a framework for mechanotransduction events at cell-ECM junctions, such as cell migration, force-regulated morphogenesis, and stem cell commitment in response to matrix stiffness.

CHAPTER 1. INTRODUCTION & SPECIFIC AIMS

Cell adhesion to extracellular matrix (ECM) proteins is regulated by integrin receptors, which are composed of α and β subunits [1]. Following binding to ECM proteins, integrins cluster together to form focal adhesion (FA) complexes, which contain structural proteins that link the ECM to the cytoskeleton and signaling effectors that regulate cell proliferation, migration, and differentiation [2]. The importance of cell-ECM adhesion is underscored by the early-stage lethality in mice that have genetic deletions or mutations for adhesion receptors, ligands, or associated components [3, 4]. Cell-ECM adhesive interactions also regulate host-implant responses for medical devices and tissue-engineered constructs, further emphasizing the importance of cell adhesion to the ECM [5]. Moreover, recent studies have identified that aberrations in cell-ECM adhesion play a critical role in pathological conditions, such as atherosclerosis, blood clotting, and cancer metastasis [6-8].

FAs also provide anchorage for the cell, by mechanically linking ECM proteins to the cell's cytoskeleton [1, 2], and transmitting adhesive forces that drive cell migration, signaling, and tissue morphogenesis [9-11]. Several systems have been developed to quantify the spatial and temporal dynamics of cell adhesive forces. These measurement systems have primarily focused on cell adhesion strength, which is defined as the amount of force required to detach the cell from the ECM [12], and cell traction forces, defined as the forces that cells exert on the ECM [9]. From the development of these measurement systems, our understanding of the forces underlying cell-ECM adhesion has increased

significantly over the past decade. Focal adhesions (FAs) are nano/micron-scale complexes of clustered integrins and structural and signaling molecules that link the ECM to the cytoskeleton and function as principal sites of force transmission and signal transduction. Despite significant progress in defining biochemical interactions driving FA assembly and signaling, very little is known about how FAs sense and transmit force and how these forces are integrated into biochemical signals. This lack of a quantitative understanding of force sensing and transmission limits functional analyses of adhesive processes and mechanotransduction pathways in diverse physiological and pathological settings.

The *objective* of this project is to analyze how FAs sense and transmit force. Our *central hypothesis* is that mechanosensing at a single FA involves a feedback loop in which vinculin is responsible for coupling FAK Y397 phosphorylation to force at single FAs and regulating YAP nuclear accumulation. This novel hypothesis is based on our evidence for important roles of FAK in adhesion strengthening through integrin activation and vinculin recruitment to FAs. We have identified important roles for (i) FAK in adhesive force through vinculin recruitment to FAs and (ii) vinculin head-tail interactions in force transfer and FA localization. We also showed that vinculin is necessary for myosin contractility-dependent adhesion strength and traction force, and its head-tail domains have distinct contributions to adhesive forces. Lastly, we observed that substrate rigidity and cytoskeletal tension influence vinculin and paxillin localization to FAs, suggesting that force influences the real-time recruitment of vinculin and paxillin to FAs.

We will test our central hypothesis by addressing 2 ***key questions*** via these ***aims***:

Q1. Do changes in adhesive force or cytoskeletal tension that perturb the local force balance at FAs regulate vinculin-paxillin localization to FAs?

SA1. Analyze the effects of local adhesive force and cytoskeletal tension on coupling force transmission and paxillin and vinculin recruitment to FAs.

We will seed cells expressing fluorescently-tagged vinculin and paxillin proteins onto mPADs of differing stiffnesses. We will assess whether vinculin-paxillin localization to single FAs is related to force and whether vinculin-paxillin residence time is related to force at FAs. We'll also assess the role of macroscopic factors, such as substrate stiffness, in regulating vinculin-paxillin localization to FAs and vinculin-paxillin residence times at FAs. Our lab previously demonstrated that vinculin residence time and force are positively related, supporting a model where forces transduced across vinculin stabilize its localization to FAs. Here, we will test this model in the context of substrate stiffness and contractility, as these two variables perturb the balance between cell-ECM and CSK forces at FAs. We anticipate that vinculin residence time will be linearly related to force at FAs, although this relationship will depend on actomyosin contractility and environmental stiffness. In contrast, we expect that paxillin residence time will be independent of force at FAs, as paxillin is primarily a signaling protein and myosin II activity is not required for paxillin recruitment to FAs.

Q2. Do talin and vinculin modulate FAK recruitment and Y397 phosphorylation at FAs and YAP nuclear accumulation?

SA2. Dissect the contributions of talin and vinculin to FAK localization and Y397 phosphorylation at FAs and determine whether vinculin and talin mediate YAP nuclear accumulation.

We hypothesize that talin- and vinculin-dependent forces at FAs regulate FAK recruitment and phosphorylation. We will use talin-depleted and vinculin-null cells expressing wild-type and mutant vinculins to analyze how vinculin and its auto-inhibited head-tail conformation modulate force-FAK phosphorylation coupling at single FAs. We will assess force-FA assembly-FAK phosphorylation profiles for a subset of mPADs formulations with different stiffness and with contractility modulators to perturb the balance of integrin-ECM force and cytoskeletal tension for cell lines derived from vinculin-null cells expressing vinculin mutants. We hypothesize that vinculin-dependent forces are required to promote FAK localization and Y397 phosphorylation at FAs. Furthermore, we anticipate that force-FAK localization and Y397 phosphorylation are coupled at single FAs, since FAK kinase activity has previously been shown to be sensitive to changes in actomyosin contractility. Although previous studies have examined whether FA proteins, such as talin, influence FAK Y397 phosphorylation at FAs, previous approaches have primarily utilized averaged or population-level metrics of FAK localization and activity. Consequently, they neglect the heterogeneity of individual FA complexes and may fail to reveal important relationships between force and FAK localization and Y397 phosphorylation at the individual FA level. Our approach has the advantage of examining

individual FAs and whether forces at single FAs can be transduced into changes in FA signaling activity. Furthermore, we will assess the role of vinculin in regulating YAP nuclear accumulation, which plays a critical role in multiple cell processes, such as proliferation, growth regulation, and differentiation. It is well-known that increases in substrate stiffness and/or actomyosin contractility result in increased YAP nuclear accumulation. Furthermore, given vinculin's important role in promoting force transmission, we hypothesize that vinculin is required to promote YAP nuclear accumulation.

This research is highly ***innovative*** because it integrates force-sensing technologies and FA mutants to analyze mechanotransduction at single FAs. As ***outcomes*** of this project, we will establish whether the local balance of adhesive force and cytoskeletal tension regulates coupled force-FAK recruitment and Y397 phosphorylation at single FAs. We will analyze the roles of FAK and vinculin in this mechanosensing. This research will generate new insights into how cell adhesive forces are generated and integrated into biochemical signals. Ultimately, this understanding will provide a general framework for early mechanotransduction events at cell-ECM junctions, such as adhesion assembly at migratory fronts, force-regulated morphogenesis, and stem cell lineage commitment in response to matrix stiffness. Furthermore, our research will generate new insights into how FAs sense force and how forces at individual FAs are transduced into biochemical and nuclear signals. Lastly, this research will provide a new framework to understand cell-ECM events as well as fundamental principles to design mechanoresponses in cell-biomaterial interactions.

CHAPTER 2. LITERATURE REVIEW

Note: Chapter 2.1 and Chapter 2.2 are adapted from Zhou DW et al. Measurement Systems for Cell Adhesive Forces, JBME, 2015. [13]

2.1 Measurement Systems for Cell Adhesion Strength

Cell adhesion strength measures cell-ECM adhesion and is strongly influenced by integrin-bond number and distribution, cell-ECM contact area and shape, and FA size and composition [14-16]. Generally, adhesion strength assays measure the ability of cells to remain attached when exposed to a detachment force (Table 1). The simplest adhesion strength assay involves seeding cells onto a substrate of interest, washing the cells with physiologic buffers, and counting the remaining cells afterwards [17]. Although these "wash" assays have identified critical components and regulatory mechanisms of cell adhesion [17], they are severely limited by poor reproducibility and sensitivity, as the washes apply largely unknown and non-uniform detachment forces [14]. Moreover, wash assays usually fail to provide sufficient detachment forces, even after short adhesion times (< 60 min) for certain strongly adherent cells. Despite its simplicity, the wash assay is undermined by poor reproducibility and sensitivity. Consequently, more robust and quantitative assays have been developed to analyze cell adhesion strength.

Several quantitative assays have been developed to apply controlled detachment forces to adherent cells. These methods are generally divided into the categories of (1) micromanipulation, (2) centrifugation, and (3) hydrodynamic shear stress. Micromanipulation encompasses several techniques that apply normal or tangential forces

with a micropipette, microprobe, atomic force microscopy (AFM) cantilever, or laser and magnetic tweezers [18-23]. These techniques provide highly sensitive (pico-nano range) real-time force-displacement relationships, and are particularly useful for analyzing isolated or low-number receptor-ligand interactions. For example, Roca-Cusachs et al. used magnetic tweezers with FN-coated magnetic beads to show that clustering of FN domains within ~40 nm increased adhesion strength six-fold via $\alpha_5\beta_1$ integrin clustering, and this increase was independent of $\alpha_v\beta_3$ integrin or talin 1 and 2 [24]. Subsequently, they concluded that $\alpha_5\beta_1$ integrin clustering supports adhesive force generation, whereas $\alpha_v\beta_3$ integrin or talin 1 and 2 are implicated in mechanotransduction and reinforce integrin-cytoskeleton linkage via talin [24]. Furthermore, Sheetz and colleagues used optical tweezers to identify and quantify the strength of a molecular slip bond between integrins and a trimer of the fibronectin (FN) integrin-binding domain (FN III-7-10) [25]. They also showed that talin1 is critical to the strength of this slip bond, suggesting that talin1 is responsible for initiating this molecular slip bond between closely packed FN-integrin complexes [25]. Kong et al. used AFM and membrane force probes to demonstrate that cyclic application of 5-25 pN forces to FN-integrin $\alpha_5\beta_1$ bond significantly increases bond lifetime, and identified a mechanism for cell adhesion strengthening by the application of cyclic forces [26]. Furthermore, they demonstrated with AFM that increasing applied force between 10-30 pN prolongs integrin $\alpha_5\beta_1$ - FN fragment bond lifetime, demonstrating catch bond behavior [27]. Although micromanipulation techniques are useful for analyzing isolated receptor-adhesive ligand interactions, they are typically not suitable for studying long-term cell adhesion strengthening responses, as the upper range of applied forces (~10

nN for AFM, ~100-1000 pN for optical and laser tweezers) is usually too small [14]. Moreover, these micromanipulation techniques often require sophisticated equipment and expertise to operate, limiting accessibility for other users.

Centrifugation assays, in contrast, provide adhesion strength measurements for large cell populations [28, 29]. In this configuration, a substrate containing adherent cells is spun at a specific speed to apply a controlled detachment force perpendicular to the cell adhesive area, and the number of cells before and after spinning is quantified. However, centrifugation applies relatively low detachment forces ($< 10^{-3}$ dyne/cell) [14], limiting its applicability to short (< 60 min) assays. Moreover, the assay is labor-intensive, as it requires many runs at different speeds to apply a wide range of forces. Alternatively, short-term cell adhesion can be analyzed as a function of ligand density at a fixed centrifugation speed. Afterwards, a non-linear profile with adherent cell fraction plotted against ligand density can be generated, and the ligand density for 50% adhesion strength can be a sensitive indicator of adhesion strength [28]. This strategy can be particularly useful for experiments involving multiple conditions, as it is significantly more high-throughput.

Hydrodynamic shear assays utilize specialized flow setups to apply a wide range of detachment forces to a large cell population, and generally provide the most robust and sensitive quantitative measurements of long-term cell adhesion strength. After shear stress exposure, cell adhesion strength is typically defined as the shear stress (τ_{50}) that produces 50% cell detachment from the ECM. For hydrodynamic shear assays, however, the net detachment force applied to an individual cell depends on the cell's area, shape, and FA size and position. Therefore, variations in cell spreading and FA geometry must be

accounted for in these assays, as τ_{50} does not accurately represent the applied detachment force if these variations are present between conditions.

Common hydrodynamic shear configurations include flow between parallel plates, radial flow between two parallel disks, and spinning or rotating disks [30-34]. With the exception of the spinning disk setup, these configurations can be combined with a microscope, which allows for the real-time monitoring of cell attachment-detachment and flow profile validation and quantification. However, the above flow configurations often provide insufficient detachment forces for well-spread or strongly adherent cells under laminar flow. Alternatively, rotating disk setups, such as the small-gap parallel disk viscometer [35] or the single spinning disk [16, 36], apply shear stresses that vary linearly with radial distance, and allow users to apply a wide range of forces to a cell population in a single experiment. Other flow setups that apply a range of detachment forces within an individual experiment include the Hele-Shaw chamber [37], jet-impingement device [38], and variable height flow channel [39]. Amongst all of these systems, however, only the spinning disk can apply a linear range of detachment forces under an individual experiment with uniform chemical conditions across the surface. For example, García and colleagues developed a robust spinning disk device that applies a wide range of detachment forces to an adherent cell population, and provides highly sensitive measurements of cell adhesion strength [36, 40]. In a typical experiment, cells are first seeded onto a circular coverslip coated with a ECM protein of interest [12]. ECM proteins can also be patterned onto the coverslip if significant differences in cell spreading are expected, as spreading differences can alter the detachment force applied to each cell [12]. Subsequently, the cells are spun at

a fixed speed, and adherent cells are counted at different radial distances, each corresponding to known shear stress values [12]. The fraction of adherent cells decreases nonlinearly with respect to applied shear stress, and the adhesion strength is typically defined as the shear stress which produces 50% cell detachment [12]. At high rotation speeds, however, flow inside the spinning disk device becomes turbulent and requires experimental validation of the flow patterns [12, 14]. To mitigate this potential issue, viscosity enhancers such as dextran can be used to increase the applied detachment force, while maintaining low rotation speeds to avoid turbulent flow.

Table 1: Measurement Systems for Cell Adhesion Strength.

Adapted from Zhou DW et al, JBME, Review: Measurement Systems for Cell Adhesive Forces.

Assay	Methodology	Force Quantification	Advantages	Disadvantages
Wash	Applies detachment force from washing with physiologic buffers	Unknown, Non-Uniform	(+) Simple/Convenient	(-) Poor reproducibility (-) Unknown forces (-) Short-Term Adhesion
Centrifugation	Conventional centrifuge applies normal force to adherent cells	$F = VRD\,\omega^2$ V = Cell Volume R = radius; ω = Rotation Speed; D = Media density	(+) Simple/Convenient (+) Population Averages	(-) Single force applied each run (-) Restricted to short-term adhesion/Low applied forces (max ~ 10^{-3} dynes/cell)
Micromanipulation	Apply force with micropipette, AFM cantilever, laser tweezers, or microprobe.	Quantified from force transducer or calibrated deflections of micromanipulator	(+) Sensitive real-time force-displacement profiles (+) Analyzes individual receptor-ligand interactions	(-) Difficult and Time-Consuming (-) Maximum Force ~ 10 nN; restricted to receptor-ligand interactions
Hydrodynamic Flow	Shear forces generated by fluid flow over adherent cells	Proportional to applied fluid shear stress	(+) Highly tunable forces (+) Provides population average	(-) Requires special flow cells (-) Force depends on cell shape (-) Flow validation required
	Radial Flow  	$\tau_w = 3\mu Q/\pi r h^2$ $\tau_{w\,max}$ ~ 600 dyn/cm² Q = Flow Rate; μ = viscosity; r = radial position; h = gap height	(+) Applied forces inversely proportional to radial position (+) Direct observation of the detachment process	(-) Flow profile validation required (-) Complex hydrodynamic conditions at impingement point
	Parallel Plate 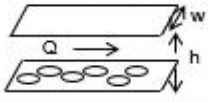 	$\tau_w = 6\mu Q/wh^2$ ($\tau_{w\,max}$ ~120 dyne/cm2) Q = Flow Rate; w = channel width; h = channel height; μ = viscosity	(+) Direct observation of detachment process (+) Flow conditions typically laminar and easily validated	(-) Relatively low detachment forces / restricted to short-term adhesion (-) Single force applied per experiment without utilizing the variable height flow channel
	Spinning Disk 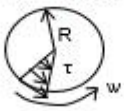 	$\tau_w = 0.8\, r\, (\rho\mu\omega^2)^{1/2}$ $\tau_{w\,max}$ ~ 2500 dyne/cm² r = radial position; ω = rotational speed; ρ = fluid density; μ = fluid viscosity	(+) High throughput; Large linear range of applied forces for each experiment (+) Uniform surface chemical properties	(-) Cell detachment cannot be visualized in real-time (-) Flow pattern validation required for high rotation speeds (~5500 RPM)

Overall, the spinning disk system produces highly robust, sensitive, and reproducible measurements of cell adhesion strength, and has been utilized for a diverse array of applications. For example, the spinning disk system has been used to characterize the dynamics of initial cell-ECM attachment, spreading, and adhesion strengthening [12, 36, 40, 41]. Furthermore, Friedland et al. utilized the spinning disk system to show that $\alpha_5\beta_1$ integrin activation via myosin II-generated cytoskeletal force strengthens $\alpha_5\beta_1$-FN bond strength, and activates subsequent signaling pathways via phosphorylation of focal adhesion kinase (FAK) [42]. The spinning disk device has also been used to identify how different FA protein mutants affect cell adhesion strength, which is indicative of FA function [3]. The spinning disk assay has also been utilized for 3D cultures, showing that fibroblasts cultured in 3D fibrillar FN matrices have significantly lower adhesion strength than fibroblasts cultured on 2D FN-coated coverslips [43]. Microscopy subsequently revealed holes inside the matrix after spinning, suggesting that cells can detach via fibril breakage in 3D, instead of integrin-matrix bond breakage in 2D [43]. Furthermore, nanopatterning has been combined with the spinning disk assay to dissect how FA geometry and size influence cell adhesion strengthening. For example, Coyer, Singh, and colleagues applied subtractive contact printing to generate nanopattern "islands" of different sizes and geometries [15]. They subsequently showed that above an individual island area of 0.11 μm^2, individual nanoisland area significantly influences cell adhesion strength, whereas the geometric arrangement of the islands (island spacing, number of islands, total area of the islands) has minimal effect on cell adhesion strength [15]. Recently, Singh et al. also used the spinning disk system to identify unique adhesion

strength values for human induced pluripotent stem cells (hiPSCs) [44]. These adhesion strength values were then used to design a flow-driven microfluidic device that purifies hiPSCs, by detaching them from an initially heterogeneous cell population. By altering the applied fluid shear stress to match the hiPSC's unique adhesion strength, users can isolate hiPSCs from the other cells, which have significantly higher adhesion strengths than the hiPSCs [44].

2.2 Traction Force Microscopy Systems

While adhesion strength measurement systems have identified key adhesion components and how they participate in the cell adhesion strengthening process, cell-ECM traction forces also significantly influence cell phenotype. It is becoming increasingly evident that cell-ECM traction forces regulate cell fate, tissue formation, and even malignant transformation [8, 9]. Traction forces also regulate FA composition and intracellular signaling, further underscoring the importance of cell traction forces [3]. Accordingly, numerous measurement systems have been developed to assess how forces, both sensed and exerted at FAs, regulate FA structure-function and cell phenotype. The majority of these measurement systems rely on linearly elastic deformable substrates, where the forces exerted by individual cells can be measured from the deformations induced in the substrate (Table 2) [9, 45, 46].

Harris et al. initiated the use of deformable substrates by flame-exposing silicone fluid to polymerize a thin "skin"-like layer on the surface, while the un-cross-linked fluid beneath serves as a lubricant [46]. These silicone film substrates are compliant to the extent

that adherent cells were able to induce wrinkle-like deformations on the film's surface as they applied contractile forces. This system offers its advantages from its simplicity, and that its mechanical properties can be tuned by altering the heat exposure time and silicone fluid viscosity. Although these substrates are not widely used today due to their qualitative nature, they helped inspire the next-generation measurement systems for cell traction forces.

Consequently, more advanced 2D traction force measurement techniques have emerged. These systems typically measure substrate deformations induced by individual cells, while utilizing engineered materials whose mechanical and chemical properties can be precisely tuned over a wide range. Amongst these measurement systems, polyacrylamide (PA) gel based traction force microscopy (TFM) and microfabricated elastomeric post array deflectors (mPADs) are currently the most widely-used, and typically provide the most sensitive and reliable measurements of 2D cell traction forces.

Wang and Dembo developed PA gel TFM, in which the PA gel is first functionalized with cell adhesive ligands, and fluorescent beads (approximately 200-500 nm in diameter) are embedded near the gel surface [45]. Cells cultured on these substrates generate traction forces that deform the gel's surface plane, which can be quantified by tracking the displacements of the fluorescent beads. This is typically done by imaging the bead fields before and after cell detachment with trypsin, so that the bead positions in both "stressed" and "unstressed" states are known [45]. As the gel deformations are generally significantly smaller than the gel thickness, the PA gel can be treated as a semi-infinitely thick, incompressible, and linearly elastic material during traction stress computation [45].

Subsequently, the traction stress field $T_\beta(r)$ and displacement field $d_{p\alpha}$ are related by the Fredholm integral equation of the first kind:

$$d_{p\alpha} = \iint g_{\beta\alpha}\left(\boldsymbol{m_p} - \boldsymbol{r}\right) T_\beta(r) dr_1 dr_2 \quad (1)$$

Where g represents a green's tensor function, and gives the displacement of the p^{th} marker 'm'. Traction stresses are exerted by a cell through its contacts on the substratum surface at position r. Given the bead displacements $d_{p\alpha}$, the integral must be inverted to solve for the traction stress field, $T_\beta(r)$ [9, 45]. However, this inversion is highly computationally intensive, and requires careful selection of mathematical constraints, such as penalty terms for higher numbers of force vectors or restriction of traction forces to the cell's edge [9, 45, 47]. Because these constraints can be subjective, an individual bead displacement field can lead to multiple different traction force fields, making the method vulnerable to user bias and error [9, 47]. However, recent experimental and computational advances have helped improve the reliability and resolution of PA gel TFM. Experimentally, the use of two different fluorescent bead markers inside the gel allows users to increase bead density and obtain a richer sampling of the displacement field, which ultimately helps improve traction force resolution [48, 49]. Improved algorithms, such as the boundary element method, Fourier-transform traction cytometry, and point force traction reconstruction, can also improve traction force resolution and reliability [48]. By combining these recent experimental and computational advances, Sabass et al. managed to reconstruct fibroblast traction force maps with a ~1 μm spatial resolution, which is a 5-10 fold improvement over earlier methods [48]. Although this is a significant improvement,

this approach usually requires a high-end confocal microscope, and tends to have difficulties computing traction forces at smaller adhesion sites [48].

Nevertheless, PA gel TFM offers numerous advantages. For example, PA is an inexpensive and convenient material, making this technique easily adaptable to many laboratories. Moreover, the mechanical and chemical properties of these gels can be precisely tuned over a wide range [6, 50-52], making these gels adaptable to a wide variety of cell types and experimental conditions. This flexibility is particularly advantageous, as substrate stiffness and ECM composition both significantly influence critical cell behaviors, such as mesenchymal stem cell differentiation [53], vascular smooth muscle cell durotaxis [54], skeletal muscle stem cell self-renewal [55], and cancer cell migration [8]. Therefore, PA gel TFM remains a widely-used experimental tool, and has uncovered multiple insights on cell traction force generation under physiological and pathological settings. For example, Huynh et al. discovered that increased substrate stiffness induces greater endothelial cell traction forces, which subsequently destabilizes cell-cell junctions, leading to increased vascular permeability to inflammatory agents during atherosclerosis progression [6]. Moreover, using PA gel TFM, Califano et al. showed that matrix mechanics and chemistry regulate traction force generation, vessel formation, and cell migration in concert [50, 56]. Furthermore, Chowdhury et al. used PA gels to demonstrate that mechanical properties of stem cells regulate stress-induced spreading, suggesting that local small forces play a critical role in early development of soft embryos [57]. PA gel TFM has also been used to better characterize basic cell adhesion and migration. Since the mechanical properties of these gels can be precisely tuned over a wide range by varying

the acrylamide to bisacrylamide ratio, numerous studies have shown that substrate stiffness typically induces greater cell spreading, FA formation, migration, and traction force generation [52, 58-61]. Overall, despite their limitations, PA gel TFM has been an invaluable tool for mechanobiology research. By allowing researchers to modulate the gel's mechanical and chemical properties over a wide range, PA gels have been utilized for a diverse array of research applications. Moreover, the strategy underlying PA gel TFM has been extended to inspire additional traction force measurement systems that utilize linearly deformable substrates.

Alternatively, methods utilizing microfabricated systems have been developed to quantify cell traction forces at discrete locations on the cell-substrate interface. Galbraith et al. initiated the use of these discrete substrates, by developing a silicon array of micro-cantilevers each tipped with a 4-25 um^2 pad coated with ECM adhesive protein [62]. By monitoring the cantilever deflections as the cell migrates across the pad, the traction force exerted by the cell at a discrete adhesion site can be quantified using basic beam theory [62]. However, the high fabrication cost required of this system is a significant limitation [62]. Moreover, the traction forces can only be measured at positions where the cell forms an adhesion, whereas continuum approaches allow for traction force measurements at virtually any point of the cell-substrate interface.

A more robust form of this approach was pioneered by Chen, and involves the use of micropost array deflectors (mPADs), which consist of silicone polydimethylsiloxane (PDMS) substrates with arrays of microposts (D ~ 3 μm, L ~ 8-12 μm) fabricated using soft lithography [9, 47, 63, 64]. The tips of the microposts are functionalized with ECM

adhesive protein, and the remaining regions are passivated to prevent cell adhesion between the posts [9]. As cells apply traction to the tips of the microposts, the microposts deflect [64].

The resulting forces, F, are calculated using Euler-Bernoulli beam theory, in which E, D, L, and δ are the Young's modulus, post diameter, height, and deflection respectively [9]:

$$F = \delta \frac{3\pi E D^4}{64 L^3}$$

Although this makes force quantification significantly easier and more reliable, mPADs have several limitations. The discrete nature of the substrate can potentially alter cell behavior and only allows force quantification where cells form adhesions to the microposts. mPADs also require sophisticated expertise and equipment to fabricate, which limits end-user accessibility. Moreover, the sensitivity of the microposts to the particular cell type may need to be optimized. If the micropost is too soft, the post deflections become very large and extend towards the nonlinear range, thus obscuring force quantification. If the microposts are too stiff, the micropost deflections will be too small to visualize, thus reducing the system's sensitivity. Therefore, optimization of the micropost dimensions may be necessary for probing traction forces for different cell types. In addition, due to the discrete nature of the substrate, ligand density quantification is more challenging. Furthermore, mPADs currently rely on the passive adsorption of large ECM proteins onto the micropost tips via microcontact printing [9]. Consequently, smaller adhesive peptides cannot be used with the current mPADs system, thus limiting the system's versatility. This

is not an issue with PA gel TFM, however, as users have previously tethered small adhesive peptides onto the gel surface [51, 52].

mPADs, however, offer multiple advantages over PA gels. For example, mPADs rely on basic elastic beam theory, which makes force quantification easier and more reliable, as there is only one traction force field for each micropost displacement map. Moreover, mPAD stiffness is modulated geometrically instead of chemically [9, 65]. By simply changing the height or diameter of the posts, the bulk substrate stiffness can be tuned over a wide range [66]. Moreover, there is no need for recording the unstressed state of the substrate, as the posts are uniformly and precisely spaced after fabrication. Since the system is microfabricated, mPADs give users excellent precision over the surface chemical properties on the micrometer scale [9, 10, 67]. For example, users have generated highly intricate ECM surface patterns to study how cell-cell contact or cell shape regulates cell phenotype and traction force generation [10, 67]. Other studies have uncovered important insights on how substrate stiffness affects stem cell traction force generation, and differentiation into adipocytes or osteoblasts [9]. At the molecular level, recent studies have characterized the role of FA protein mutations on traction force generation [3], and examined how the cytoskeleton affects traction force generation and rigidity sensing [68]. Others have used mPADs to investigate the endothelial cell traction force response to laminar (atheroprotective) vs. disturbed (atheroprone) fluid shear stress, further underscoring the many diverse uses of the mPADs system [65]. Overall, mPADs offer users easier and more reliable force quantification compared to PA gel TFM, and give

researchers substantial flexibility over matrix mechanics and chemistry to suit their experimental application.

In addition to traction forces at the ECM surface, the tension applied across the ECM-FA-cytoskeleton interface can also significantly influence cell behavior [69, 70]. Schwartz and colleagues pioneered the development of molecular sensors to quantify these forces [70, 71]. For example, a vinculin tension sensor was engineered to contain the mTFP1-Venus fluorophore pair between the vinculin head and tail domains [70]. The tension (~2.5 pN/FA average) applied across the sensor influences the spacing between the two fluorophores, which changes the sensor's fluorescence emission due to Förster Resonance Energy Transfer (FRET) [70]. Subsequently, the change in fluorescence can be used to quantify the tension across the sensor with pN sensitivity after sensor calibration and validation [70]. Using the vinculin tension sensor, this group showed that vinculin tension is highest during FA assembly and enlargement, and lowest during FA disassembly or sliding [70]. Schwartz and colleagues also developed similar FRET tension sensors for endothelial cell VE-cadherin and PECAM-1 junctions [71], which play a critical role in vascular endothelial cell signaling and cytoskeletal alignment to laminar arterial-level (>10 dyne/cm^2) fluid shear stress [6, 71, 72]. Subsequently, this group showed that laminar fluid shear stress at 15 dyne/cm^2 triggers a rapid (< 30 sec) decrease in junctional VE-cadherin tension and a simultaneous increase in junctional PECAM-1 tension (~2.0 pN/molecule average) that was dependent on vimentin [71]. Taken together, their results suggest that fluid shear stress initiates cytoskeletal reorganization, which then alters forces across cell-cell junction receptors [71]. Overall, these FRET tension sensors allow for the real-time

monitoring of dynamic changes in molecular tension with pN sensitivity. However, these FRET sensors may not be adaptable to all cell types and proteins, depending on the cell type and sensor structure and sensitivity. Additionally, converting FRET change to molecular force requires the use of fluorescence lifetime imaging microscopy (FLIM), which is not accessible to most laboratories.

To further characterize how molecular forces regulate integrin and notch signaling and initial cell-ECM adhesion, Wang and Ha developed a "tension gauge tether" (TGT) approach, where the ligand is immobilized onto a surface through a rupturable DNA-based tether [73]. The TGT rupture strength was tuned over the 12-56 pN range to restrict the maximal tension underlying the receptor-ligand interaction over several different values. Using this system, the authors showed that a peak tension of ~40 pN is critical to single integrin-ligand bonds during initial cell-ECM adhesion, although cells require significantly less force (< 12 pN) to activate Notch receptors [73]. Therefore, TGT not only measures forces across individual integrin-ligand receptors, but also provides molecular mechanical cues to regulate important cell behaviors, such as cell spreading, FA formation, and signaling [73]. Recently, another fluorescent sensor was developed to measure tension between integrins and adhesive ligands for cells cultured on 2D substrates [69]. Liu et al. developed a spring-like PEG chain (MW ~ 3400) coupled to a gold nanoparticle anchor on one end and both a fluorescent dye and an adhesive peptide on the other end. Under relaxed conditions, the fluorophore is close to the nanoparticle and the fluorescence is quenched from nanometal surface energy transfer (NSET) [69]. However, if the PEG chain is under tension, the fluorophore is pulled 1-20 nm away from the gold nanoparticle, and the

quenching effect is abrogated to produce a significant change in detected fluorescence on the order of $1/r^4$ [69]. This change in fluorescence can be used to quantify molecular tension between the integrin receptors and adhesive peptide. Subsequently, they utilize the sensor to quantify tensions on the order of 1-15 nN across the integrin-ECM interface. Moreover, this system offers high spatial (< 1 μm) and temporal (100 ms) resolution [69]. In fact, the authors report a sensitivity 3 orders of magnitude greater than PA gel TFM or mPADs [69]. The system also allows users to incorporate different adhesive ligands onto the PEG chain, increasing the flexibility of the system, and allowing users to probe tension across specific integrin receptors. This system can also probe "clusters" of integrins instead of only one integrin receptor, as done in traditional micromanipulation techniques, such as AFM. However, the system currently requires specialized reagents and sophisticated expertise to operate, limiting its accessibility.

Although significant progress has been made on understanding 2D cell traction forces, little is known about how cells generate traction forces in 3-dimensional (3D) environments. Although nearly all traction force studies to-date have been performed on 2D substrates, many cellular processes are altered in 3D environments. For example, cells encapsulated in a 3D matrix exhibit significantly different cytoskeletal and FA structure [74], and sometimes form invasive protrusions to migrate and spread [75, 76]. In a pathological context, certain cancer cells in 3D exhibit significantly different gene expression, drug resistance, and metastatic behavior compared to cells cultured in 2D [77, 78], further underscoring the importance of moving to 3D substrates for certain cell types. Therefore, measurement systems for quantifying the spatial and temporal nature of 3D cell

traction forces are paramount to attaining a more physiologically relevant understanding of how mechanical events drive cell function (Table 2).

Table 2: Traction Force Microscopy Techniques.

Adapted from Zhou DW et al, JBME, Review: Measurement Systems for Cell Adhesive Forces.

Schematic	Methodology	Advantages	Limitations
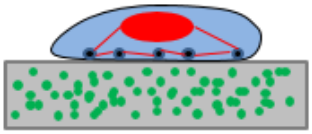	Elastic gels: Microscopy tracks bead (green) displacements to quantify cell traction forces (43).	(+) Simple/Convenient (+) Flexibility over matrix chemistry/mechanics	(-) Potentially unreliable traction force maps
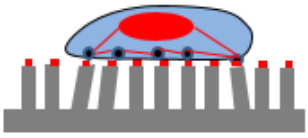	Micropost Array Deflectors: Micropost first functionalized with ECM protein (red) and cells seeded on top. Micropost deflections are used to quantify cell traction forces (45, 62).	(+) Reliable traction force quantification (+) Flexibility over substrate chemistry and mechanics	(-) Discrete nature of substrate (-) Requires special expertise and equipment to fabricate
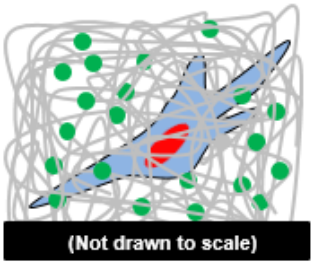 (Not drawn to scale)	3D hydrogels: Cells embedded into 3D matrix (gray) that is functionalized with adhesive peptides and cross linked. High resolution microscopy tracks bead (green) displacements to estimate cell traction forces (76, 79, 80).	(+) More physiologically relevant environment for certain cell types (+) Flexibility over matrix chemistry, mechanics, and topography	(-) Potentially unreliable traction force maps (-) Highly computationally intensive; requires expensive high-resolution microscopy

3D TFM was first initiated through the use of 3D gels made from biological polymers, such as collagen or fibrin. For example, Koch et al. embedded carcinoma cells and 1 μm beads inside a 3D collagen matrix, and used the bead displacements to generate a strain energy map of the cell [78]. Although precise measurement of traction force is not possible due to the nonlinearity of the matrix material, these strain energies were used to approximate cell traction stresses. Nevertheless, these biological matrices are still used today, as a qualitative measurement of cell traction force generation can sometimes be sufficient. For example, Kraning-Rush et al. showed that contractility inhibition abrogates

traction force generation in both 2D and 3D, demonstrating that cytoskeletal contractility is similarly important for traction force generation in 2D and 3D [79]. Other users have modified this strategy to quantify forces underlying tissue morphogenesis, where fluorescent deformable microdroplets are functionalized with adhesive ligands and embedded inside embryonic tissue matrices [80]. Cells subsequently adhere to the droplets, and the droplet deformations can be used to estimate local stresses inside the tissue [80]. Using this strategy, the authors show that cells within mammary epithelial 3D aggregates generate stresses on the order of 3.4 $nN/\mu m^2$, which is nearly two-fold higher than the stresses generated by cells inside the embryonic tooth mesenchyme, further underscoring the importance of forces during development [80].

Alternatively, the use of 3D polyethylene glycol (PEG) gels allows for more reliable cell traction force quantification, as the material is linearly elastic [81, 82]. Chen and colleagues first demonstrated this technique by tethering adhesive peptides onto the PEG macromer, and crosslinking the functionalized PEG macromers with protease-sensitive linkers to encapsulate the cells [81]. This ultimately creates a dense hydrogel network with pores on the nanometer scale [81, 82]. The adhesive peptides allow cells to adhere, while the protease-sensitive linkers allow cells to remodel the matrix to invade, migrate, and spread via protease secretion [81]. As the pore sizes are approximately an order of magnitude smaller than the beads, the beads are physically entrapped inside the hydrogel, which allows users to track bead displacements to estimate cell traction stresses [81]. Just like 2D PA gel TFM, the bead fields are imaged before and after cell detachment or contractility inhibition, so that the bead positions in both the “stressed” and “unstressed”

state are known [81]. Using the finite element method, a strain map is subsequently generated to estimate the cell traction stresses [81]. Although the geometry is different, the mathematical derivation of the cell's traction stresses is very similar to 2D PA gel TFM, although inversion of the green's function integral is significantly more computationally intensive. 3D gel TFM similarly requires regularization constraints, such as penalty terms for higher numbers of force vectors, restriction of traction forces to cell edges, or requiring that the net traction force is close to zero [81, 82]. Because these constraints can be subjective, an individual bead displacement field can lead to multiple different traction force maps, making the method susceptible to user bias and error. Imaging can also be a significant challenge for 3D hydrogels. Typically, high-magnification objectives are required to visualize beads and individual cells, but usually have significant working distance limitations into the gels. Recent studies also suggest the possibility of different hydrogel structural and mechanical properties as a function above the glass coverslip between 0 and 200 μm, which causes cells to be encapsulated in "2.5D" near the coverslip, and further compounds the working distance problem [83]. Moreover, this method suffers from uncertainties in tracking the bead positions and displacements, although uncertainty analysis can be performed to estimate these potential inaccuracies [81, 82]. Furthermore, 3D PEG gel TFM usually requires the use of a high-end confocal microscope to eliminate out-of-focus light, making the system less accessible to others.

However, 3D PEG gel TFM does offer numerous advantages. For example, the gel's mechanical properties can be adjusted, by modulating gel composition and crosslinking. However, this can potentially alter the gel's architecture, which can influence

cell behavior [84, 85]. Likewise, the chemical properties can be adjusted to incorporate different adhesive ligands and other bioactive molecules, such as growth factors [86]. Therefore, 3D PEG hydrogels are a versatile traction force measurement system, and adaptable to a wide variety of different cell types and experimental conditions. Moreover, by allowing cells to be cultured in 3D, this technique allows us to examine cell mechanics in a significantly more physiologically relevant context.

Although most studies still utilize 2D force measurement systems, 3D PEG gel traction force measurements are rapidly gaining in popularity. 3D gel TFM has also been used already to better characterize stem cell differentiation and cancer cell migration. For example, recent studies identify how stem cells form protrusions inside the matrix to generate force and migrate during differentiation [87]. Furthermore, several studies have uncovered insights between traction force generation and risk of cancer metastasis [78]. Although it is a relatively new experimental tool, 3D gel TFM is a rapidly growing system that will identify important insights on 3D cell-matrix mechanosensory interactions in the coming future.

2.3 Vinculin and FA Mechanotransduction

Integrin-mediated adhesion is a highly regulated process involving integrin activation and mechanical coupling to ECM ligands [29, 40, 88-90]. Integrins regulate their affinity for ligands by undergoing conformational activation through “inside-out” signaling via binding of talin to the integrin tail [1, 91-93]. Following ligand binding, integrins cluster into FAs [1, 69]. These structures consist of integrins and actins separated by a ~40 nm

core that includes cytoskeleton elements, such as vinculin, talin and α-actinin, and signaling molecules, including FAK, Src and paxillin [15, 94-97]. FAs transmit forces required for anchorage, spreading and migration by modulating their size/composition and force transfer between the ECM and cytoskeleton [15, 98-100]. This function has been likened to a "mechanical clutch" between an engine and transmission. Several FA components regulate adhesive forces, including vinculin, talin, α-actinin, and FAK [79, 101-109].

In addition to transmitting force, FAs are mechanosensitive. Direct application of external forces to adhesion complexes revealed that FAs respond to external forces by altering their size and composition [25, 110, 111]. Comprehensive mass spectrometry-based analyses have established that recruitment of various proteins, including LIM-domain proteins, to FAs requires myosin II-mediated contractility [16, 64, 111, 112]. Force-dependent changes in binding rates ("catch" bonds, where bond lifetimes increase with force) and protein unfolding to expose binding sites provides potential mechanisms for these mechanoresponses [18, 19, 111, 113]. For instance, Sheetz and colleagues elegantly demonstrated that forces applied across talin can expose additional binding sites for vinculin and other FA proteins [111]. Also, force application to integrin complexes increases recruitment and activities of the RhoA activators GEF-H1 and LARG [114]. Lastly, actomyosin contractility involving myosin II and the Rho GTPase effector ROCK regulates the assembly of FAs and stress fibers. Myosin II activity is also required for recruitment of vinculin and FAK, but not integrin, talin or paxillin, to FAs, and myosin II-dependent FAK phosphorylation of paxillin promotes vinculin localization to FAs [115].

Force-dependent FA maturation provides a basis for ECM stiffness sensing [116-118]. Substrate stiffness modulates FA size and traction force [6, 8, 50, 61, 68, 79, 118]. In the current model, myosin contractility-based cytoskeletal tension is dynamically tuned in response to ECM stiffness to regulate FA size, and consequently, adhesion maturation decreases on soft ECM substrates and is increased in cells attaching to stiff substrates [61, 116]. FAK, vinculin, and α-actinin have been implicated in this matrix stiffness sensing mechanism [115, 116]. Additionally, cooperative interactions between β1 and β3 integrins contribute to stiffness sensing [24, 119]. Furthermore, Sheetz proposed that a key aspect of stiffness sensing is the 'mechanical cycle,' by which integrins bind to the matrix, attach to the cytoskeleton, transduce force, aggregate, unbind, and are recycled [120]. Notably, Waterman elegantly showed that FAs dynamically sample rigidity by applying fluctuating pulling forces to the ECM, and FAK-paxillin-vinculin signaling defines the rigidity range over which this sensing process operates to guide cell migration [116, 121]. Although these findings support our hypothesis for a local force-sensing module involving FAK and vinculin, how force and FAK activation are coupled and the roles of FAK and vinculin in force sensing remain poorly understood.

Myosin contractility-driven recruitment of proteins to FAs and force-dependent unfolding of single FA proteins to expose binding sites provide mechanotransduction mechanisms [111], yet very little is known about how FAs sense and transmit force and how these forces are integrated into biochemical signals. For example, YAP/TAZ functions as a master regulator of mechanotransduction by relaying extracellular mechanical signals to the nucleus to initiate gene expression and biochemical signaling [122-124]. Recent

studies implicate YAP/TAZ in force-dependent stem cell responses to biomaterials [125]. Nevertheless, the relationship between YAP nuclear localization and force at FAs remains poorly understood.

Vinculin regulates force transmission between the cell and its ECM [3]. Vinculin consists of a globular head domain (V_H) that is linked to a tail domain (V_T) by a proline-rich strap [126]. The V_H domain contains binding sites for talin and α-actinin [127, 128]. The V_T domain includes binding sites for actin, phosphatidylinositol 4,5-biphosphate (PIP2) and paxillin [128]. Furthermore, the proline-rich strap contains binding sites for vasodilator-stimulated phosphoprotein (VASP), actin-related protein 2/3 (Arp 2/3), and vinexin [128]. Vinculin displays high-affinity head-tail binding, which leads to auto-inhibition and regulates vinculin's interactions with its binding partners at the head and tail domains [129, 130]. Vinculin activation is hypothesized to occur at FAs, upon simultaneous binding between talin and actin [94, 127, 128]. Moreover, recent reports show that actomyosin contractility and substrate stiffness influence vinculin recruitment to FAs [115, 131-133]. Our lab previously demonstrated that vinculin plays a critical role in force transmission, using MEFs transduced with various eGFP-tagged vinculin constructs. Specifically, we demonstrated that vinculin-null MEFs displayed a significant defect in force transmission. Furthermore, expression of a Vinculin Head mutant displayed a significant force transmission defect, suggesting that the vinculin head domain is not sufficient for force transmission but rather a full-length vinculin molecule is necessary to link vinculin to the CSK to support maximal force transmission. Taken together, these data provide new insights on the molecular mechanisms behind vinculin's role in force

transmission and underscore vinculin's crucial role in cell mechanotransduction. Furthermore, given vinculin's important role in force transmission, we anticipate that vinculin-dependent forces at FAs will regulate FAK localization and Y397 phosphorylation at FAs and YAP nuclear accumulation.

In current models of FA mechanotransduction, myosin contractility-based CSK tension is dynamically tuned in response to ECM stiffness to regulate FA size, and consequently, FA size decreases on soft ECM substrates and is increased in cells attaching to stiff substrates [134]. FAK, talin, vinculin, and α-actinin have all been implicated in this matrix stiffness sensing mechanism [115, 116, 135]. Additionally, cooperative interactions between β1 and β3 integrins contribute to stiffness sensing [119]. Notably, FAs dynamically sample rigidity by applying fluctuating forces to the ECM, and FAK-paxillin-vinculin signaling defines the rigidity range over which sensing operates to guide cell migration [116]. Talin unfolding has also been implicated in matrix rigidity sensing [136]. Although these studies identify important roles for these molecules in ECM stiffness sensing, **how force and FAK phosphorylation are coupled and regulated at FAs and the roles of these FA components in force sensing remain poorly understood**. It is this void that we will address in this project.

CHAPTER 3. EFFECTS OF SUBSTRATE STIFFNESS & ACTOMYOSIN CONTRACTILITY ON VINCULIN-PAXILLIN RECRUITMENT TO FOCAL ADHESIONS.

This chapter and the corresponding figures are adapted from Zhou DW et al, Molecular Biology of the Cell, Effects of Substrate Stiffness and Actomyosin Contractility on Coupling Between Force Transmission and Vinculin-Paxillin Recruitment at Single Focal Adhesions. 2017. [137]

3.1 Abstract

Focal adhesions (FAs) regulate force transfer between the cytoskeleton and ECM-integrin complexes. We previously showed that vinculin regulates force transmission at FAs. Vinculin residence time in FAs correlated with applied force, supporting a mechanosensitive model in which forces stabilize vinculin's active conformation to promote force transfer. In the present study, we examined the relationship between traction force and vinculin-paxillin localization to single FAs in the context of substrate stiffness and actomyosin contractility. Substrate stiffness and contractility regulated vinculin localization to FAs, and vinculin auto-inhibition is a crucial regulatory step in this process that overrides the effects of cytoskeletal tension and substrate stiffness. Vinculin and paxillin FA area did not correlate with traction force magnitudes at single FAs, and this was consistent across different ECM stiffness and cytoskeletal tension states. Vinculin residence time at FAs linearly varied with applied force for stiff substrates, but this

coupling was disrupted on soft substrates and in the presence of contractility inhibitors. In contrast, paxillin residence time at FAs was independent of force, substrate stiffness, and cytoskeletal contractility. Lastly, substrate stiffness and cytoskeletal contractility regulated whether vinculin and paxillin turnover dynamics are correlated to each other at single FAs. This analysis sheds new insights on the coupling among traction force, substrate stiffness, and FA dynamics.

3.2 Introduction

Cell adhesion to the extracellular matrix (ECM) is regulated by integrin receptors [1]. Following binding to ECM proteins, integrin clustering occurs to form focal adhesion (FA) complexes, which contain structural proteins that link the cell cytoskeleton to the ECM and signaling effectors that regulate cell division, migration, and differentiation [132, 138, 139]. FAs provide cell anchorage by mechanically linking ECM proteins to the cytoskeleton [1, 2], and transmitting adhesive forces that drive signaling, proliferation, and tissue morphogenesis [9, 11, 139]. Actomyosin contractility plays a critical role in generating cell adhesive forces [47, 115, 140], and influences FA composition and size [99, 141]. Single molecule experiments support a model for force-induced talin unfolding, which exposes cryptic binding sites for vinculin [111]. Furthermore, actomyosin contractility controls the recruitment of several FA proteins, such as vinculin and focal adhesion kinase (FAK) [115].

Mechanosensitive responses to ECM stiffness influence diverse cell behaviors, such as cell fate commitment, migration, spreading, and FA assembly [53, 58]. Previous analyses revealed that stiffer substrates promote increased cell spreading and traction force

generation [142] and larger FAs [61]. FAs have also been implicated as principal sites for stiffness mechanosensing, through modules such as a FAK-phospho-paxillin-vinculin signaling axis [116], talin isoforms [136], or vinculin through its head-tail interactions [143]. Furthermore, localization of certain FA proteins, such as vinculin, is significantly influenced by substrate stiffness, whereas localization of other FA proteins, including paxillin, is relatively insensitive to substrate stiffness [115].

Although previous studies examined the effects of substrate stiffness and cytoskeletal tension on FA assembly, it is still unclear how FA assembly is related to local adhesive force generation at the single FA level. In particular, the relationship between traction force and FA assembly is poorly understood. Both positive correlation [47, 112, 144] and inverse correlation between force and FA size for FAs along the leading edge of cells [93] have been reported. Furthermore, others have reported lower forces during FA disassembly, whereas increases in force are correlated with FA assembly [70]. Indeed, coupling between FA size and traction force is only limited to the initial period during FA growth, where in the absence of growth history, FA size is a poor predictor of traction force [145]. Regardless of these conflicting results, it is well accepted that applied forces regulate FA size by modulating FA kinetics [3, 133].

Vinculin regulates force transmission between the cell and its ECM [3]. Vinculin consists of a globular head domain (V_H) that is linked to a tail domain (V_T) by a proline-rich strap [126]. The V_H domain contains binding sites for talin and α-actinin [127, 128]. The V_T domain includes binding sites for actin, phosphatidylinositol 4,5-biphosphate (PIP2) [146] and paxillin [107]. Furthermore, the proline-rich strap contains binding sites

for vasodilator-stimulated phosphoprotein (VASP) and actin-related protein 2/3 (Arp 2/3) [147]. Vinculin displays high-affinity head-tail binding, which leads to auto-inhibition and regulates vinculin's interactions with its binding partners at the head and tail domains [129, 130]. Vinculin activation is hypothesized to occur at FAs, upon simultaneous binding between talin and actin [94, 127, 128]. Moreover, recent reports show that actomyosin contractility and substrate stiffness influence vinculin recruitment to FAs [115, 131-133].

Paxillin is a multi-domain protein that localizes to FAs and functions as a scaffold for the recruitment of numerous structural and signaling FA proteins that control cell-ECM adhesion, cytoskeletal organization, and signaling pathways necessary for cell migration and proliferation [148]. Furthermore, paxillin coordinates the spatiotemporal activation of Rho GTPases, which regulate the actin cytoskeleton, by recruiting GTPase activator, suppressor, and effector proteins to FAs [148]. Binding partners to paxillin include vinculin, tubulin, and FAK. Furthermore, paxillin localizes to FAs independently of actomyosin contractility and substrate stiffness [115].

In this study, we examined how substrate stiffness and cytoskeletal tension regulate the relationship between force transmission and vinculin-paxillin recruitment at single FAs. Substrate stiffness and contractility regulated vinculin localization to FAs, and vinculin auto-inhibition overrides these effects. Vinculin and paxillin FA area did not correlate with traction force magnitude at single FAs, and this was consistent across different ECM stiffness and cytoskeleton tension states. Vinculin residence time at FAs linearly varied with applied force for stiff substrates, but this coupling was disrupted on soft substrates and in the presence of contractility inhibitors. In contrast, paxillin residence

time at FAs was independent of force, substrate stiffness, and cytoskeletal tension. Finally, substrate stiffness and cytoskeletal tension regulate whether vinculin and paxillin turnover dynamics are correlated to each other at single FAs.

3.3 Methods

Cells and Reagents

eGFP-WT-vinculin and eGFP-T12-vinculin MEFs have been described previously [3]. MEFs were lentivirally transduced to express TagRFP-paxillin using EMD Millipore's LentiBrite system. After transduction, TagRFP-paxillin positive cell populations were enriched by Fluorescence Activated Cell Sorting (FACS). Cells were maintained in DMEM containing 10% FBS, 1% sodium pyruvate, and 1% penicillin-streptomycin.

Traction Force Microscopy

Microfabricated post array deflection (mPAD) device silicon masters were prepared as described previously [22]. In brief, elastomeric micropost arrays were fabricated using PDMS replica molding. To make microfabricated post array templates, 1:10 PDMS prepolymer was cast on top of silanized mPAD device silicon masters, cured at 110 °C for 30 min, peeled off gently, oxidized with oxygen plasma (Plasma-Preen; Terra

Universal), and silanized overnight with (tridecafluoro-1,1,2,2,- tetrahydrooctyl)-1-trichlorosilane (Sigma–Aldrich) vapour under vacuum. To make the final PDMS mPAD device, 1:10 PDMS pre-polymer was cast on the template, degassed under vacuum for 20 min, and cured at 110 ℃ for 20 h and gently peeled off the template on a 25 mm diameter #1 circular coverslip (Electron Microscopy Services). Peeling induced collapse of the mPADs was rectified by sonication in 100% ethanol, followed by supercritical drying in liquid CO2 using a critical point dryer (Samdri-PVT-3D; Tousimis). Flat PDMS stamps were generated by casting 1:20 PDMS pre-polymer on flat and silanized silicon wafers. Stamps were coated in a saturating concentration of fibronectin (Thermo Fisher D307) (50 μg/ml in PBS) for 1 h. These stamps were washed in sterile distilled water and dried under a stream of nitrogen gas. Subsequently, fibronectin-coated stamps were placed in contact with surface-oxidized mPAD substrates (UVO-Model 342; Jelight). mPAD substrates were labelled with 5 μg/ml DiD' (Invitrogen) in distilled water for 10 min. mPAD substrates were subsequently transferred to a solution of 0.2% Pluronics F127 (Sigma–Aldrich) for 30 min, to prevent nonspecific protein absorption. MEF cells were seeded in growth medium and then allowed to spread overnight. On the following day, mPAD substrates were transferred to an aluminium coverslip holder (Attoflour Cell Chamber; Invitrogen) for live cell microscopy and placed in a stage top incubator that regulated temperature, humidity and CO_2 (Live Cell; Pathology Devices). Confocal images were taken with a Nikon C2-Confocal Module connected to a Nikon Eclipse Ti inverted microscope, using a high magnification objective (CFI Plan Apochromat total internal reflection fluorescence (TIRF) 60 × oil, N.A. 1.49; Nikon). Post images were captured using a 640-nm laser with

a 685/50 filter, vinculin images were captured using a 488 nm laser and 525/50 filter, and paxillin images were captured using a 561 nm laser and 595/50 filter. For force measurements, the top and bottom of the posts were sequentially imaged and the deflection measured. The resulting force, *F*, was calculated using Euler-Bernoulli beam theory, in which *E*, *D*, *L* and δ are the Young's modulus, post diameter, post height, and post deflection respectively:

$$F = \delta \frac{3\pi E D^4}{64 L^3}$$

Fluorescence Recovery after Photobleaching (FRAP)

A confocal microscope head (Nikon C2) and inverted microscope (Nikon Eclipse Ti) equipped with a Melles-Griot Argon 488 laser and Coherent Sapphire 561 laser under the control of Nikon C2 Elements software were used for FRAP experiments. MEFs expressing eGFP-vinculin and TagRFP-paxillin were seeded overnight on fibronectin-coated mPADs of varying stiffness. Cell-seeded mPADs were loaded into an Attofluor cell chamber (Invitrogen) and allow to equilibrate for >20 min. A 60x APO TIRF (1.49 N.A.) objective (Nikon) was used for imaging. Initial fluorescence intensity was measured using low laser power (0.3 - 1.0%) followed by photo-bleaching of a 0.85-μm-diameter circle inside FAs at 25% laser power (488) and 3.5% (561) laser power for 1 zoomed pass (bleached circle is defined within 512 × 512 pixel box). The recovery of fluorescence was monitored every 8 sec until a plateau in recovery was reached (5 pre-bleach and 35-40 post-bleach images were acquired in each series recorded). Image series were analyzed in Nikon NIS-Elements Software, where background subtraction and correction for incidental

bleaching during image acquisition were applied to data extracted from the bleached region. Curves were fit to single exponential recovery model by assuming a reaction-dominated system and disregarding any effects of diffusion, and the characteristic recovery time ($t_{1/2}$) was calculated as previously described [3].

Statistical Analysis

Regression analyses were performed using GraphPad Prism. ANOVA, Kruskal-Wallis nonparametric tests, and post hoc tests were performed in GraphPad Prism. A p-value < 0.05 was considered significant.

3.4 Results

Vinculin, but not paxillin, recruitment to FAs is dependent on substrate stiffness and CSK contractility

We first analyzed the effects of stiffness and CSK contractility on vinculin and paxillin localization to single FAs. We used mouse embryonic fibroblasts (MEFs) expressing fluorescent FA proteins. We chose to use MEFs because they are a commonly used cell type for adhesion studies and these cells generate robust FAs and forces [3]. Vinculin-null MEFs expressing enhanced green fluorescent protein (eGFP)-vinculin were lentivirally transduced to express Tag red fluorescent protein (TagRFP)-paxillin. Cells were cultured overnight on micropillar array detectors (mPADs) coated with fibronectin. This platforms allows for measurement of cell traction forces, by tracking the deflections of micropillars [9, 47, 63]. We used mPADs presenting a range of substrate stiffness values. The effective substrate stiffness of mPADs was modulated by changing micropost heights, where increasing the post height decreased the effective substrate stiffness [9]. One advantage of mPADs is their ability to mimic tissue stiffnesses found within biological tissues. We were able to tune mPAD stiffnesses between 3 and 17 kPa, which are comparable to multiple tissue types within the human body. For instance, neural and lung tissue are often around the 100-400 Pa range [149]. However, aortic and stromal tissue are around 3 kPa while smooth muscle tissue is at ~5 kPa and skeletal muscle tissue is at ~12 kPa [149].

We found that substrate stiffness significantly influences the recruitment of vinculin to FAs, consistent with previous work [115]. There was poor localization of vinculin to FAs on 3 kPa mPADs (Fig. 1A). Vinculin showed improved localization to FAs on 5 and 14 kPa mPADs (Fig. 1A). We observed significant paxillin localization to FAs for substrates with different stiffness (3, 5, and 14 kPa) (Fig. 1B). Vinculin FA area increased on stiffer substrates (Fig. 1C). In contrast, paxillin area at FAs was independent of substrate stiffness (Fig. 1D). These results demonstrate that substrate stiffness significantly regulates vinculin, but not paxillin, localization to FAs.

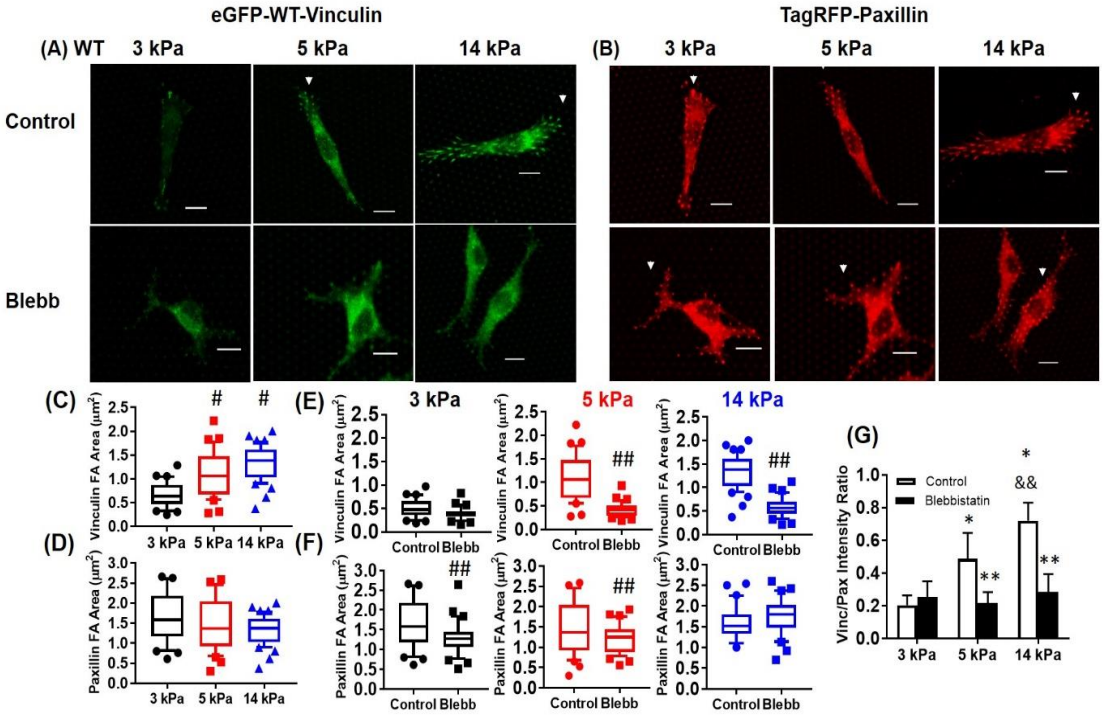

Figure 1. WT vinculin recruitment is dependent on substrate stiffness and cytoskeletal tension. (A) vinculin (green) and (B) paxillin (red) on mPADs of 3, 5, and 14 kPa in the presence or absence of 20 μM blebbistatin for 1 h. White arrowheads indicate FAs. Scale bar 10 μm. Effects of substrate stiffness (C, D) and blebbistatin treatment (E, F) on vinculin and paxillin FA area, plotted as box-whisker plots (median, 10th, 25th, 75th, and 90th percentile, n > 25). For WT vinculin FA area, P < 0.01 for one-way ANOVA for substrate

stiffness. # $P < 0.01$ vs. 3 kPa, ## $P < 0.05$ vs. blebbistatin. (G) Effects of substrate stiffness and actomyosin contractility on vinculin/paxillin intensity ratio at single FAs ($n > 25$, mean +/- SD). * $P < 0.01$ vs. 3 kPa, ** $P < 0.01$ vs. respective WT control, && $P < 0.01$ vs. 5 kPa WT.

We next examined the effects of actomyosin contractility on vinculin and paxillin FA localization to FAs on fibronectin-coated mPADs. Treatment with blebbistatin (20 μM, 1 h), a potent and selective inhibitor of myosin II activity [150], significantly reduced vinculin localization to FAs and vinculin area at FAs for 5 and 14 kPa substrates (Fig. 1A,E). Although paxillin localization to FAs was evident in the presence of blebbistatin (Fig. 1B), inhibition of contractility did reduce paxillin area at FAs for 3 and 5 kPa substrates (Fig. 1F). In contrast to vinculin, blebbistatin treatment had no effect on paxillin FA area for the stiff 14 kPa substrate (Fig. 1F).

The images in Fig. 1A and B show good co-localization of vinculin and paxillin to FAs, especially for stiffer substrates. We therefore computed the ratio of vinculin intensity to paxillin intensity at single FAs. This intensity ratio has been previously used as a metric to compare vinculin and paxillin co-localization to FAs [131]. The vinculin-to-paxillin ratio increased with substrate stiffness, indicating increased co-localization of vinculin and paxillin (Fig. 1G). Blebbistatin treatment eliminated the substrate stiffness-dependent increases in vinculin-to-paxillin ratio, demonstrating that actomyosin contractility is required for vinculin-paxillin co-localization to FAs.

Vinculin auto-inhibition is crucial to FA localization and overrides the effects of CSK contractility and substrate stiffness

Craig and colleagues previously showed that simultaneous vinculin head binding to talin and vinculin tail binding to the actin CSK promotes vinculin activation and FA localization [127]. However, this model has not been tested as a function of both substrate stiffness and CSK contractility. Therefore, we sought to determine the role of vinculin's auto-inhibition in FA localization, and whether this was dependent on substrate stiffness or CSK tension. We used a MEF line that expresses eGFP-T12-vinculin [3]. The T12 vinculin mutant is a full-length variant with mutations on the head-tail interface that reduce head to tail binding affinity by 100-fold, resulting in an open conformation that can readily bind actin and talin [129]. We also lentivirally transduced the eGFP-T12-vinculin MEFs to express TagRFP-paxillin to assess the co-localization between T12 vinculin and paxillin.

We observed significant localization of both T12 vinculin and paxillin to FAs on soft (3 kPa), moderate (5 kPa), and stiff (14 kPa) mPAD substrates (Fig. 2A-B). Both T12 vinculin and paxillin area at FAs were independent of substrate stiffness (Fig. 2C-D). Although we still observed significant vinculin and paxillin localization at FAs, blebbistatin treatment significantly decreased vinculin and paxillin area at FAs for 3 and 5 kPa substrates, but not for stiffer 14 kPa mPADs (Fig. 2E-F).

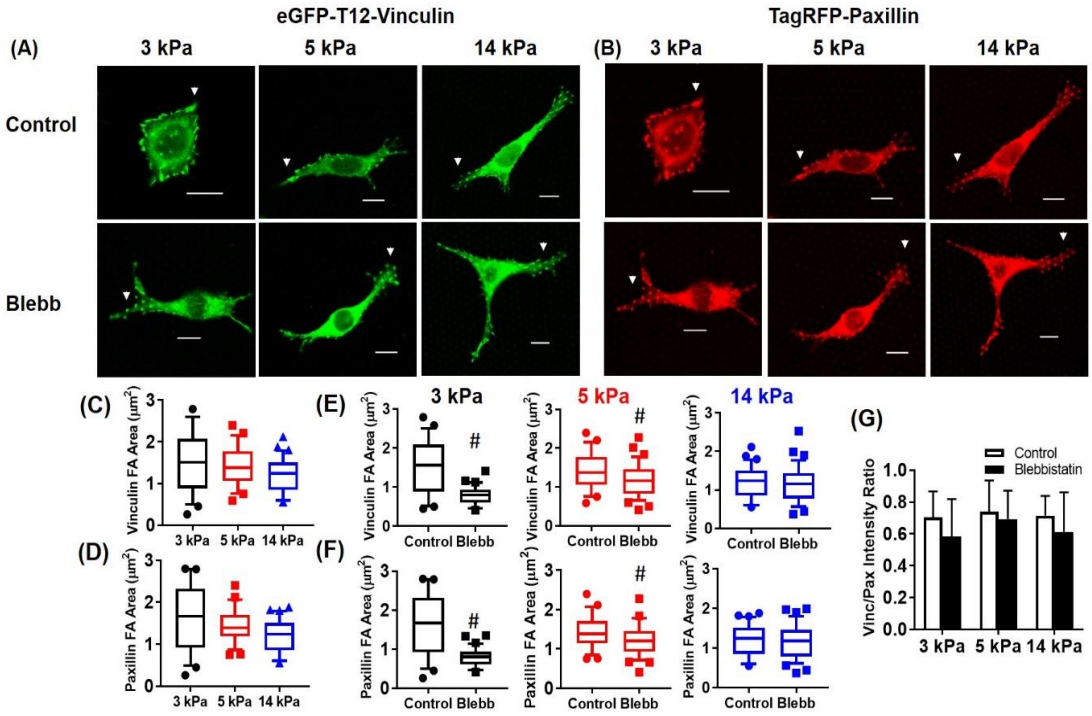

Figure 2: T12 vinculin and paxillin recruitment to FAs are independent of substrate stiffness and actomyosin contractility. (A) T12 vinculin (green) and (B) WT paxillin (red) on mPADs of 3, 5, and 14 kPa in the presence or absence of 20 μM blebbistatin for 1 h. White arrowheads indicate FAs. Scale bar 10 μm. Effects of substrate stiffness (C-D) and blebbistatin treatment (E-F) on T12 vinculin and paxillin FA area plotted as box-whisker plots (median, 10^{th}, 25^{th}, 75^{th}, and 90^{th} percentile, $n > 25$). # $P < 0.01$ vs. blebbistatin. (G) Effects of substrate stiffness and actomyosin contractility on T12 vinculin/paxillin ratio at single FAs ($n > 25$, mean +/- SD).

We also measured the ratio between T12 vinculin intensity and paxillin intensity at FAs, and found that the intensity ratio was high and equivalent across different substrate stiffness and CSK contractility state (Fig. 2G). This result indicates that T12 vinculin and paxillin co-localization to FAs is independent of substrate stiffness and actomyosin contractility. Taken together, our results demonstrate that substrate stiffness and contractility regulate vinculin localization to FAs, and vinculin auto-inhibition is a crucial regulatory step in this process that overrides the effects of CSK tension and substrate

stiffness. In contrast to vinculin, paxillin localization to FAs was insensitive to substrate stiffness and actomyosin contractility and independent of vinculin head-tail auto-inhibition.

Coupling between force transmission and vinculin-paxillin localization at single FAs

A key advantage of mPADs is the ability to analyze traction force at single FAs for different substrate stiffness values. Although previous studies have explored the effects of vinculin's head-tail interactions in driving FA localization [151], it is not understood how this process is related to force at the single FA level. Therefore, we used mPADs to measure traction forces for MEFs expressing either WT or T12 eGFP-vinculin. Traction forces were computed by measuring micropost deflections and multiplying the deflections with known micropost stiffnesses [3, 64]. This allows for simple quantification of forces, compared to polyacrylamide gel traction force measurements, which often require sophisticated computer algorithms [48]. We analyzed forces at single FAs on 3, 5, and 14 kPa mPADs with or without blebbistatin treatment. WT vinculin-expressing MEFs exhibited significantly higher forces at single FAs on 14 kPa mPADs compared to cells cultured on 3 or 5 kPa substrates (Fig. 3A). Blebbistatin treatment (20 μM, 1 h) significantly reduced forces at single FAs for all substrate stiffness values evaluated. We next analyzed the relationship between traction force and vinculin or paxillin area at single FAs. Consistent with a previous report [152], we found that vinculin or paxillin area did not correlate with traction force at the single FA level on 3, 5, and 14 kPa mPADs (Fig. 3B-C). We observed

similar results, albeit with lower traction forces, for MEFs treated with blebbistatin on 3, 5, and 14 kPa mPADs as well (Fig. 3B-C).

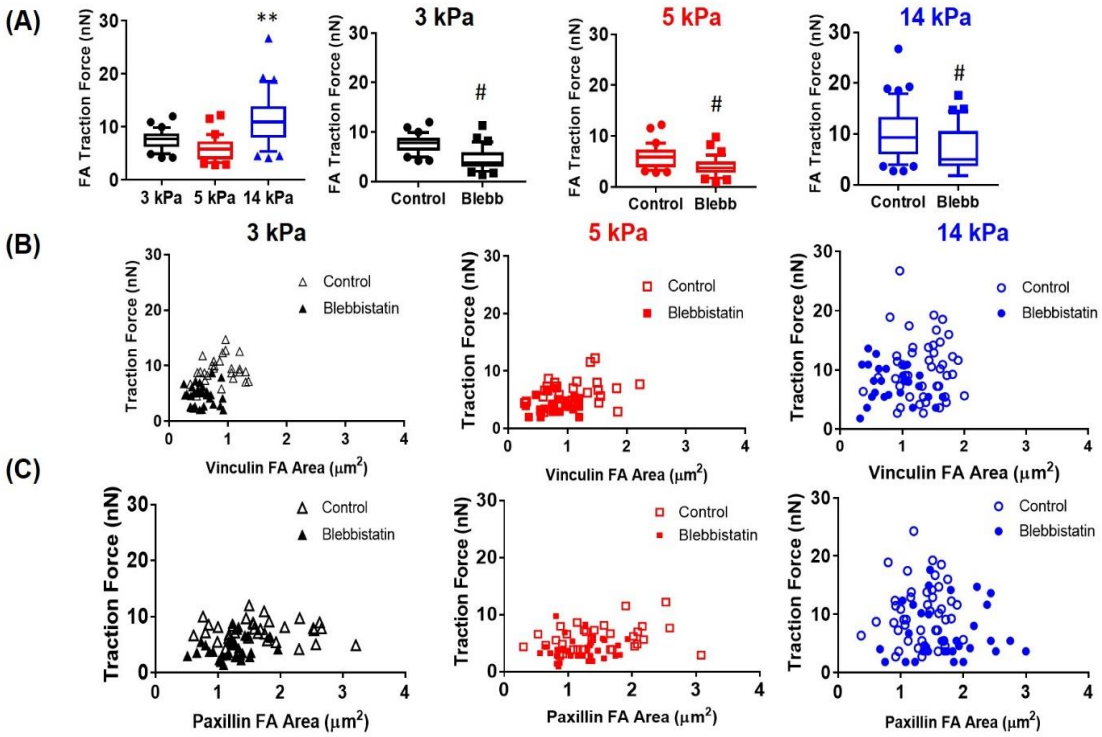

Figure 3**:** Traction forces at single FAs for MEFs expressing WT vinculin and WT paxillin, in the presence or absence of blebbistatin. (A) Traction forces at single FAs for WT MEFs cultured on mPADs of 5, 9, and 14 kPa (n > 25 FAs, randomly selected from 6 cells on each condition). $P < 0.01$ for one-way ANOVA, ** $P < 0.01$ vs. 3 and 5 kPa, # $P < 0.01$ vs. blebbistatin. (B) Relationship between traction force and FA area at single FAs.

We repeated this analysis for MEFs expressing T12 vinculin, and observed similar results, where T12 vinculin-expressing cells displayed higher forces at FAs on stiffer substrates (Fig. 4A). Furthermore, blebbistatin treatment significantly reduced forces at FAs on all stiffness values (Fig. 4A). T12 vinculin or paxillin FA area correlated poorly with traction

force at the single FA level for all substrate stiffness values examined and in the presence of blebbistatin (Fig. 4B-C). Gardel and colleagues previously reported that without knowledge of FA assembly history, FA size is a poor predictor of the degree of tension exerted on the ECM [145]. Here, we extend these findings for both vinculin and paxillin for varying substrate stiffness and CSK tension states.

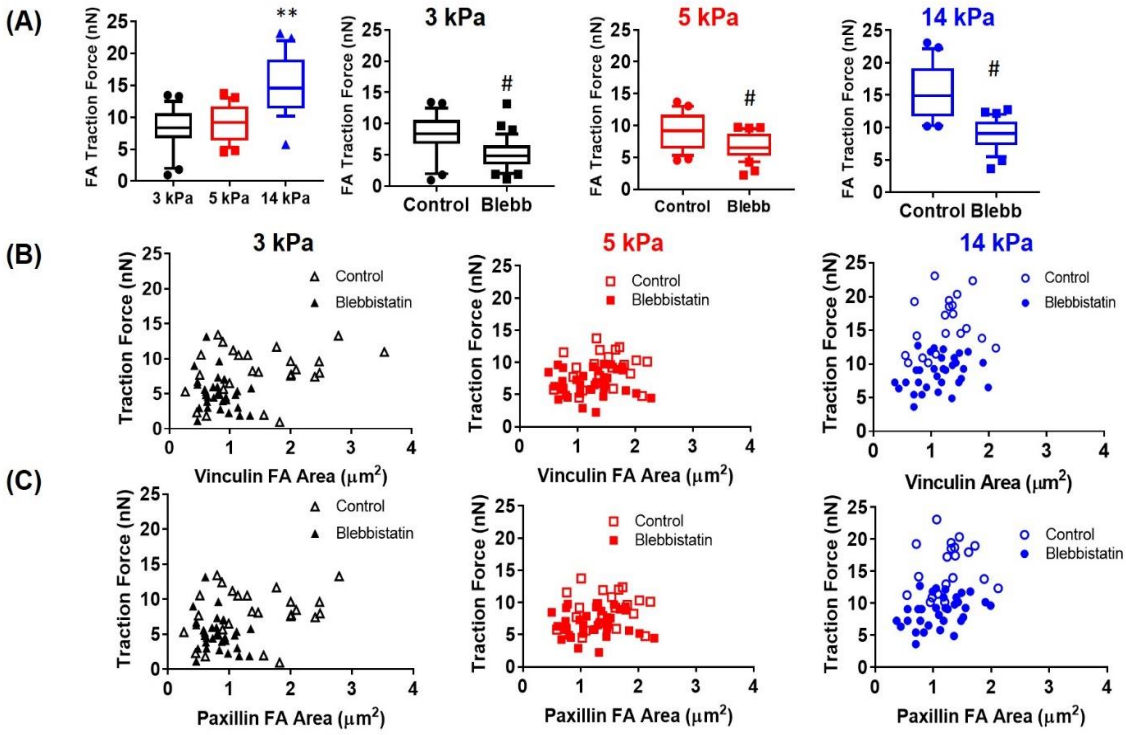

Figure 4: Traction forces at single FAs for MEFs expressing T12 vinculin and WT paxillin, in the presence or absence of blebbistatin. (A) Traction forces for T12 MEFs cultured on mPADs of 5, 9, and 14 kPa (n > 25 FAs, randomly selected from 6 cells for each condition). $P < 0.01$ for one-way ANOVA, ** $P < 0.01$ vs. 3 and 5 kPa, # $P < 0.01$ vs. blebbistatin. (B) Relationship between traction force and FA area at single FAs.

Effects of substrate stiffness on vinculin and paxillin residence time at FAs

FA turnover rate regulates cell migration and spreading [133, 153]. Furthermore,

FAs function as sites for stiffness mechanosensing and force transmission [3, 47, 94, 112]. Although others have analyzed turnover of different FA proteins and whether CSK contractility modulates FA turnover rates [133], most of these studies have been performed on glass substrates, with mechanical properties that poorly represent physiological values. Furthermore, how force is related to FA turnover is poorly understood. We previously reported a model of vinculin turnover at FAs, where forces applied across the vinculin molecule increase vinculin's residence time at FAs [3]. We therefore sought to examine the relationship between traction force and vinculin-paxillin turnover at single FAs in the context of substrate stiffness and CSK contractility.

We examined the relationship between vinculin and paxillin residence times at FAs and applied force by performing FRAP experiments on cells on mPADs of different stiffness values. We examined recovery times after photobleaching for eGFP-vinculin and TagRFP-paxillin-containing FAs associated with posts with known deflections. In this fashion, we could monitor vinculin dynamics at FAs under force. Fig. 5 demonstrates representative recovery images and profiles for both vinculin and paxillin, under varying levels of traction force. Furthermore, we previously demonstrated that during FRAP experiments, there are negligible changes in force generation at a single FA that was photobleached during the recovery time course [3].

We first analyzed the effects of substrate stiffness on vinculin and paxillin turnover at single FAs on 5, 9, 14, and 17 kPa mPADs (Fig. 6). We did not include 3 kPa mPADs for the FRAP studies, as WT vinculin recruitment to FAs was significantly attenuated on this substrate (Fig. 1), making it challenging to reliably photobleach vinculin at FAs. To

quantify turnover, our primary metric was the half-life recovery time ($t_{½}$), which is the time it takes for 50% fluorescence recovery after photobleaching.

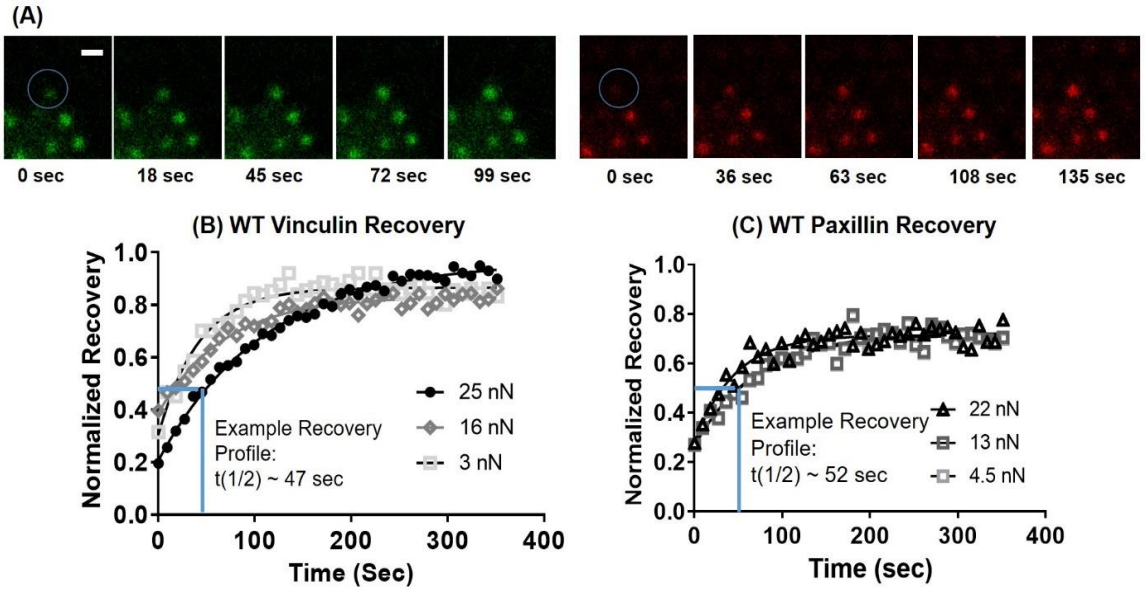

Figure 5: FRAP at single FAs. (A) Sample recovery images for vinculin (green) and paxillin (red) for an FA under high (24 nN) force. Scale bar 4 µm. Blue circle indicates photobleached region. FRAP recovery curves for (B) WT vinculin and (C) WT paxillin recovery at FAs transmitting different forces.

For WT vinculin, vinculin turnover rate at FAs was relatively insensitive to substrate stiffness, although vinculin $t_{½}$ on 17 kPa mPADs (~30 sec) was significantly lower than that of 5 kPa mPADs (~58 sec) (Fig. 6A). However, linear regression analyses for vinculin $t_{½}$ and substrate stiffness showed no relationship (Fig. S1). We then tested whether CSK contractility influenced vinculin turnover rate, and whether this was dependent on substrate stiffness. To inhibit contractility, we used Y27632, a potent and selective ROCK inhibitor [154], because blebbistatin exhibits photo-toxicity effects during live cell imaging [155]. For WT vinculin, contractility inhibition by Y27632 (10 µM, 30

min) did not alter vinculin turnover rate at FAs for 5, 9, 14, and 17 kPa mPADs (Fig. 6B). These results indicate that substrate stiffness and CSK contractility state do not significantly influence vinculin residence times at single FAs.

We performed similar analyses for paxillin turnover rate at FAs. Substrate stiffness had modest effects on paxillin residence time (Fig. 6C). Paxillin $t_{½}$ values on 14 kPa substrates (~46 sec) was higher compared to 5, 9, and 17 kPa mPADs (~34 sec), but only by 25%. Linear regression analyses showed no relationship between paxillin residence time and substrate stiffness (Fig. S1). Y27632 treatment (10 μM, 30 min) resulted in higher paxillin $t_{½}$ for 5 and 9 kPa substrates but had no effects on stiffer substrates (Fig. 6D). These results indicate that paxillin residence time at FAs depends on CSK tension, but only for soft substrates.

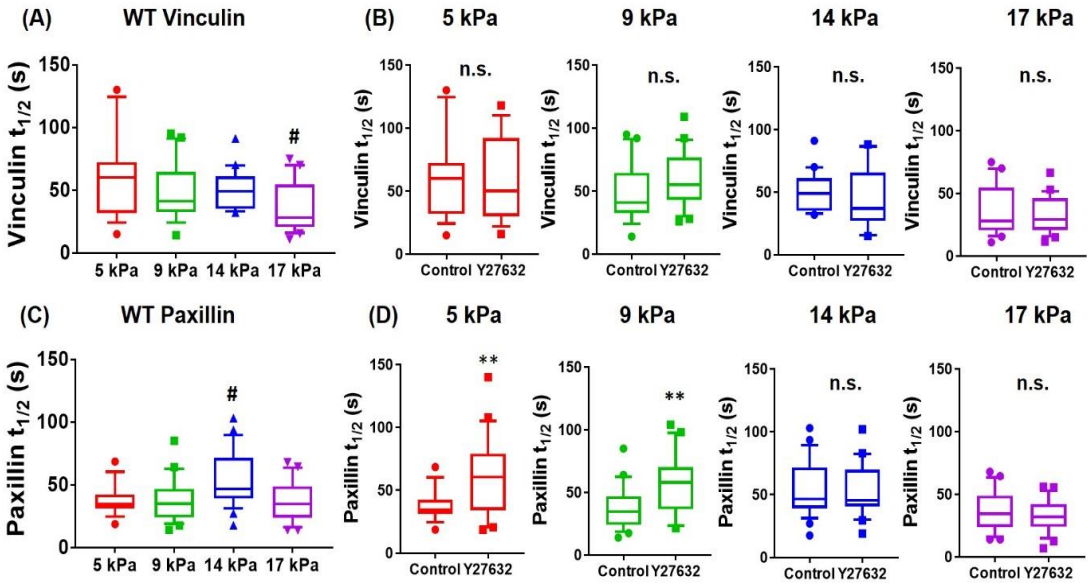

Figure 6: Effects of substrate stiffness on (A-B) vinculin and (C-D) paxillin residence times at single FAs, plotted as box-whisker plots (median, 10th, 25th, 75th, and 90th percentile, n = 18-25 FAs for each condition). For both vinculin and paxillin, $P < 0.01$ for one-way ANOVA for substrate stiffness. For WT vinculin, # $P < 0.01$ vs. 5 kPa. For paxillin, # $P < 0.01$ vs. 5, 9, 17 kPa, ** $P < 0.01$ vs. Y27632.

Correlation between force transmission and vinculin-paxillin turnover at FAs

We next examined the relationship between vinculin-paxillin turnover rate and applied traction force at single FAs for different substrate stiffness values. We observed a linear relationship between applied traction force and residence time at FAs for WT vinculin for stiffer mPADs of 14 and 17 kPa (Fig. 7). This linear relationship was abrogated on softer mPADs of 5 and 9 kPa. Furthermore, Y27632 eliminated the linear relationship between recovery time and force for vinculin on stiff mPADs of 14 and 17 kPa. These findings support a mechanosensitive model for vinculin activation in which forces applied across vinculin maintain the molecule in active conformation to increase

residence times at FAs to transfer force under stiffer substrates. However, this relationship only holds on stiff substrates and in the presence of sufficient CSK contractility. In contrast to vinculin, paxillin residence times at FAs did not vary with applied traction force for any substrate stiffness (Fig. 8). Taken together, these data suggest that substrate stiffness and actomyosin regulate the coupling between vinculin turnover rate and local traction force at single FAs, but there is no coupling between paxillin residence time and applied force, substrate stiffness, or CSK contractility.

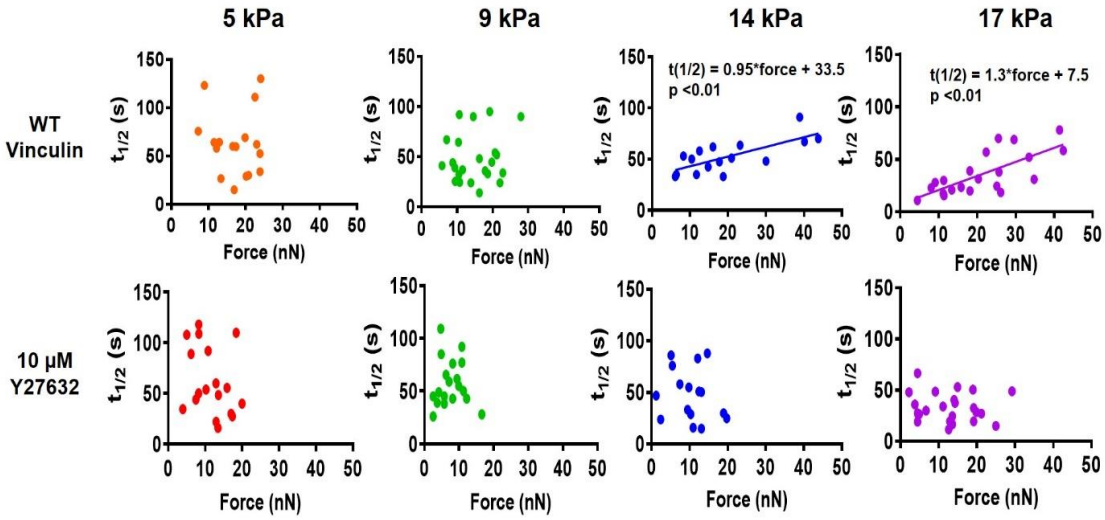

Figure 7: Coupling between vinculin $t_{1/2}$ and force at single FAs for MEFs cultured on difference substrate stiffness with and without Y27632 treatment. Vinculin $t_{1/2}$ and force are linearly coupled on 14 and 17 kPa, while this coupling is abrogated on softer substrates and after Y27632 treatment.

Simultaneous measurement of vinculin and paxillin turnover rates at single FAs

The differences between vinculin and paxillin on the dependence of turnover rate on traction force and substrate stiffness prompted us to compare their residence times at

the same FA under a given applied traction force. On stiff 14 and 17 kPa mPADs, where we observed linear coupling between vinculin residence time and force, there was no significant relationship between vinculin and paxillin residence time (Fig. 9). However, on softer 5 and 9 kPa mPADs, a linear relationship between vinculin residence time and paxillin residence time was observed. Strikingly, Y27632 treatment resulted in a linear relationship between vinculin and paxillin residence times all mPAD stiffness values (Fig. 9). Overall, these results show that soft substrates or contractility inhibition yields a strong correlation between vinculin and paxillin residence times at single FAs. However, on stiffer substrates in the presence of actomyosin contractility, vinculin and paxillin residence times are not correlated.

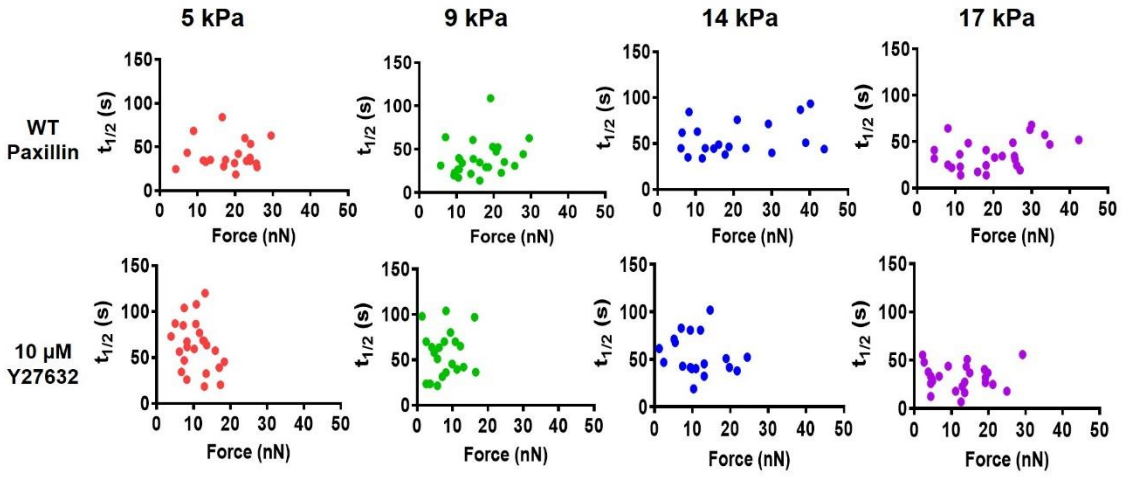

Figure 8**:** Correlation between paxillin $t_{1/2}$ and force at single FAs for MEFs cultured on difference substrate stiffnesses with or without Y27632 treatment. Paxillin $t_{1/2}$ and force are not correlated on any stiffness values or with or without Y27632 treatment.

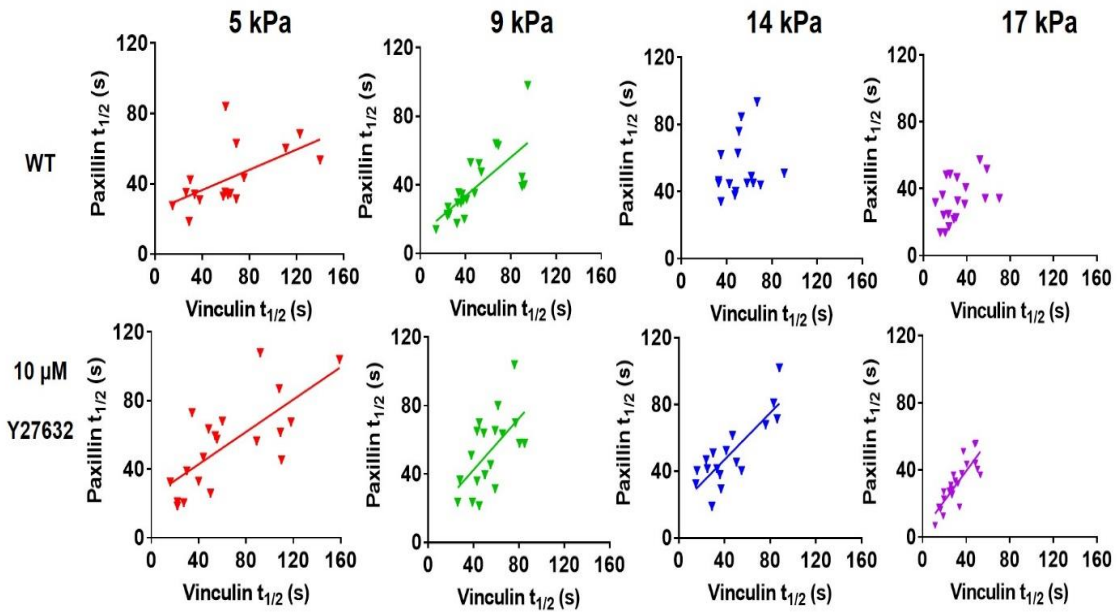

Stiffness	Y27632	Slope ± SE	P-value vs. Zero Slope	t-test for Y27632
5 kPa	Control	0.288 ± 0.103	P < 0.05	
5 kPa	Treatment	0.472 ± 0.107	P < 0.01	n.s. to control
9 kPa	Control	0.563 ± 0.117	P < 0.01	
9 kPa	Treatment	0.752 ± 0.247	P < 0.01	n.s. to control
14 kPa	Control	N/A	n.s.	
14 kPa	Treatment	0.704 ± 0.122	P < 0.01	N/A
17 kPa	Control	N/A	n.s.	
17 kPa	Treatment	0.889 ± 0.129	P < 0.01	N/A

Figure 9: Correlation between paxillin $t_{1/2}$ and vinculin $t_{1/2}$ at single FAs for MEFs cultured on different substrate stiffness with or without 10 µM Y27632 treatment. Linear coupling between paxillin $t_{1/2}$ and vinculin $t_{1/2}$ at single FAs for MEFs cultured on 5 and 9 kPa substrates and/or after treatment with Y27632.

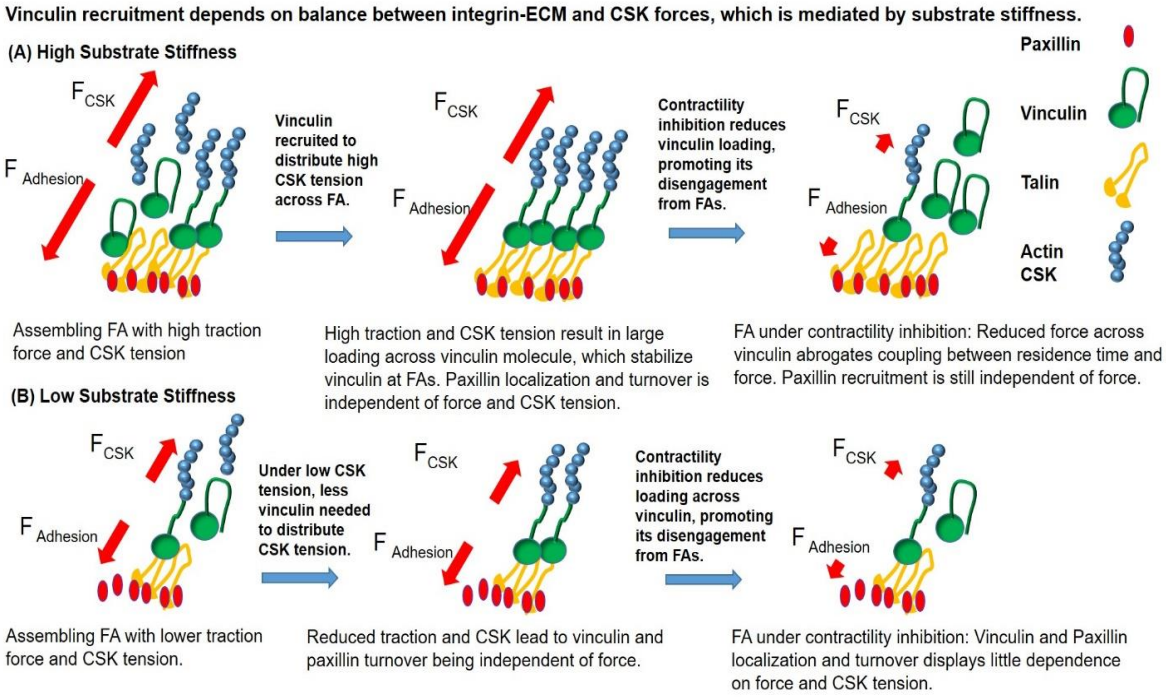

Figure 10**:** Model for vinculin-dependent force transfer and localization to FAs. (A) On stiff substrates, vinculin is recruited to better distribute high applied forces across FA. High forces applied across vinculin stabilize vinculin at FA to promote force transfer. Contractility inhibition unloads vinculin molecule, and promotes it disengage from FA. Paxillin recruitment is independent of stiffness and CSK tension. (B) On soft substrates, less vinculin is recruited, as there is less force to distribute across FA. Consequently, vinculin recruitment occurs through force-independent mechanisms. Contractility inhibition unloads vinculin molecule, and promotes its disengagement from FA, while paxillin recruitment is independent of stiffness and CSK tension.

3.5 Discussion

How force regulates FA assembly is poorly understood. In this study, we examined the relationship between traction force and vinculin-paxillin localization to single FAs in the context of substrate stiffness and actomyosin contractility. Substrate stiffness and contractility regulated vinculin localization to FAs, whereas they had minimal effects on

paxillin localization to FAs. In contrast to WT vinculin, T12 vinculin localization to FAs was independent of substrate stiffness and CSK contractility. This result indicates that vinculin auto-inhibition is a crucial regulatory step in vinculin localization to FAs that overrides the effects of CSK tension and substrate stiffness.

We also found that vinculin and paxillin FA area do not correlate with traction force magnitude at a single FA, and this observation holds consistent across different ECM stiffness and CSK tension states. However, vinculin residence time at FAs varied linearly with traction force for stiff substrates, but this coupling was disrupted on soft substrates and in the presence of contractility inhibitors. In contrast, paxillin residence time at FAs was independent of traction force, substrate stiffness, and CSK contractility. Furthermore, substrate stiffness and CSK contractility regulate whether vinculin and paxillin turnover dynamics are correlated to each other at single FAs. We showed that vinculin turnover and paxillin turnover at the same FA are linearly correlated with each other on soft substrates (5 and 9 kPa), and also in the presence of contractility inhibition. On stiff substrates (14 and 17 kPa), however, this coupling is abrogated, whereas vinculin residence time and force become linearly correlated. These findings suggest that vinculin functions as a mechanosensor for substrate stiffness, contractility, and traction force by modulating vinculin residence time at FAs whereas paxillin residence time at FAs is insensitive to these mechanical stimuli.

We previously reported that vinculin residence time at FAs correlate with traction force, supporting a mechanosensitive model, in which forces stabilize vinculin's active conformation to promote force transfer [3]. Expression of T12 vinculin, however, disrupted

the relationship between applied force and residence time, underscoring the importance of head-tail inhibition in regulating vinculin residence time. Based on our new data, we propose that vinculin serves a mechanosensor and integrator of forces at FAs via its head-tail auto-inhibition. At FAs, ECM-integrin traction forces must be balanced by CSK tension arising from actomyosin contractility for mechanical equilibrium [15]. Vinculin regulates this force balance by localizing to FAs and transferring forces across the ECM-CSK linkage [3]. Fig. 10 presents a conceptual model that captures experimental results for perturbations of the ECM-CSK force balance:

Substrate stiffness: On stiff substrates, cells generate high traction forces, which are balanced by high CSK tension that is necessary for spreading. This results in high forces across the FAs, but if the CSK tension is too high, the adhesive cluster will detach [15]. Because vinculin residence time at FAs varies linearly with traction force on stiff substrates, these elevated forces result in longer vinculin residence times and consequently, larger vinculin FA area. The increased FA area distributes the applied force across the FA to reduce the load for each ECM-CSK linkage and prevent the linkages from failing. Conversely, on soft substrates, low traction forces are balanced by low CSK tension, and therefore, low forces are transmitted across the FA. Accordingly, vinculin molecules at the FA carry lower forces and vinculin residence time at FAs is dominated by head-tail auto-inhibition and independent of force.

Contractility inhibition: Treatment with blebbistatin or Y27632 inhibits actomyosin contractility to reduce CSK tension and lower traction forces. The reduced CSK tension yields lower force transmission across vinculin molecules at the FA. For these lower forces,

vinculin auto-inhibition controls residence times at FAs and reduces vinculin FA area. Furthermore, during contractility inhibition, vinculin turnover occurs through force-independent mechanisms; these mechanisms may be similar to those of paxillin, as we observed significant correlation between vinculin and paxillin residence time on soft substrates or in the presence of contractility inhibitors.

Although factors like diffusion may influence vinculin localization within the cell, we stipulate that vinculin's conformational switch is the primary factor that regulates its recruitment to FAs. In the auto-inhibited conformation, vinculin exhibits head-tail binding that prevents it from localizing to FAs. However, simultaneous binding of vinculin to talin and actin works with actomyosin contractility to separate the head and tail domains, leading to vinculin's open conformation and localization to FAs. Indeed, this idea is supported by previous findings [151], showing that a mutated vinculin with reduced head-tail auto-inhibition has significantly longer residence time at FAs and increased talin binding. Furthermore, other mechanisms, such as vinculin tail binding to PIP2 [156], which is enriched at FAs, provide compelling explanations for vinculin's specific recruitment to FAs.

Our lab previously proposed a model where forces transmitted across vinculin stabilizes its open conformation and localization at FAs to promote force transfer. However, it is unclear how directionality of actin-vinculin binding influences vinculin-actin catch bond lifetime. Dunn and colleagues previously showed using a single-molecule optical trap assay that vinculin forms a catch bond with F-actin through its tail domain [157]. Strikingly, the vinculin-actin bond lifetime strongly depended on the

directionality of applied force. Specifically, forces applied towards the (-) end of actin resulted in bonds with a mean lifetime (12 seconds) 10 times as long as the mean lifetime of the bond when force was applied toward the barbed (+) actin end [157]. Taken together, these data indicate that force directionality regulates vinculin's role in FA mechanosensing. Although this model was further validated using a computational model of a cell protrusion [157], further validation within living cells, such as measurement of vinculin on and off dynamics at FAs under different directionality of vinculin-actin binding, is critical to confirm the authors' hypothesis.

In contrast to vinculin, paxillin localization to FAs is relatively insensitive to substrate stiffness or actomyosin contractility. We observed significant paxillin localization to FAs on all substrate stiffness values and CSK tension states. Furthermore, no significant relationship between force and paxillin residence time was observed for any of the substrate stiffness values evaluated. These findings are consistent with the fact that paxillin has not been implicated as a regulator of force transmission at FAs, but rather as an important component of the integrin signaling layer [95]. Paxillin, however, may still have important functions for mechanotransduction at FAs. For instance, phospho-paxillin facilitates vinculin recruitment to FAs [115], and a FAK-phospho-paxillin-vinculin signaling is involved in stiffness sensing during cell migration [116]. Taken together, the present analysis sheds new insights on the coupling among traction force, substrate stiffness, and FA dynamics.

CHAPTER 4. VINCULIN REGULATES FORCE-FAK LOCALIZATION AND FORCE-FAK Y397 PHOSPHORYLATION COUPLING AT INDIVIDUAL FOCAL ADHESIONS AND YAP MECHANOSENSING.

4.1 Abstract

Integrin-mediated adhesion to extracellular matrices (ECM) provides forces and signals that direct cell processes central to tissue organization, homeostasis, and disease. Recent studies suggest that forces generated at focal adhesions (FAs) lead to FA growth and maturation, yet it remains unclear how forces are transduced into adhesive signals. We seeded fibroblasts onto ECM-coated micropost-array-detectors (mPADs) and examined whether levels of FAK recruitment and Y397 phosphorylation were related to force at individual FAs. We found that force-FAK localization and force-pY397-FAK levels are linearly coupled at single FAs on stiff substrates. On soft substrates or upon contractility inhibition, these linear couplings are eliminated. We also assessed the roles of talin and vinculin, which are important force transducing proteins, in regulating FAK recruitment and Y397 phosphorylation at FAs and YAP nuclear accumulation. We found that talin is required for FAK localization and Y397 phosphorylation at FAs and mediates force-FAK linear coupling at FAs via talin-FAK binding. Furthermore, vinculin is not required for averaged levels of FAK localization and Y397 phosphorylation at FAs. However, a full-length vinculin molecule that binds talin and actin is required for linear coupling between force-FAK localization and force-FAK Y397 phosphorylation at individual FAs. Lastly,

we demonstrate that a full-length vinculin molecule that binds talin and actin is required to promote YAP nuclear accumulation.

From these data, we propose a sequential model where talin and actomyosin contractility-dependent forces promote talin-dependent FAK localization to FAs, where FAK Y397 phosphorylation then occurs. As FA growth occurs, a FAK-talin-vinculin complex is necessary to couple force generation and continued FAK recruitment and Y397 phosphorylation at individual FAs, whereas an integrin-talin-vinculin complex, FAK kinase activity, and contractility are required to enhance YAP nuclear accumulation. Lastly, talin, vinculin, contractility, and pY397-FAK promote YAP nuclear accumulation. These findings demonstrate that force generation and FAK recruitment-Y397 phosphorylation are coupled at FAs and underscore the role of talin and vinculin in regulating force-signaling coupling at FAs and YAP nuclear accumulation. Taken together, we anticipate that our results generate new insights into how cell adhesive forces are integrated and transduced into biochemical and nuclear signals.

4.2 Introduction

Cell adhesion to the extracellular matrix (ECM) is regulated by integrin membrane receptors, which are composed of α and β subunits [1]. Following integrin-ECM binding, integrins cluster and form focal adhesion (FA) complexes, which contain structural proteins that link the cytoskeleton (CSK) to bound integrins and signaling effectors (e.g. paxillin, FAK, Src) that regulate processes, such as migration [138], differentiation [2], and development [158]. Cell-ECM adhesive interactions regulate host-implant responses for medical devices and tissue-engineered constructs and play a crucial role in disease and pathogenesis (e.g. cancer, atherosclerosis) [6, 117, 159], further underscoring the importance of cell-ECM adhesion [5].

FAs provide support and anchorage for the cell, by mechanically linking ECM proteins to the CSK [1, 2] and transmitting forces that regulate cell migration, survival, and tissue morphogenesis [9-11]. Our lab previously proposed a force-equilibrium model for ECM area-regulated assembly of stable FAs [15]. Talin-activated integrins bind to ECM and assemble into clusters containing talin and vinculin. CSK tension applies force to FAs via actomyosin contractility. This CSK force is balanced by the adhesive force generated by integrin-FN clusters [15]. Below an area threshold, the adhesive force cannot support the CSK tension and the cluster is unstable and detaches from FN. Above this area threshold, the integrin-FN cluster is large enough to generate sufficient adhesive force to support the applied CSK tension [15]. Consequently, our model suggests that a balance of integrin-ECM force and CSK tension modulates FA activity and mechanotransduction.

Vinculin regulates adhesive force transmission between the cell's integrin receptors and surrounding ECM proteins [3]. Vinculin consists of a globular head domain (V_H) that is linked to a tail domain (V_T) by a proline-rich strap [126]. The V_H domain contains binding sites for talin and α-actinin [127, 128]. The V_T domain includes binding sites for actin, paxillin, and phosphatidylinositol 4,5-biphosphate (PIP2) [128]. Vinculin displays high-affinity head-tail binding, which leads to auto-inhibition [129, 130]. Vinculin activation is hypothesized to occur at FAs, upon engagement to talin via V_H and actin via V_T, which consequently leads to head-tail domain separation, FA localization, and force transmission [3, 94, 127, 128]. Furthermore, we previously found a positive linear relationship between force and vinculin residence time at FAs on stiff substrates, supporting a model where forces applied across vinculin stabilize its open conformation and localization at FAs [3, 137].

Whereas mechanotransduction research analyzes force-transducing proteins like vinculin, other FA proteins such as focal adhesion kinase (FAK) are key signaling regulators at FAs [5]. FAK is a 125 kDa non-receptor tyrosine kinase that localizes to the integrin signaling layer in FAs [95]. FAK is comprised of an N-terminal FERM (band 4.1-ezrin-radixin-moesin) domain, central kinase domain, and a C-terminal FAT (focal adhesion-targeting) domain that helps recruit FAK to FAs [138]. The FERM and kinase domains are usually bound to each other, resulting in a closed auto-inhibited conformation [97, 138]. FAK activity is primarily regulated by Tyr397 (Y397) auto-phosphorylation, which in turn leads to Src association and Src-mediated phosphorylation at Y576/577, promoting FAK's open conformation and enhancing signaling activity [138]. FAK

phosphorylation targets include paxillin, p130Cas, Src, VE-cadherin, and α-actinin [3]. Furthermore, recent computational models have proposed that forces applied across FAK are directly responsible for regulating its phosphorylation and promoting FAK signaling activity [160]. However, experimental studies assessing how force and FAK are coupled at FAs are currently lacking.

Yes-associated protein (YAP) is a mechanosensitive transcriptional factor that regulates cancer, development, and organ size [123, 161, 162]. YAP can localize to either the cytoplasm or the nucleus, where it binds and activates TEAD transcription factors [123]. YAP can be regulated by a combination of biochemical and mechanical cues [123]. At the biochemical level, the Hippo pathway regulates YAP activity by Lats-mediated phosphorylation, which inhibits YAP and promotes cytoplasmic localization [162]. Furthermore, recent work by Meng et al demonstrates that increased ECM stiffness is transduced into decreased RAP2 activity, which in turn enhances YAP nuclear accumulation [163]. At the mechanical level, ECM stiffness [164], cytoskeletal assembly [165], or cell spreading area [122], can regulate YAP nuclear accumulation. Furthermore, Roca-Cusachs and colleagues have proposed a mechanical model of YAP nuclear accumulation, where integrin-ECM-nuclear mechanical coupling promotes YAP nuclear localization in response to ECM stiffness [166]. However, it is unclear how FA proteins, such as vinculin, can regulate YAP nuclear accumulation. Although previous studies have shown that vinculin depletion results in reduced nuclear YAP levels, the mechanism by which vinculin regulates YAP nuclear activity remains unclear [167].

The relationship between FA signaling and force generation and whether structural proteins like vinculin influence FA signaling, in particular FAK phosphorylation, remains poorly understood. Although experiments involving averaged or cell population-level measurements (e.g. Western blotting or immunostaining) show that actomyosin contractility is required for FAK Y397 phosphorylation [115], how force regulates FAK Y397 phosphorylation at individual FAs remains unclear. In the present study, we seeded mouse embryonic fibroblasts (MEFs) expressing mutated FA constructs onto mPADs and assessed whether FAK localization and Y397 phosphorylation were related to force at FAs.

For WT MEFs, we found that force and FAK localization are linearly coupled at single FAs on stiff (14 kPa) substrates. However, on low stiffness (5 kPa) or after contractility inhibition, the relationship between FAK localization and force is eliminated. Furthermore, force and pY397-FAK levels at FAs are linearly coupled on stiff (14 kPa) substrates. Subsequently, we assessed the role of force-transducing proteins, such as vinculin and talin, in regulating FAK localization and Y397 phosphorylation at FAs. We demonstrate that talin is required for FAK localization and Y397 phosphorylation and mediates force-FAK linear coupling at individual FAs via talin-FAK binding. Although vinculin is not required for FAK localization and Y397 phosphorylation at FAs, a full-length vinculin molecule that binds to talin and actin is required to linearly couple force-FAK localization and force-FAK Y397 phosphorylation at FAs. We also demonstrated that FAK's kinase function is required to promote FAK Y397 phosphorylation, although force-FAK localization linear coupling still occurs in kinase dead FAK-expressing cells. Lastly, FAK kinase activity, actomyosin contractility, talin, and vinculin enhance YAP nuclear

accumulation, and a full-length vinculin molecule that binds talin and actin is necessary to promote YAP nuclear accumulation.

4.3 Materials and Methods

Cells and Reagents

eGFP-WT-vinculin, eGFP-V_H-vinculin, eGFP-A50I-vinculin, eGFP-T12-vinculin, and vinculin-null MEFs have been described previously [3]. Cells were maintained in DMEM containing 10% FBS, 1% sodium pyruvate, and 1% penicillin-streptomycin. WT GFP-FAK, E1015A GFP-FAK, K454R GFP-FAK (kinase dead), and FAK-null MEFs have been described previously [104, 158] and were kindly provided by David Schlaepfer (UCSD). Talin-1 was depleted using talin-1 shRNA lentiviral particles (Santa Cruz Biotechnology) in DMEM containing 6 µg/mL polybrene. Control cells were treated with scrambled shRNA lentiviral particles (Santa Cruz Biotechnology). After addition of lentiviral particles, cells were centrifuged at 1,200 xg for 30 min in a swinging bucket rotor and then incubated for 24 hours at 37°C and 5% CO_2. Afterwards, the cell culture media was aspirated and replaced with fresh media. The transduced cells were then selected using 4 µg/mL puromycin for 3-4 days, expanded, and either used for experimentation or cryopreserved. Knock-down of talin-1 was confirmed using Western blotting.

Traction Force Microscopy

Microfabricated post array detector (mPAD) device silicon masters were prepared as described previously [22]. In brief, elastomeric micropost arrays were fabricated using PDMS replica molding. To make microfabricated post array templates, 1:10 PDMS prepolymer was cast on top of silanized mPAD device silicon masters, cured at 110 °C for 30 min, peeled off gently, oxidized with oxygen plasma (Plasma-Preen; Terra Universal), and silanized overnight with (tridecafluoro-1,1,2,2,- tetrahydrooctyl)-1-trichlorosilane (Sigma–Aldrich) vapour under vacuum. To make the final PDMS mPAD device, 1:10 PDMS pre-polymer was cast on the template, degassed under vacuum for 20 min, and cured at 110 ℃ for 20 h and gently peeled off the template on a 25 mm diameter #1 circular coverslip (Electron Microscopy Services). Peeling induced collapse of the mPADs was rectified by sonication in 100% ethanol, followed by supercritical drying in liquid CO2 using a critical point dryer (Samdri-PVT-3D; Tousimis). Flat PDMS stamps were generated by casting 1:20 PDMS pre-polymer on flat and silanized silicon wafers. Stamps were coated in a saturating concentration of fibronectin (Thermo Fisher D307) (50 μg/ml in PBS) and AF647-fibrinogen (Thermo F35200, 20 µg/mL) for 1 hr. These stamps were washed in sterile distilled water and dried under a stream of nitrogen gas. Subsequently, fibronectin-coated stamps were placed in contact with surface-oxidized mPAD substrates (UVO-Model 342; Jelight). mPAD substrates were subsequently transferred to a solution of 0.2% Pluronics F127 (Sigma–Aldrich) for 30 min, to prevent nonspecific protein absorption. MEF cells were seeded in growth medium and then allowed to spread overnight. On the following day, mPAD substrates were transferred to an aluminium

coverslip holder (Attoflour Cell Chamber; Invitrogen) for live cell microscopy and placed in a stage top incubator that regulated temperature, humidity and CO_2 (Tokai Hit). Confocal images were taken with a Nikon C2-Confocal Module connected to a Nikon Eclipse Ti inverted microscope, using a high magnification objective (Plan Apo VC Water Immersion 60X, N.A. 1.2; Nikon). Post images were captured using a 640-nm laser with a 685/50 filter, vinculin images were captured using a 488 nm laser and 525/50 filter, FAK or YAP images were captured using a 561 nm laser and 595/50 filter, and pY397-FAK images were captured with a 405 nm laser and 450/40 filter. For force measurements, the top of the posts were labeled with AF647-fibrinogen and were sequentially imaged and the deflection measured using custom MATLAB code. The resulting force, *F*, was calculated using Euler-Bernoulli beam theory, in which *E*, *D*, *L*, and δ are the Young's modulus, post diameter, post height, and post deflection respectively:

$$F = \delta \frac{3\pi E D^4}{64 L^3}$$

Immunofluorescence Staining

For staining of FAs, cells cultured overnight were fixed in a mixture of 50% cytoskeleton-stabilizing buffer (0.5% Triton X-100, 10 mM PIPES buffer, 50 mM NaCl, 150 mM sucrose, 3 mM $MgCl_2$, 1 μg/mL leupeptin, 1 μg/mL aprotinin) and 50% PBS with 10% paraformaldehyde. Subsequently, samples were permeabilized with CSK buffer with 0.5% Triton-X100, incubated in 0.1M glycine solution to quench free aldehydes, and blocked in 33% goat serum in PBS for 1 hour, and incubated with primary

antibodies against FA components overnight at 4°C in PBS with 33% goat serum and 0.02% tween. On the following day, samples were incubated with secondary antibody in PBS with 33% goat serum and 0.02% Tween-20 at room temperature for 1 hour. Confocal images of FAs were taken with a Nikon C2 module connected to a Nikon Eclipse Ti inverted microscope with a high magnification objective (60X Plan Apo VC Water Immersion objective, NA 1.2, Nikon) Cell spreading and FA size and intensity were quantified using Nikon NIS-Elements Analysis Software and ImageJ. The following antibodies were used: pY397-FAK: Abcam ab39967, Rb polyclonal to pY397-FAK, 1:300. Total FAK: Millipore 4.47, Mouse monoclonal to FAK, 1:200. YAP: Santa Cruz 63.7, Mouse monoclonal to YAP, 1:200.

Western Blotting

Cells were washed with ice-cold PBS containing calcium and magnesium and lysed in cold radioimmunoprecipitation assay buffer [1% Triton X-100, 1% sodium deoxycholate, 0.1% SDS, 150 mM NaCl, 150 mM Tris-HCl (pH 7.2)] supplemented with Protease Inhibitor Cocktail (Thermo) and Phosphatase inhibitor cocktail (Thermo) for 20 min. Lysates were sonicated briefly and then clarified by centrifugation at 14,000 xg for 15 min. Protein concentration was then determined using a BCA protein assay kit (Pierce). Equal amounts of protein (10 μg) were boiled in Laemmli sample buffer [2% SDS, 10% glycerol, 100 mM DTT, 60 mM Tris·HCl (pH 6.8), and 0.001% bromophenol blue] for 5 min and separated by SDS-PAGE. Proteins were transferred by electrophoresis onto 0.45 μm PVDF

membranes and blocked with LICOR Blocking Buffer for 1 hour at room temperature. Membranes were incubated with appropriate antibodies in LICOR Blocking Buffer supplemented with 0.1% tween overnight at 4°C. Membranes were washed in PBS-0.1% Tween (3 washes, 10 minutes each) and incubated in near-infrared conjugated-secondary antibodies (LICOR Biosciences) for 45 min followed by 30 min washing in PBS-0.1% Tween. Membranes were imaged with a LI-COR Odyssey Imager (LI-COR Biosciences). The following primary antibodies were used: Mouse Monoclonal anti-Talin (Sigma, clone 8d4, 1:200), Rabbit Polyclonal anti-Talin-1 (ab71333, Abcam, 1:1000), and Mouse Monoclonal anti-Vinculin (Sigma V284, 1:8000).

Statistical Analysis

Regression analyses were performed using GraphPad Prism. ANOVA, Kruskal-Wallis nonparametric-tests, and post hoc tests were performed in GraphPad Prism. A p-value < 0.05 was considered significant. To assess force-FAK recruitment and force-pY397-FAK coupling at FAs, only FAs at the edge of the cell were analyzed. We analyzed as many FAs on the edge as possible for each individual cell. For statistical analyses, FAs taken from different cells were pooled together and linear regression was performed to determine whether the force-FAK relationship at FAs was linear.

4.4 Results

Force-FAK localization and force-FAK Y397 phosphorylation are linearly coupled at single FAs.

We first analyzed how force, FAK localization, and FAK-Y397 phosphorylation were related at individual FAs. We used vinculin-null mouse embryonic fibroblasts (MEFs) expressing eGFP-WT-vinculin, which were previously described [3]. We chose to use MEFs because they generate robust FAs and forces and are a commonly used cell type for mechanotransduction studies [3, 104, 168]. Cells were cultured overnight on micropost-array-detectors (mPADs) coated with fibronectin (FN) that had an effective elastic moduli (E) of 14 kPa. This platform allows for measurement of cell traction forces, by tracking the deflections of the micropillars, as described previously [9, 47, 63]. One advantage of mPADs is their ability to mimic tissue stiffnesses found within biological tissues. We were able to tune mPAD stiffnesses between 3 and 17 kPa, which are comparable to multiple tissue types within the human body. For instance, neural and lung tissue are often around the 100-400 Pa range [149]. However, aortic and stromal tissue are around 3 kPa while smooth muscle tissue is at ~5 kPa and skeletal muscle tissue is at ~12 kPa [149]. Additionally, the use of mPADs as our experimental platform is advantageous, as it decouples changes in substrate stiffness from changes in the microscopic material properties that could affect ligand binding and cell responses [47, 169]. With mPADs, FAs will assemble at individual pillars, which are mechanically isolated from each other, which allows us to reliably map force values to individual FAs

[47]. This is a key advantage over using flat deformable substrates, where measured forces at an FA can be influenced by the forces generated by nearby FAs [48].

After overnight incubation on the mPADs, the cells were fixed and stained for total FAK and pY397-FAK and visualized with confocal microscopy. To measure FAK localization at single FAs, we quantified the area and mean intensity of FAK at an individual FA. We then multiplied FAK FA area with FAK FA mean intensity to get the FAK integrated intensity at an individual FA. We used the same approach to compute pY397-FAK integrated intensity at individual FAs. We chose to use the integrated intensity metric (FA size x mean FA intensity), as it combines important FA parameters into one metric. Furthermore, this metric has been utilized in published reports analyzing force generation and FA protein recruitment [112].

At individual FAs, we found that force and FAK integrated intensity were linearly related on 14 kPa mPADs (Figure 11B, G). In addition, we found that force and pY397-FAK integrated intensity were linearly related on 14 kPa mPADs (Figure 12A, E). These observations were further validated in multiple different individual cells on 14 kPa mPADs (Figure 13 A-B). On 14 kPa mPADs, the pY397-FAK/total FAK ratio was relatively constant between different values of applied force at FAs (Figure 13C). This finding supports a model where FAK Y397 phosphorylation occurs upon FAK localization to the FA.

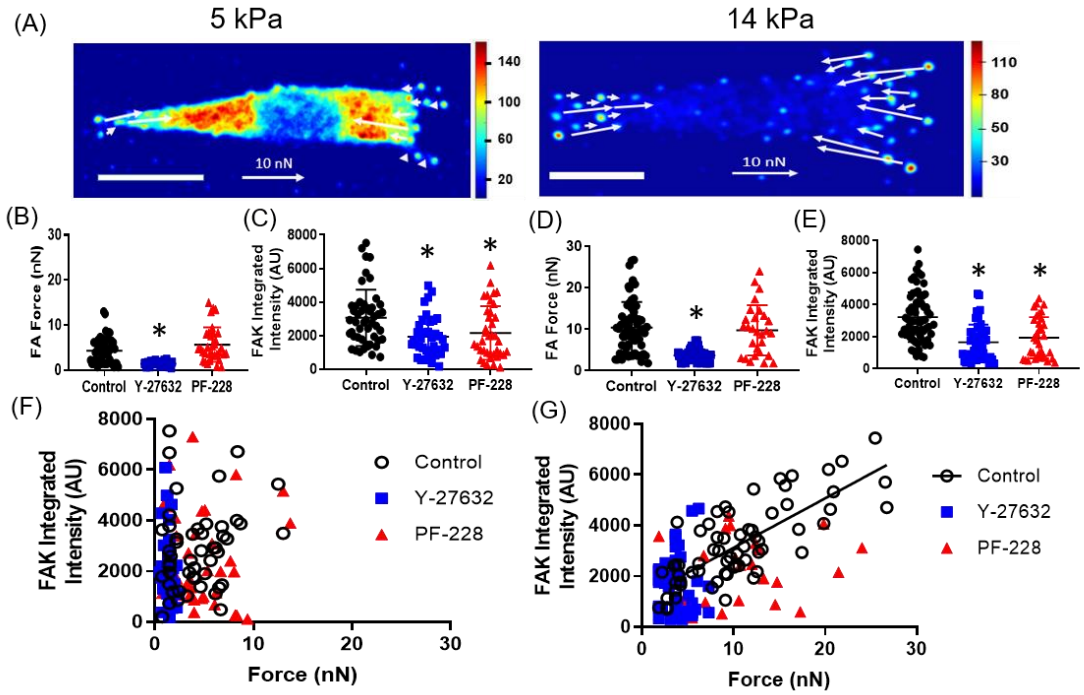

Figure 11: Force and total FAK integrated intensity are linearly coupled at single FAs. (A) Heatmap of total FAK staining on mPADs of differing stiffness values. White arrows indicate force magnitudes and directions. Scale bar 5 µm. (B) Comparison of force at single FAs. $P < 0.01$ Kruskal-Wallis Test and * $P < 0.01$ vs control and PF-228. (C) Comparison of total FAK integrated intensity at single FAs between Y-27632 (10 µM, 90 min) and PF-228 (10 µM, 90 min) treated cells vs control on 5 and 14 kPa mPADs. $P < 0.02$ Kruskal-Wallis Test. * $P < 0.03$ vs corresponding control. (D) Comparison of force at single FAs. $P < 0.01$ Kruskal-Wallis Test and * $P < 0.01$ vs control and PF-228. (E) Comparison of total FAK integrated intensity at single FAs between Y-27632 (10 µM, 90 min) and PF-228 (10 µM, 90 min) treated cells vs control on 5 and 14 kPa mPADs. $P < 0.02$ Kruskal-Wallis Test. (F, G) Correlation between force and FAK integrated intensity at single FAs. Linear regression on 14 kPa: FAK Integrated Intensity = 195 x force + 1179, $P < 0.0001$. $R^2 = 0.48$ (n = 60 FAs, taken from 9 cells). Y-27632 (n = 44 FAs, taken from 6 cells) or PF-228 (FAK inhibitor) (n = 27 FAs, taken from 5 cells) treatment eliminates linear relationship between FAK integrated intensity and force at single FAs ($P = 0.89$ and 0.21 respectively) on 14 kPa mPADs. Linear regression for 5 kPa: $P = 0.12$, 0.19, and 0.99 for

control (n = 49 FAs, 7 cells), Y-27632 (n = 35 FAs, 6 cells), and PF-228 (n = 44 FAs, 8 cells) respectively.

Substrate stiffness, actomyosin contractility, and FAK catalytic activity regulate the linear coupling between force-FAK localization and force-FAK Y397 phosphorylation at individual FAs.

We next analyzed the effects of substrate stiffness, actomyosin contractility, and FAK catalytic activity on FAK localization to single FAs. The effective substrate stiffness of mPADs was modulated by changing micropost heights, where increasing the post height decreased the effective substrate stiffness. Importantly, the cross-sectional area of individual posts and the spacing between posts are consistent for mPADs with different stiffness values [9]. We first measured forces at single FAs and found that Y-27632 (ROCK inhibitor) treatment significantly reduces FA forces on 5 and 14 kPa, while PF-228 (FAK kinase inhibitor) did not significantly influence FA forces on 5 and 14 kPa mPADs (Figure 11B, D). This observation is consistent with other reports utilizing deformable substrates and immunostaining, suggesting that FAK kinase activity is dispensable for force transmission at FAs [170]. Furthermore, we found that Y-27632 and PF-228 treatment significantly reduced levels of total FAK at FAs on both 5 and 14 kPa mPADs (Figure 11C, E), which is consistent with previously published data by Waterman and colleagues [116]. Importantly, whereas we observed a strong linear coupling between force and FAK integrated intensity at individual FAs on 14 kPa mPADs, this linear coupling is eliminated

for cells cultured on 5 kPa mPADs and after Y-27632 or PF-228 treatment on 14 kPa mPADs (Figure 11F, G).

Similar to FAK localization to FAs, we found that Y-27632 or PF-228 treatment significantly reduced pY397-FAK levels at FAs (Figure 12 B,C), which is consistent with previous observations [116]. Remarkably, we also observed a strong linear relationship between pY397-FAK integrated intensity and force at single FAs on 14 kPa mPADs, but Y-27632 or PF-228 treatment or culture on 5 kPa substrates abrogated this relationship (Figure 12D, E). Taken together, our data demonstrate that force and FAK recruitment and force and Y397 phosphorylation at individual FAs are linearly coupled, and substrate stiffness, actomyosin contractility, and FAK catalytic activity are required for maintaining force-FAK linear coupling at FAs. Furthermore, our data show that contractility and FAK catalytic activity support FAK localization and Y397 phosphorylation at FAs. In addition, our results support a model where local applied forces promote FAK localization and subsequent Y397 phosphorylation at FAs on stiff substrates. As demonstrated with the FAK inhibitor, PF-228, FAK kinase activity is not required to promote force generation at FAs. Although FAK kinase activity can promote the recruitment of force-transducing proteins [115], such as vinculin, to FAs, there are other mechanisms, such as simultaneous binding to talin and actin, by which vinculin can be recruited to FAs [94, 151]. One limitation of our approach, however, is that PF-228 may have off-target inhibitory effects on other kinases within the cell, due to structural similarities of the ATP-binding domain between many other kinases [171]. In fact, studies have shown that the biological effects of PF-228 in platelets result from its off-target effects rather than FAK kinase inhibition

[171]. We therefore later examined force and FAK localization-Y397 phosphorylation coupling at FAs in MEFs expressing a kinase dead FAK variant (Figure 19).

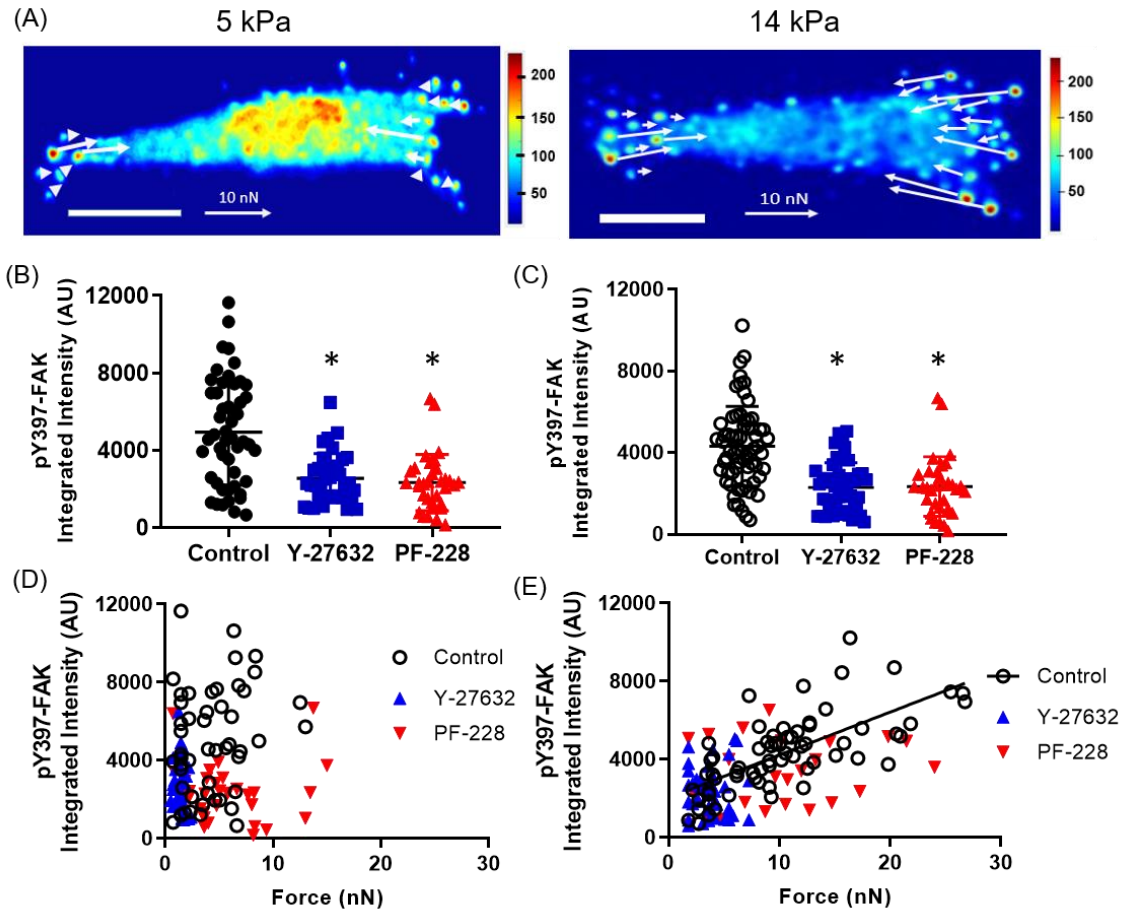

Figure 12: Force and pY397-FAK integrated intensity are linearly coupled at single FAs. (A) Heatmap of pY397-FAK staining on mPADs of differing stiffness values. White arrows indicate force magnitudes and directions. Scale bar 5 μm. (B) $P < 0.01$ Kruskal-Wallis Test. * $P < 0.01$ vs control. (C) $P < 0.01$ Kruskal-Wallis Test. * $P < 0.01$ vs control. (D, E) Correlation between force and pY397-FAK integrated intensity at single FAs from multiple cells. Linear regression for 5 kPa: $P = 0.11, 0.29, 0.89$ for control (n = 49 FAs, 7 cells), Y-27632 (n = 35 FAs, 6 cells), and PF-228 (n = 44 FAs, 8 cells) respectively. Linear regression on 14 kPa: pY397-FAK Integrated Intensity = 220 x force + 203, $P < 0.0001$. $R^2 = 0.48$, n = 60 FAs, 9 cells. On 14 kPa substrate, Y-27632 (n = 44 FAs, taken from 6 cells) or PF-228 (n = 27 FAs, taken from 5 cells) treatment eliminates linear relationship

between pY397-FAK integrated intensity and force at single FAs (P = 0.80 and 0.23 respectively).

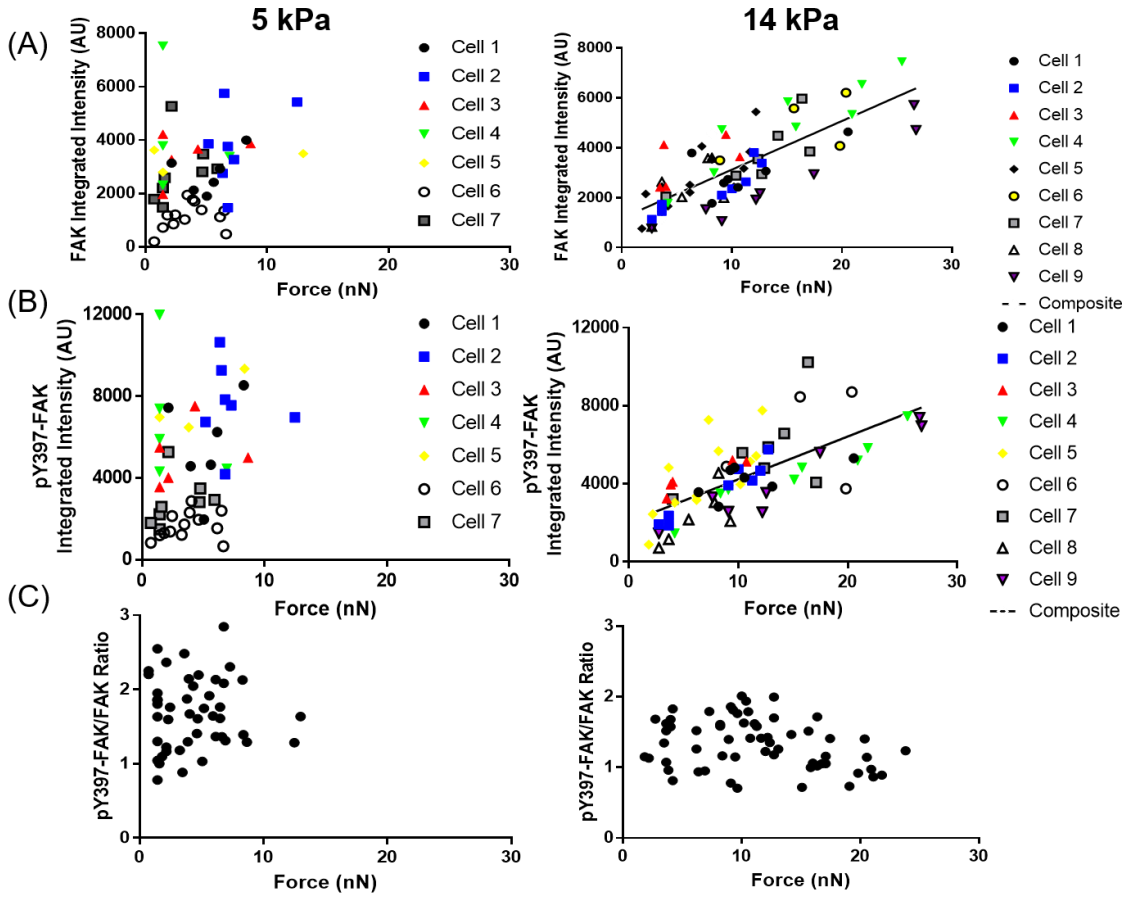

Figure 13: Correlation between pY397-FAK/total FAK ratio and force at single FAs. (A) Correlation between force and FAK integrated intensity at single FAs from multiple cells on 5 and 14 kPa mPADs. Linear regression on 14 kPa: FAK Integrated Intensity = 195 x force + 1179, $P < 0.001$, $R^2 = 0.60$, n = 60 FAs. Linear regression on 5 kPa: P = 0.12 (n = 49 FAs). (B) Correlation between force and pY397-FAK integrated intensity at single FAs from multiple cells on 5 and 14 kPa mPADs. Linear regression on 14 kPa: pY397-FAK Integrated Intensity = 220 x force + 203, $P < 0.0001$, $R^2 = 0.48$, n = 60 FAs. Linear regression on 5 kPa: P = 0.11, n = 49 FAs. (C) Correlation between pY397-FAK integrated intensity and FAK integrated intensity ratio and force at single FAs. Linear regression on 5 and 14 kPa: P = 0.91, 0.03 ($R^2 = 0.08$) respectively.

Talin is required for FAK localization and Y397 phosphorylation at FAs as well as force-FAK and force-Y397 phosphorylation coupling at individual FAs.

We next examined whether talin is required for FAK localization and Y397 phosphorylation at individual FAs. Talin is a ~270 kDa FA protein that exists in two isoforms, talin-1 and talin-2 [172]. Furthermore, talin is hypothesized to play a critical role in FA assembly and force transmission [172]. Although talin-1 is expected to be the predominant isoform expressed in fibroblasts [173], it is well-documented that talin-1 depletion can lead to talin-2 over-expression and compensation for the loss of talin-1 [173]. Furthermore, the relationship between talin and FAK remains complex. Lawson et al demonstrated that FAK is required for talin recruitment to nascent FA complexes but dispensable for talin localization to mature FAs [104]. Others have proposed models where talin is required for FAK Y397 phosphorylation at FAs. For instance, Roca-Cusachs and colleagues demonstrated that talin-1 and talin-2 depletion leads to significantly reduced pY397-FAK levels at FAs [134]. In the following studies, we sought to examine whether talin was required for FAK localization, Y397 phosphorylation, and force-FAK coupling at individual FAs.

We depleted talin-1 by treating WT MEFs with a talin-1 shRNA lentiviral construct (Figure 14). We also treated WT MEFs with a control scrambled shRNA lentiviral construct. After antibiotic selection of transduced cells, we measured talin-1 depletion through Western blotting. We found that talin-1 depletion was successful (87% reduction compared to control shRNA-treated cells) via Western blotting for talin-1 (Figure 14E).

We also measured total talin levels with the pan-talin 8d4 antibody and found that total talin levels were reduced by 60% in the talin-1 shRNA-treated cells (Figure 14E). We measured cell spreading and total traction force generation (quantified by summing up all the individual forces from the pillars that the cell is attached to) in the control shRNA- and talin-1 shRNA-treated MEFs (Figure 14A-C). We found that talin-1 shRNA-treated MEFs had significant spreading and traction force generation defects compared to the control shRNA-treated MEFs (Figure 14A-D). These observations are consistent with previous reports describing the effects of talin depletion on cell behavior [134].

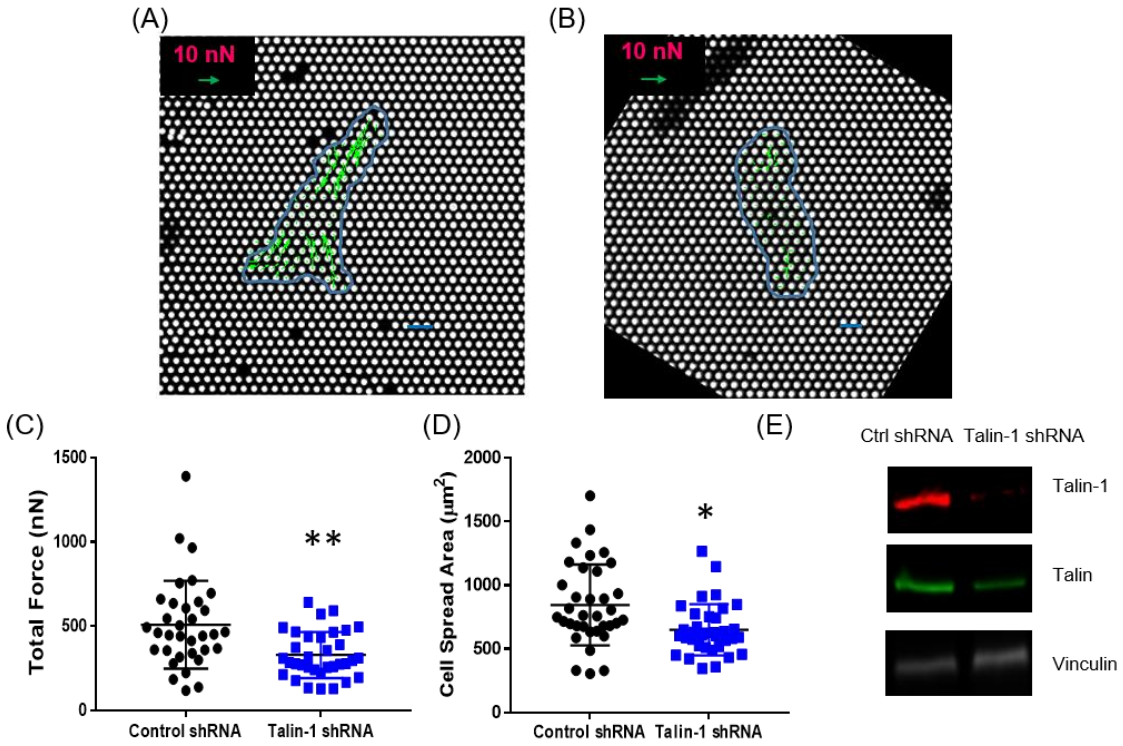

Figure 14: Talin promotes cell spreading and traction force generation. (A, B) Cells treated with ctrl shRNA (A) and talin-1 shRNA (B) spread on mPADs (posts labeled white) showing force vectors (green) and spreading (blue outline). Scale bar 10 μm. (C) Comparison of total force generation between scrambled shRNA treated and talin-1 shRNA treated cells. ** $P < 0.001$. (D) Effects of talin-1 depletion on cell spreading. * P <

0.01 (E) Western blots confirming talin-1 depletion compared to ctrl shRNA treated WT MEFs. Vinculin was used as a loading control.

We noticed significant reductions in average levels of total FAK and pY397-FAK at FAs in talin 1-depleted fibroblasts (Figure 15). Importantly, whereas control shRNA-treated MEFs exhibited linear coupling for force-FAK localization and force-FAK Y397 phosphorylation at individual FAs, this relationship is eliminated in talin-1 shRNA-treated MEFs (Figure 15C, D). Taken together, our data demonstrate that talin-1 is essential for FAK localization and Y397 phosphorylation at FAs as well as force-FAK localization and force-Y397 phosphorylation linear coupling at individual FAs.

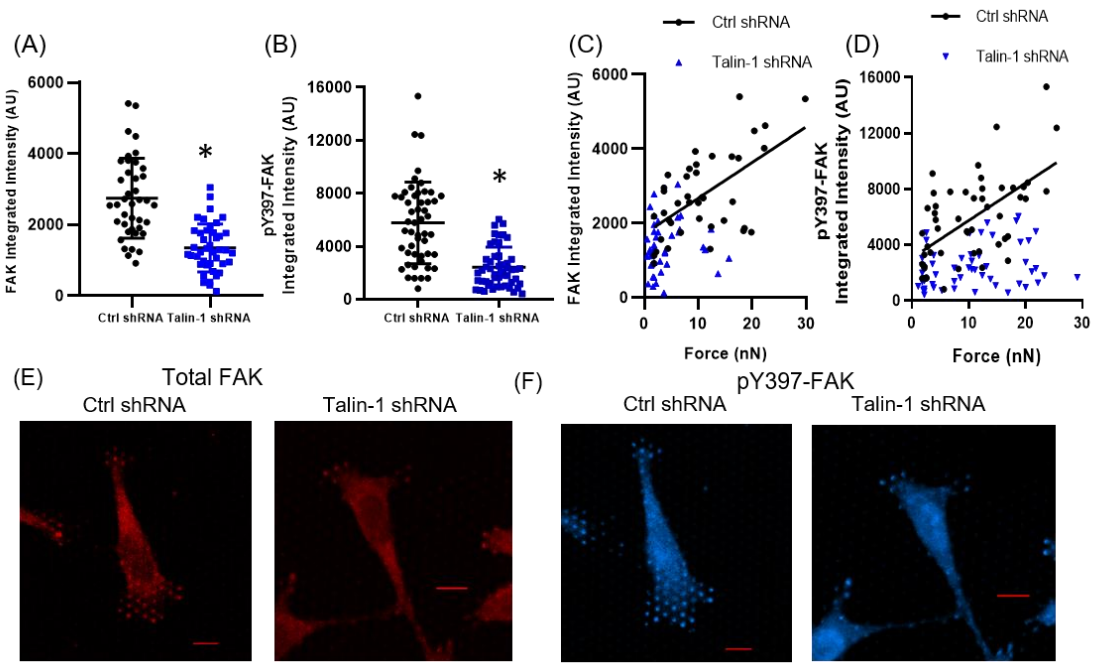

Figure 15: Talin regulates FAK localization and Y397 phosphorylation and force-FAK linear coupling at individual FAs. (A, B) Depletion of talin-1 significantly reduces total FAK and pY397-FAK levels at FAs (* indicates P< 0.001). (C, D) Talin-1 depletion also eliminates coupling between force-FAK localization and force vs. pY397-FAK levels at single FAs. Linear regressions for ctrl shRNA: FAK integrated intensity = 1710 + 96.1*force, $P < 0.001$, $R^2 = 0.35$, n = 41 FAs, 6 cells. pY397-FAK integrated intensity = 3060 + 268*force, $P < 0.001$, $R^2 = 0.35$, n = 51 FAs, 7 cells. Linear regressions for talin-1 shRNA: FAK integrated intensity vs force: $P = 0.61$, n = 42 FAs, 6 cells. pY397-FAK integrated intensity vs force: $P = 0.08$, n = 53 FAs, 7 cells. (E, F) Representative staining of total FAK and pY397-FAK. Scale bar 10 µm.

Vinculin is not necessary for FAK localization and Y397 phosphorylation at FAs, but a full-length vinculin molecule that binds talin and actin is required to maintain linear coupling for force-FAK localization and force-Y397 phosphorylation at FAs.

Because our data indicates that actomyosin contractility-dependent forces are necessary for FAK localization and Y397 phosphorylation at FAs, we next examined the role of vinculin, an important force-transducing protein [3], in regulating FAK localization and Y397 phosphorylation at FAs. To investigate the contributions of vinculin domains to FAK localization and Y397 phosphorylation at FAs, we used cell lines expressing various eGFP-vinculin constructs that were derived from vinculin-null MEFs (Figure 16A) [3]. In addition to WT vinculin and vinculin-null MEFs, we examined several mutants, which were described previously [3]: (i) a vinculin mutant comprising only V_H (1–851) and lacking most of the proline-rich strap and actin-binding tail [129], (ii) a full-length molecule (T12) with mutations along the head–tail interface that reduce head–tail binding affinity by 100-fold and render the molecule in an open conformation that can bind talin and actin [151], and (iii) a full-length variant (A50I) with a head domain mutation that significantly reduces it binding to talin [3, 102]. The A50I mutant has reduced association to FAs due to its talin-binding defect [102].

MEFs expressing mutant and control vinculin were seeded onto 14 kPa mPADs and allowed to attach and spread overnight. On the next day, the cells were fixed and stained for total FAK and pY397-FAK and visualized with confocal microscopy. We first found that forces at FAs were similar between WT, T12, and A50I- vinculin expressing MEFs. Although we previously showed that T12 vinculin-expressing MEFs exhibit higher

levels of spreading and total force generation compared to WT MEFs, we did not characterize spreading and traction force generation in A50I vinculin-expressing MEFs [3]. However, V_H MEFs and vinculin-null MEFs had significant force generation defects compared to WT MEFs, which is consistent with our previously published data [3]. Interestingly, we found that vinculin is not required for FAK localization and Y397 phosphorylation to occur at FAs (Figure 18). In Figure 16, we show that average levels of total FAK and pY397-FAK at individual FAs are equivalent between WT vinculin and vinculin-null MEFs. Furthermore, MEFs expressing V_H and A50I constructs exhibited amounts of FAK and pY397-FAK staining at FAs that were comparable to levels in WT MEFs (Figures 16C, D, 18). However, T12 MEFs had significantly higher amounts of FAK localization and Y397 phosphorylation at FAs compared to WT MEFs (Figure 16C), which is consistent with previous reports showing that T12 vinculin promotes FA enlargement [102]. Taken together, these data demonstrate that averaged levels of FAK and pY397-FAK at FAs are relatively insensitive to vinculin expression. Furthermore, this finding is consistent with previous findings by Reinhart-King and colleagues, where they used Western blotting to show that vinculin depletion does not significantly alter pY397-FAK levels in cells on 2D substrates [174].

We subsequently measured whether vinculin influences the relationship between force and FAK localization and force and Y397 phosphorylation at individual FAs. We observed linear relationships for force and FAK localization and force and Y397 phosphorylation at individual FAs in WT- and T12 vinculin-expressing MEFs (Figure 16). However, these relationships are eliminated in the vinculin-null MEFs or MEFs expressing

A50I or V_H constructs (Figure 16E,F). These results demonstrate that a full-length vinculin molecule that binds talin and actin is required for linear coupling for force-FAK localization and force-Y397 phosphorylation at individual FAs. Although A50I vinculin is a full-length vinculin molecule, its binding defect with talin reduces its ability to localize to FAs, demonstrating that vinculin-talin interactions are required to maintain force-FAK coupling at FAs. Interestingly, we observed that both force-FAK localization and force-FAK Y397 phosphorylation exhibit a linear relationship for T12 vinculin-expressing MEFs (Figure 16), although T12 and WT vinculin had similar slope values in force-FAK localization and force-FAK Y397 phosphorylation linear coupling.

Lastly, we found that T12 and V_H vinculin mutants exhibited greater average vinculin integrated intensity values at FAs compared to WT MEFs (Figure 17A), which is consistent with previously published data [106]. Also, we found that force and vinculin integrated intensity are linearly coupled at single FAs for WT and T12 vinculin-expressing MEFs (Figure 17B,C) although the slopes for these two linear regressions were not significantly different. However, in V_H MEFs, force-vinculin coupling is eliminated, demonstrating that a full-length vinculin molecule that localizes to FA and binds actin is necessary for force-vinculin recruitment coupling at individual FAs (Figure 17D). We were unable to measure force-vinculin coupling in vinculin-null MEFs and MEFs expressing the A50I-vinculin construct, as A50I vinculin signal was very diffuse and challenging to measure at individual FAs and vinculin-null cells do not express vinculin. These data show that force-vinculin recruitment are linearly coupled at FAs, supporting a model where forces applied at FAs enhance vinculin recruitment to support higher traction forces.

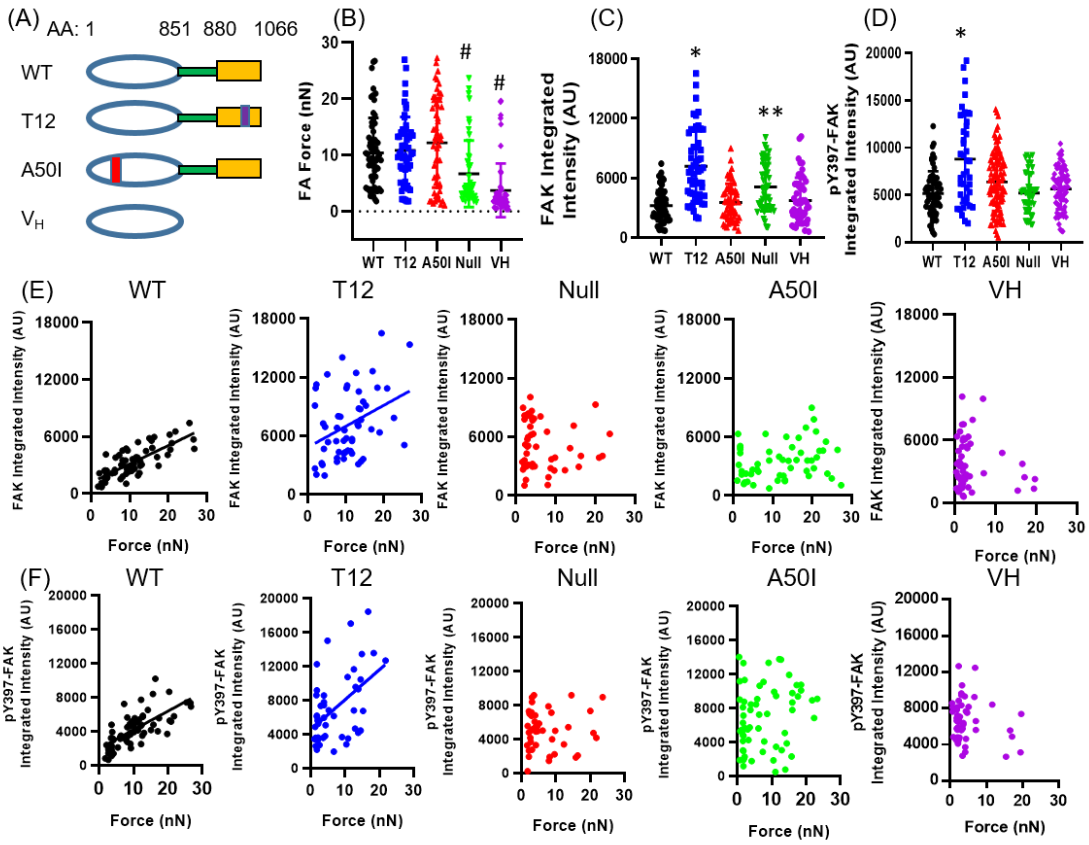

Figure 16: Vinculin mediates force transmission and force-FAK linear coupling at single FAs. Vinculin mediates force transmission and force-FAK coupling at single FAs. (A) Overview of vinculin mutants. (B) Forces at FAs for different vinculin mutants. # indicates $P < 0.01$ vs WT, T12, and A50I. (C) Comparison of pY397-FAK integrated intensity at single FAs between different vinculin mutants on 14 kPa mPADs ($n > 42$ FAs per condition, taken from 7-12 cells per condition). $P < 0.01$ Kruskal-Wallis Test. * indicates $P < 0.01$ vs WT, VH, A50I, and vinculin null MEFs. (D) Comparison of FAK integrated intensity at single FAs between different vinculin mutants on 14 kPa mPADs ($n > 42$ FAs per condition, taken from 7-12 cells per condition). $P < 0.01$ Kruskal-Wallis Test. * indicates $P < 0.01$ vs WT, VH, A50I, and vinculin null MEFs. ** indicates $P < 0.01$ vs WT and A50I vinculin MEFs. (E) Correlation between force and FAK integrated intensity at single FAs from multiple WT cells ($n = 58$ FAs, taken from $n > 8$ different cells). $P < 0.001$, $R^2 = 0.60$. T12 vinculin linear regression: $P < 0.01$, $R^2 = 0.13$. Vinculin null linear regression: $P = 0.71$. A50I linear regression: $P = 0.08$. V_H linear regression: $P = 0.23$. (F) Linear regression for WT vinculin: pY397-FAK Integrated Intensity = 220 x force + 2027, $P < 0.0001$. $R^2 = 0.48$. T12 vinculin linear regression: pY397-FAK Integrated Intensity = 353 x force + 4587, $P < 0.0001$. $R^2 = 0.26$. A50I, VH linear regression: $P = 0.08$, $P = 0.64$ (respectively)

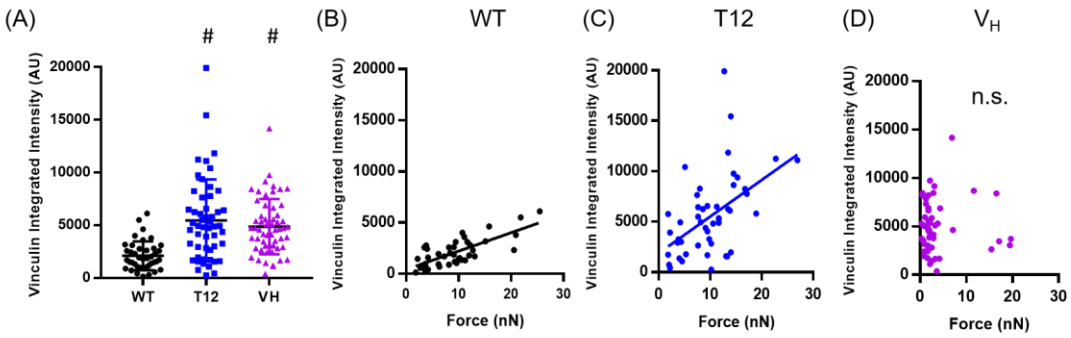

Figure 17: Force and vinculin integrated intensity are linearly coupled at individual FAs on 14 kPa mPADs. (A) Comparison of vinculin integrated intensity at FAs for different mutants. $P < 0.01$ one-way Kruskal-Wallis Test. # indicates $P < 0.01$ vs WT. (B) WT Vinculin Linear Regression: Vinculin Integrated Intensity = 417 + 180*force, $P < 0.001$, $R^2 = 0.56$, n = 40 FAs, 5 cells. (C) T12 Vinculin Linear Regression: Vinculin Integrated Intensity = 1880 + 363*force, $P < 0.001$, $R^2 = 0.24$, n = 49 FAs, 8 cells. (D) VH Linear Regression: $P = 0.84$, n = 57 FAs, 8 cells.

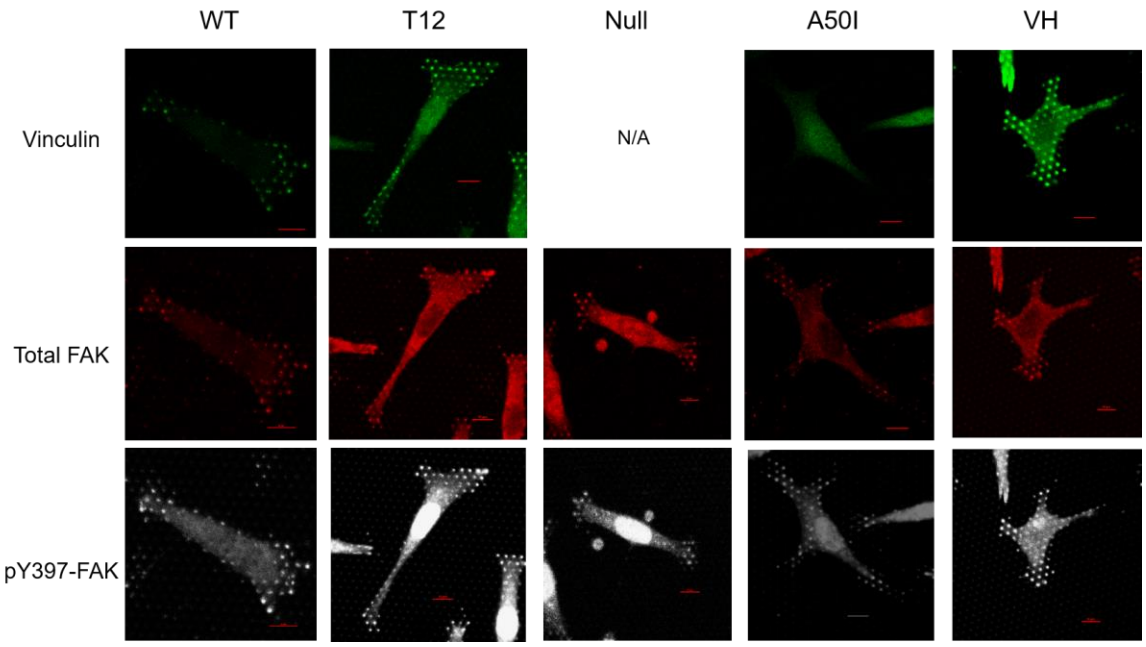

Figure 18: Representative IF Staining of Vinculin Mutants on 14 kPa mPADs. Vinculin (green), total FAK (red) and pY397-FAK (white) staining. Scale bar 10 μm.

Effects of talin-FAK Binding and FAK catalytic function on cell traction force generation

Talin is also known to bind to FAK's E1015 residue [104]. Lawson et al previously demonstrated that the E1015A mutation prevents FAK from binding talin [104]. Moreover, MEFs expressing E1015A-FAK have significantly reduced talin localization to nascent FAs, although talin can still localize to mature FAs [104]. However, it is unknown whether talin-FAK binding influences force generation and force-FAK linear coupling at FAs. We first analyzed whether talin-FAK binding and FAK catalytic function regulate cell traction force generation in MEFs expressing mutated FAK constructs. Although we previously used clonal cell lines with tetracycline-regulated FAK expression [175], we used newer

lines derived from FAK-floxed mice from David Schlaepfer's lab in the present study. We used FAK-null and p53-null MEFs that have been previously transduced with retroviral WT, E1015A, and K454R (kinase dead) GFP-FAK constructs [104, 158]. The p53 deficiency in these cells is necessary, as FAK-null cells are not able to proliferate without p53 depletion [158, 176]. This experimental strategy has several advantages over routine approaches utilizing transient FAK expression or clonal cell lines: (i) the experiments are based on the same cell population, eliminating batch-to-batch variability in transfection and expression levels, (ii) expression of target FAKs in cells lacking endogenous FAK expression avoids confounding effects of endogenous FAK, and (iii) the retroviral system has high transduction efficiencies, resulting in a polyclonal population of engineered cells and avoiding issues associated with clonal lines.

For cells expressing WT, E1015A, and K454R (kinase dead) FAK constructs, we measured their spreading and traction forces from the corresponding micropost deflections on 14 kPa mPADs (Figure 19). The magnitude of traction forces varied significantly across a single cell, where the highest forces were usually located at the periphery (Figure 19A). Figure 19 represents plots for the total traction force per cell, which represents the sum of the magnitudes of force vectors in each cell and is often used for reporting traction forces [169]. FAK-null cells have a significant spreading defect but still generate considerable traction forces (~650 nN), indicating that FAK is dispensable for traction force generation. WT FAK expression increased cell spread area by 64% and total traction force by 80%, indicating that FAK expression promotes cell spreading and traction force generation (Figure 19C-D). Interestingly, E1015A FAK-expressing cells had a ~24% reduction in

traction force generation and ~26% reduction in spreading compared to WT FAK cells, suggesting that FAK-talin interactions contribute to cell traction force generation and spreading (Figure 19C-D). Lastly, we found that WT- and K454R FAK-expressing cells have equivalent levels of traction forces, but K454R FAK expressing cells exhibit a 28% reduction in spread area (Figure 19C-D). This finding is consistent with previous reports analyzing how FAK inhibitors influence cell traction force generation [170]. Taken together, we demonstrate that FAK-talin binding at FAK's E1015 residue promotes higher levels of force generation and spreading, whereas FAK catalytic function has minimal effects on force generation but promotes cell spreading.

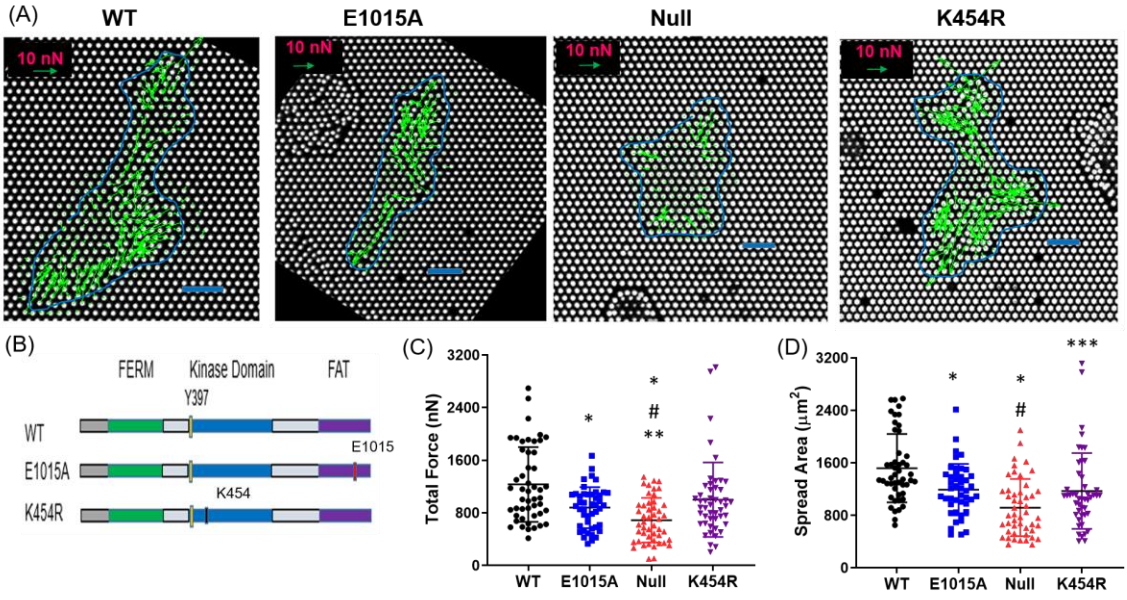

Figure 19: Traction force and spreading measurements for FAK mutants analyzed. (A) Cells spread on mPADs (posts labeled white) showing force vectors (green) and spreading (blue outline). Scale bar 20 μm. (B) Overview of FAK mutants. (C, D) Scatter plots for total traction force and spread area. Total force and spread area for FAK cell lines were measured on micropillar array detectors (mPADs). * indicates $P < 0.05$ compared to WT. # indicates $P < 0.05$ compared to E1015A. ** $P < 0.01$ vs K454R. N = 44-48 cells for each

condition. $P < 0.001$ Kruskal-Wallis for Total Force and $P < 0.001$ one-way ANOVA for cell spread area. *** $P < 0.01$ vs WT.

Talin-FAK binding and FAK catalytic function are required for force-FAK linear coupling at individual FAs.

Because talin-FAK binding promotes traction force generation (Figure 19), we hypothesized that it may also influence linear coupling for force-FAK localization and force-FAK Y397 phosphorylation at individual FAs. We seeded MEFs expressing WT-GFP-FAK, E1015A-GFP-FAK, and K454R-GFP-FAK constructs onto 14 kPa FN-coated mPADs and allowed them to attach and spread overnight. On the next day, we fixed the cells and stained for total FAK and pY397-FAK and visualized FAK and pY397-FAK staining using confocal microscopy. For cells expressing WT GFP-FAK, we found that force and FAK localization and force and Y397 phosphorylation were linearly coupled at individual FAs (Figure 20B). However, this linear relationship was eliminated in the E1015A FAK MEFs (Figure 20C). Furthermore, while force and FAK localization were linearly coupled at FAs for the K454R-FAK MEFs, there was very little pY397-FAK found at the FAs (Figure 20D).

In summary, we found that talin-FAK binding at FAK's E1015 residue are dispensable for maintaining FAK localization and Y397 phosphorylation at FAs, but required for force-FAK coupling at individual FAs (Figure 20). Our data also show that FAK catalytic function is required for pY397-FAK at FAs but not FAK localization to FAs (Figure 20). Furthermore, force-FAK localization linear coupling is independent of FAK

kinase function. This observation supports a model where force promotes FAK localization to the FA and then FAK kinase activity is required for Y397 phosphorylation once FAK localizes to the FA. However, this finding is contrary to our data with the PF-228 FAK kinase inhibitor (Figure 11), which showed that PF-228 eliminates force-FAK localization coupling at FAs. However, PF-228 treatment can lead to multiple off-target effects [171], such as inhibition of CDK1, CDK7, Fyn, and MKK [177], which makes data interpretation from more challenging. In particular, Fyn is known to interact with FAK, so off-target Fyn inhibition can lead to confounding effects on FAK localization to FAs [178]. Consequently, we submit that the data generated from the kinase dead FAK mutant is more reliable than the data generated with PF-228.

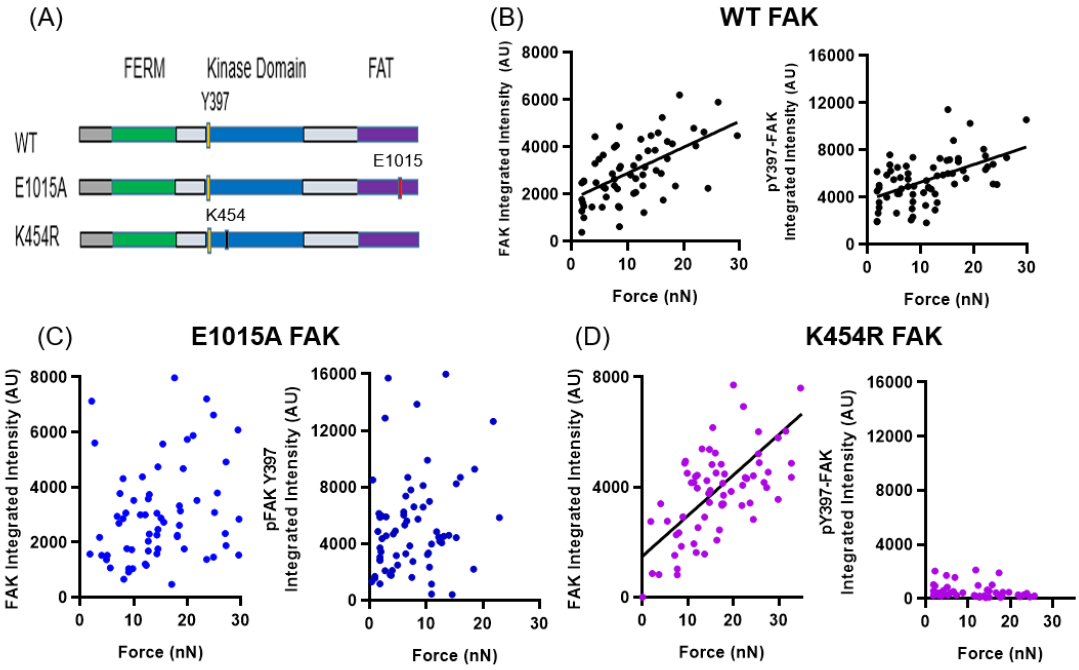

Figure 20: Effects of talin-FAK binding and kinase domain function on force-FAK coupling at single FAs. (A) Overview of FAK mutants analyzed. (B) Linear regression for MEFs expressing WT GFP-FAK variant: Linear regression for WT GFP-FAK: Total FAK Integrated Intensity = 110 x force + 1780, $P < 0.0001$. $R^2 = 0.34$, n = 68 FAs, 10 cells. pY397-FAK Integrated Intensity = 150 x force + 3778, $P < 0.0001$, $R^2 = 0.28$, n = 68 FAs,

10 cells. (C) E1015A GFP-FAK pY397-FAK vs force linear regression: P = 0.09, n = 68 FAs, 7 cells. E1015A GFP-FAK linear regression: P = 0.06, n = 64 FAs, 7 cells. (D) K454R GFP-FAK pY397-FAK vs force linear regression: P = 0.08, n = 47 FAs, 6 cells. K454R GFP-FAK linear regression: Total FAK integrated intensity = 148 x force + 1491, P < 0.0001, R^2 = 0.48, n = 68 FAs, 7 cells.

Vinculin and FAK Kinase Activity Enhance YAP Nuclear Accumulation

So far, we have demonstrated that a full-length vinculin that binds talin and actin is necessary for force-FAK localization and force-Y397 phosphorylation linear coupling at individual FAs. Furthermore, talin is necessary for FAK localization and Y397 phosphorylation at FAs as well as force-FAK linear coupling. Meng et al previously showed that FAK kinase activity is necessary for YAP nuclear accumulation [163]. Since we found that vinculin and talin were necessary for force-FAK linear coupling at FAs, we next examined whether vinculin and talin were necessary for YAP nuclear accumulation. YAP is a transcriptional factor that can localize into the nucleus or cytosol [161, 162]. YAP is sensitive to changes in ECM stiffness, where higher stiffness promotes increased YAP nuclear accumulation [164]. Consequently, it is hypothesized that ECM stiffness signals are transduced from FAs into changes in YAP nuclear accumulation, which ultimately regulates downstream processes, such as cell proliferation and differentiation [123]. We first tested whether FAK kinase activity and actomyosin contractility influenced YAP nuclear accumulation in WT MEFs on 14 kPa mPADs. FAK kinase inhibition with PF-228 or myosin II inhibition with blebbistatin significantly reduced YAP nuclear accumulation compared to control cells (Figure 21), consistent with previous reports [163, 165].

Because vinculin is important for actomyosin-mediated force generation [3] and force-FAK linear coupling at FAs, we next assessed whether vinculin influences YAP

nuclear accumulation. We seeded vinculin-null MEFs expressing WT, T12, A50I, and V_H constructs onto 14 kPa mPADs overnight (Figure 22). On the next day, cells were fixed and stained for YAP, and YAP was visualized via confocal microscopy. To quantify YAP nuclear localization, we separated individual cells with YAP staining into three categories, which has been described previously [163]: $N < C$, less YAP in nucleus than in cytoplasm; $N = C$, similar levels of YAP in cytoplasm and nucleus; $N > C$, more YAP in nucleus than in cytoplasm. We used the Chi-squared test to compare YAP localization distributions among vinculin lines. We found that vinculin is required for YAP nuclear accumulation, as we observed a significant deficiency in nuclear YAP in MEFs expressing the V_H vinculin construct and vinculin-null MEFs (Figure 22).

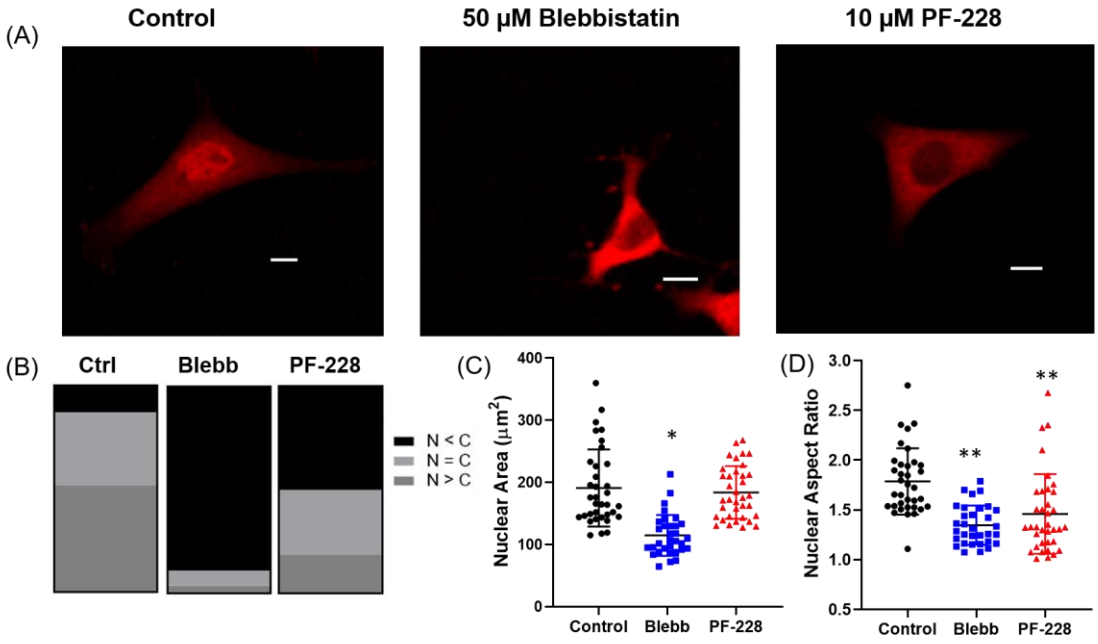

Figure 21: Effects of blebbistatin and PF-228 on YAP nuclear accumulation. (A) Representative YAP staining for MEFs. Scale bar 10 μm. (B) Quantification of YAP localization in MEF cells. $N < C$, less YAP in nucleus than in cytoplasm; $N = C$, similar levels of YAP in cytoplasm and nucleus; $N > C$, more YAP in nucleus than in cytoplasm.

Chi-Squared Test: $P < 0.001$ Ctrl vs Blebbistatin and Ctrl vs. PF-228. $N = 25\text{-}33$ cells per condition. (C) Nuclear size comparison between different groups. $P < 0.001$ Kruskal-Wallis Test. * indicates $P < 0.001$ vs control and PF-228. (D) Nuclear aspect ratio between different groups. $P < 0.01$ Kruskal-Wallis Test. ** indicates $P < 0.01$ vs control.

We also measured YAP nuclear localization in A50I vinculin-expressing MEFs. Although A50I MEFs had higher levels of nuclear YAP than vinculin-null MEFs, A50I vinculin-expressing MEFs still had significantly less nuclear YAP than WT vinculin-expressing MEFs (Figure 22B). We also examined whether vinculin auto-inhibition influenced YAP nuclear accumulation. In the T12 vinculin -expressing MEFs, we observed similar levels of nuclear YAP compared to WT MEFs (Figure 22B), suggesting that further increases in vinculin activity and vinculin-dependent force generation do not necessarily lead to further increases in nuclear YAP. Taken together, our data support a model where a full-length vinculin molecule that binds talin and actin is necessary to promote YAP nuclear accumulation. Lastly, consistent with previous reports [134], we found that talin-1 depletion led to significantly reduced YAP nuclear localization compared to MEFs treated with control shRNA lentiviral particles (Figure 22C-D), showing that talin-1 is essential for YAP nuclear localization.

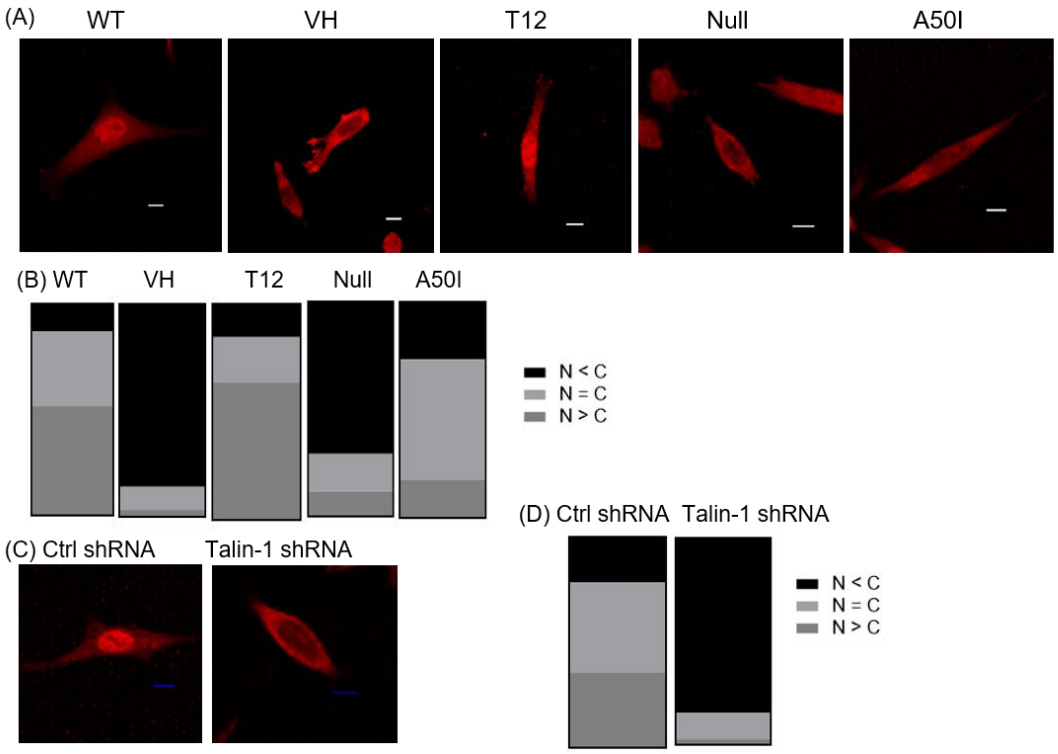

Figure 22: Vinculin and talin regulate YAP nuclear accumulation. (A) Representative YAP staining for MEFs expressing various vinculins and vinculin null MEFs. Scale bar 10 μm. (B) Quantification of YAP localization in MEF cells. *N* < C, less YAP in nucleus than in cytoplasm; *N* = C, similar levels of YAP in cytoplasm and nucleus; *N* > C, more YAP in nucleus than in cytoplasm. Chi-Squared Test: P < 0.01 for WT vs null, VH, and A50I. P < 0.01 for A50I vs null. (C) Representative YAP staining for MEFs treated with control scrambled shRNA and talin-1 shRNA lentiviral constructs. (D) Quantification of YAP localization (same categories as panel B) Chi-Squared Test: P < 0.001 vs ctrl shRNA vs talin-1 shRNA. N = 25-34 cells.

Recent work by Roca-Cusachs and colleagues suggests that forces transmitted from integrin-ECM linkages can lead to nuclear elongation, nuclear pore deformation, and subsequent YAP entry into the nucleus via nuclear-cytoskeletal mechanical coupling [166]. We first measured nuclear size and elongation for WT MEFs treated with blebbistatin and PF-228 (Figure 21), as both inhibitors led to significant decreases in nuclear YAP (Figure 21). Blebbistatin treatment significantly reduced nuclear size, elongation, and YAP nuclear accumulation (Figure 21), which is consistent with Roca-Cusach's model [166]. PF-228

treatment significantly reduced nuclear elongation and YAP nuclear localization but had no significant effects on nuclear size (Figure 20). This observation suggests that FAK kinase activity could promote increased nuclear YAP by increasing nuclear elongation. However, FAK kinase activity is not required for promoting force generation (Figures 12 and 18), which was an important aspect of Roca-Cusach's model, where force generation and nuclear-cytoskeletal mechanical coupling lead to nuclear elongation and pore deformation. Additional studies measuring nuclear transport dynamics and nuclear-cytoskeletal coupling in the presence or absence of FAK inhibitors are needed to assess whether FAK kinase activity alters nuclear morphology to regulate YAP nuclear accumulation. Lastly, recent studies have elegantly shown how FAK kinase activity leads to decreases in RAP2 activity to promote increased nuclear YAP and provide a compelling explanation for FAK kinase activity's effects on YAP nuclear accumulation [163].

To assess whether vinculin affects nuclear morphology, we measured nuclear size and aspect ratio in MEFs expressing the WT, A50I, T12, and V_H constructs and vinculin-null MEFs. We found that there were no significant differences in nuclear aspect ratio between the different vinculin mutants analyzed (Figure 23). Although vinculin is a critical mediator of force transmission (Figure 16), the nuclei for each of the vinculin mutants exhibited similar values of aspect ratio, which is an important component of Roca-Cusach's model [166]. Furthermore, we were unable to correlate changes in nuclear size towards changes in nuclear YAP levels (Figure 23). In particular, V_H MEFs have the largest nuclei of the different cells analyzed (Figure 23) yet exhibit very low levels of nuclear YAP

(Figure 22). Taken together, our data suggest that vinculin mediates YAP nuclear accumulation independently of changes in nuclear size or elongation.

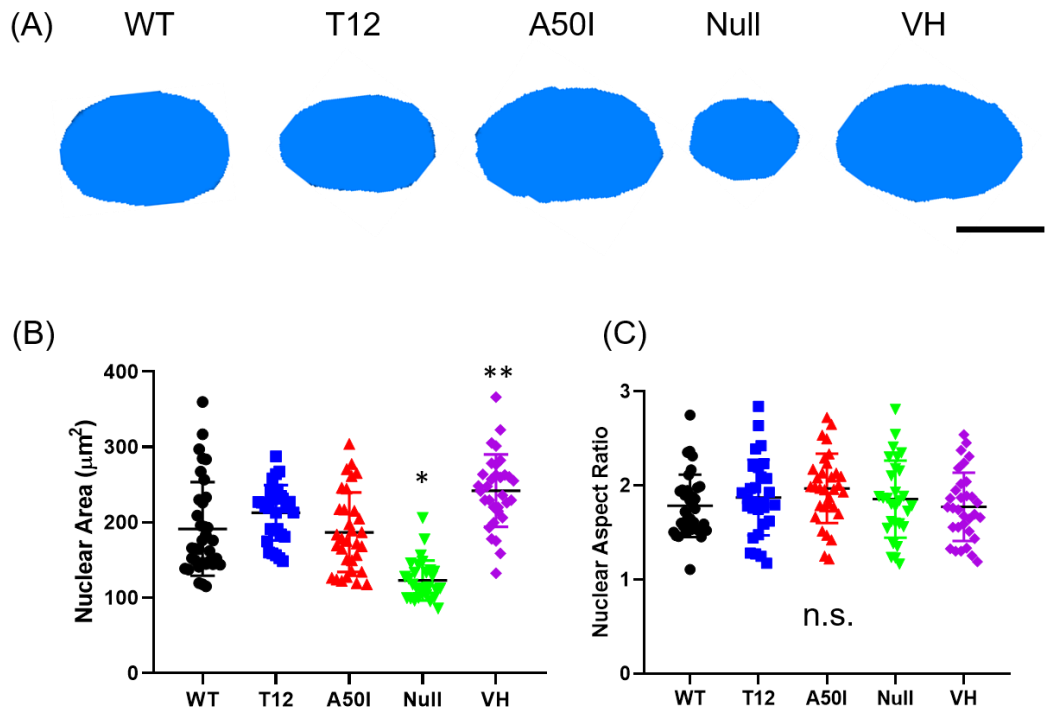

Figure 23: Nuclear Morphology of Vinculin Mutants. (A) Representative DAPI staining for vinculin mutants. Scale bar 10 μm. (B) Nuclear size of vinculin mutants. $P < 0.01$ Kruskal-Wallis Test. * indicates $P < 0.01$ vs WT, T12, and A50I. ** indicates $P < 0.01$ vs WT, A50I, and null. (C) Nuclear aspect ratios of vinculin mutants. $P = 0.22$ one-way ANOVA.

Recently, Meng et al proposed a model where increased ECM stiffness leads to decreased RAP2 activity, which in turn enhances YAP nuclear accumulation [163]. On 40 kPa hydrogels, RAP2 activity was significantly reduced compared to 1 kPa hydrogels, which in turn led to increased YAP nuclear accumulation compared to 1 kPa hydrogels

[163]. Their model suggests that RAP2 is a critical mediator in transducing ECM stiffness signals towards changes in YAP nuclear localization. Specifically, they proposed the following sequence of biochemical events from focal adhesions to changes in Lats activity, which mediate YAP nuclear accumulation:

Increased substrate stiffness → increased FA assembly→ increased PLCγ1 activity→ decreased PtdIns(4,5)P2 levels → decreased phosphatidic acid (PA) → decreased PDZGEF → decreased active RAP2 → decreased LATS → increased nuclear YAP.

Hanks and colleagues previously showed that FAK Y397 phosphorylation upregulates PLCγ1 activity [179]. Furthermore, RAP2 activity is hypothesized to function downstream of FAK and PLC to regulate YAP nuclear localization [163]. From this model, we hypothesize that a full-length vinculin molecule that binds talin and actin increases PLCγ1 activity to decrease RAP2 activity, which in turn enhances YAP nuclear accumulation.

To test this model, we began by inhibiting RAP2 activity in WT, A50I vinculin MEFs and vinculin-null MEFs. Although there are no commercial RAP2 inhibitors available, Meng et al demonstrated that BML-279, which is a phospholipase-D1/D2 (PL-D1/2) inhibitor, inhibits RAP2 activity to promote YAP nuclear accumulation on soft 1 kPa substrates [163]. Subsequently, we characterized whether BML-279 influences nuclear YAP levels in MEFs expressing WT and A50I vinculin and vinculin-null MEFs. We observed that on 14 kPa mPADs, BML-279 treatment (10 μM, overnight) had minimal effects on YAP nuclear accumulation in WT Vinculin MEFs (Figure 24). However, BML-

279 significantly increased nuclear YAP levels in vinculin-null and A50I MEFs on 14 kPa mPADs (Figure 24), demonstrating that PL-D1/2 and RAP2 activity may significantly influence YAP nuclear localization. These data suggest that vinculin regulates PL-D1/2 and RAP2 activity to influence YAP nuclear accumulation. However, more experimental analyses, such as measurement of PLCγ1 and RAP2 activity within different vinculin mutants, must be performed to confirm whether this is indeed the case.

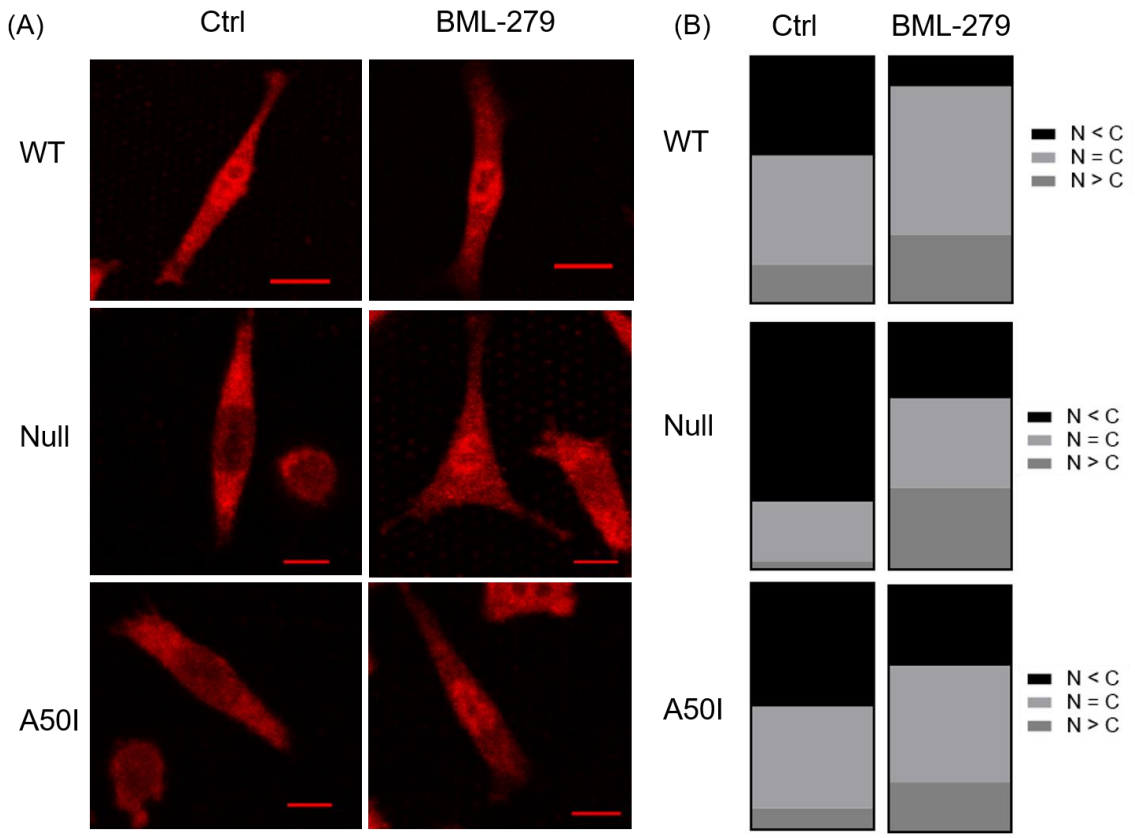

Figure 24: Effects of BML-279 on YAP nuclear accumulation for cells on 14 kPa mPADs. (A) Representative YAP staining for MEFs treated with either BML-279 (10 μM overnight) or vehicle (DMSO) overnight. Scale bar 20 μm. (B) Quantification of YAP localization in MEF cells. *N* < C, less YAP in nucleus than in cytoplasm; *N* = C, similar levels of YAP in cytoplasm and nucleus; *N* > C, more YAP in nucleus than in cytoplasm. Chi-Squared Test: P < 0.001 ctrl vs BML-279 for A50I vinculin and vinculin-null MEFs. P = 0.27 ctrl vs BML-279 for WT MEFs. N = 25-35 cells analyzed per condition.

4.5 Discussion

How force regulates FA signaling, such as FAK Y397 phosphorylation and YAP nuclear localization, is poorly understood at the individual FA level. We first examined the relationship between traction force and FAK localization and force and Y397-FAK phosphorylation at individual FAs in the context of substrate stiffness, actomyosin contractility, and FAK kinase function. On 14 kPa mPADs, we observed a linear coupling for both force and FAK localization and force and Y397-FAK phosphorylation at individual FAs. In addition, our data demonstrate that FAK recruitment and Y397 phosphorylation are coupled, as the pY397-FAK/total FAK ratio was relatively constant under different values of applied force at individual FAs on 14 kPa mPADs. On 5 kPa mPADs, FAK localization and Y397 phosphorylation at FAs can still occur, although force-FAK linear coupling is eliminated. We also found that FAK kinase inhibition with PF-228 or contractility inhibition with Y-27632 reduces FAK localization and Y397 phosphorylation and eliminates force-FAK coupling at FAs on 14 kPa mPADs. However, as described previously, PF-228 can have off-target inhibition effects, which makes data interpretation more challenging [171]. Consequently, this motivated us to use MEFs expressing a kinase dead FAK variant in later studies, where we found that FAK's kinase activity is not required for force-FAK localization coupling at FAs. Taken together, these data support a model where on stiff substrates, actomyosin contractility-dependent forces applied at FAs promote FAK localization, and Y397 is then phosphorylated upon FAK localization to the FA. Furthermore, perturbation of the integrin-ECM and cytoskeletal

force balance via contractility inhibition or talin-1 depletion reduces FAK localization and Y397 phosphorylation at FAs.

During these studies, the use of mPADs as our experimental platform is advantageous, as it decouples changes in substrate stiffness from changes in the microscopic material properties that could affect ligand binding and cell responses [47, 169]. In addition, the force measured at each post is independent of nearby FAs [47]. Furthermore, our approach has the advantage of assessing local forces at individual FA sites, whereas previous analyses have focused on averaged or population-level measurements (e.g. Western blotting, IF staining) of FAK Y397 phosphorylation [115, 180]. These routine analyses may not capture important relationships at the cell-material interface due to the heterogeneity of individual FAs in terms of force and composition. In particular, by analyzing force and FAK levels at single FAs, we were able to demonstrate that force and FAK localization-Y397 phosphorylation are coupled at individual FAs. However, direct force application to FAs and measurement of FAK localization and Y397 phosphorylation are still needed to fully validate this model. FAK's binding partners, such as talin, paxillin, and Src, could also provide indirect mechanisms for its force-regulated recruitment and Y397 phosphorylation. Lastly, force-dependent FAK recruitment and Y397 phosphorylation at individual FAs represents another mechanism that complements mechanosensitive pathways at FAs, such as integrin–FN binding [42] and talin stretching to expose cryptic binding sites for other FA proteins, such as vinculin, to promote force transmission and FA growth [111].

We next examined whether vinculin influences force-FAK localization and force-FAK Y397 phosphorylation linear coupling at FAs. Although vinculin is not required for FAK localization and Y397 phosphorylation to occur at FAs, a full-length vinculin molecule that binds to talin and actin is required to couple force-FAK localization and force-FAK Y397 phosphorylation at FAs. Consequently, we hypothesize that vinculin is responsible for regulating signaling events at FAs and "fine-tuning" cell FA assembly by modulating force-FAK linear coupling at individual FAs. We also observed that WT vinculin MEFs have comparable levels of FAK localization and Y397 phosphorylation at FAs to vinculin-null MEFs. Previously, we demonstrated that vinculin-null MEFs still generated significant amount of traction forces, although WT vinculin expression was necessary to enhance force transmission [3]. Consequently, the forces transmitted by integrin-talin-actin linkages in vinculin-null cells may still be sufficient to allow for FAK localization and Y397 phosphorylation to occur at FAs. However, a full-length vinculin molecule that binds talin and actin is necessary to linearly couple force-FAK localization and force-FAK Y397 phosphorylation at individual FAs. Furthermore, our finding that a full-length vinculin that binds talin and actin enhances force-FAK coupling at FAs, but V_H and A50I vinculin completely disrupts this coupling indicates that vinculin is a key regulator of mechanotransduction and demonstrates a unique and previously unknown function for vinculin in cell mechanosensing.

Similar to vinculin, talin is important for regulating FA growth and force transmission [134]. However, talin's effects on FA signaling remain unclear. We demonstrated that talin is required for FAK localization and Y397 phosphorylation and

mediates force-FAK linear coupling at individual FAs via talin-FAK binding. We also demonstrated with a kinase dead FAK mutant that FAK's kinase function is not required for force-FAK localization linear coupling at FAs, although FAK's kinase function is essential for Y397 phosphorylation. Lastly, FAK kinase activity, actomyosin contractility, talin, and vinculin are critical for enhancing YAP nuclear accumulation, where a full-length vinculin molecule that binds talin and actin is necessary to promote YAP nuclear accumulation.

From these data, we propose a sequential model where talin- and actomyosin contractility-dependent forces promote FAK localization to FAs, where FAK Y397 phosphorylation then occurs. Talin mediates force-FAK linear coupling at individual FAs via talin-FAK binding at FAK's E1015 residue. Talin, vinculin, actomyosin contractility, and pY397-FAK promote YAP nuclear accumulation. As FA growth occurs, a FAK-talin-vinculin complex is necessary to linearly couple force generation and continued FAK recruitment and Y397 phosphorylation at individual FAs, whereas an integrin-talin-vinculin complex, FAK kinase activity, and contractility are required to enhance YAP nuclear accumulation. From this model, we stipulate that talin-FAK interactions are responsible for "tuning" cell FA assembly, by coupling force-FAK localization and force-FAK Y397 phosphorylation at FAs. This idea is further supported by data showing that MEFs expressing the GFP-E1015A-FAK construct have reduced migration speed, impaired proteolytic cleavage of talin to drive cell migration, and increased paxillin residence time at FAs compared to MEFs expressing GFP-WT-FAK [104]. Interestingly, our data is contrary to observations from Lawson et al, where the authors knocked out talin-

1 in human umbilical vein endothelial cells (talin-1 is presumed to be the only isoform expressed in these cells) and demonstrated that talin-1 is not necessary for FAK recruitment to FA sites [104]. However, these measurements were performed on cells seeded at early timepoints (15 minutes) on nascent FAs, whereas our analyses involve an overnight (16 hour+) timepoint, where the cells are at a quasi-equilibrium state. Consequently, this time-point difference may lead to differing findings.

Conceptual Model:

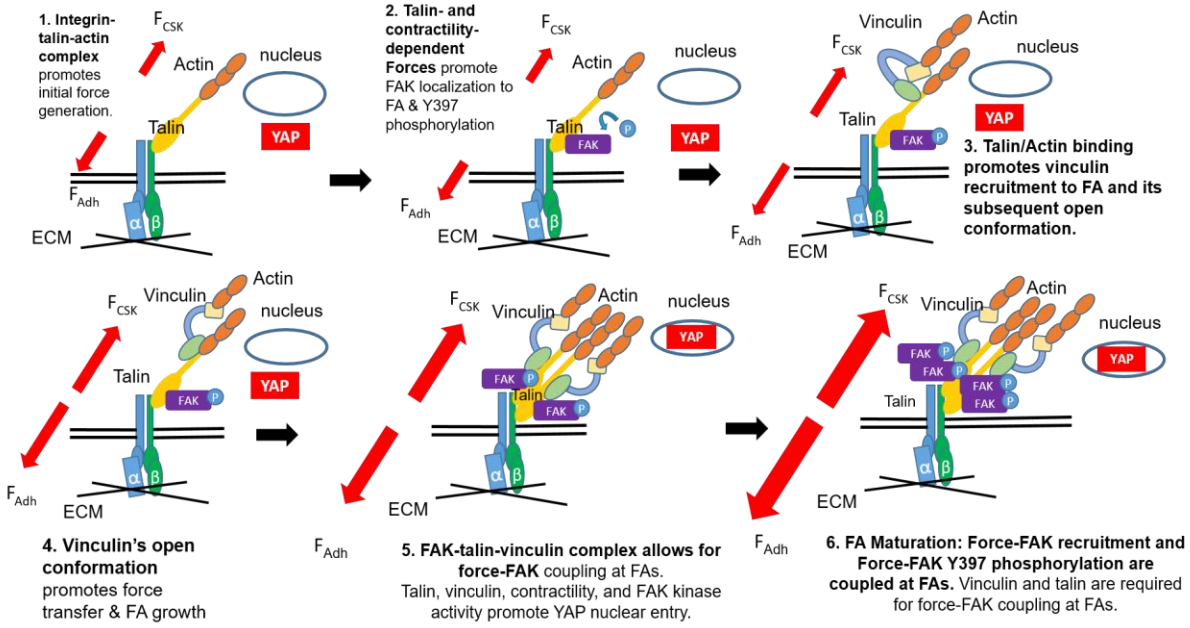

Figure 25: Conceptual Model. Talin and contractility dependent forces promote initial FAK localization to FAs, where Y397 phosphorylation then occurs. Talin, vinculin, contractility, and pY397-FAK promote YAP nuclear accumulation. As FA growth occurs, a FAK-talin-vinculin complex is necessary to couple force generation and continued FAK recruitment and Y397 phosphorylation at individual FAs, whereas an integrin-talin-vinculin complex, FAK kinase activity, and contractility are essential for YAP nuclear accumulation. Lastly, talin mediates force-FAK coupling at individual FAs via talin-FAK binding. Although vinculin is not required for FAK localization and Y397 phosphorylation at FAs, a full-length vinculin that binds talin and actin is required to linearly couple force-FAK localization and force-FAK Y397 phosphorylation at FAs and promote YAP nuclear accumulation.

Lastly, vinculin-null MEFs exhibit large amounts of FAK localization and Y397 phosphorylation at FAs but significant YAP nuclear localization defects, suggesting that FAK requires vinculin to enhance YAP nuclear accumulation. Furthermore, we showed that vinculin modulates YAP nuclear accumulation via mechanisms that are independent of changes in nuclear size and elongation (Figure 20). Recently, Meng et al proposed a model where increases in substrate stiffness decrease RAP2 activity to increase YAP

nuclear accumulation [163]. Since increases in substrate stiffness promote vinculin recruitment to FAs [137], we hypothesize that vinculin recruitment to FAs may decrease RAP2 activity to enhance YAP nuclear accumulation. We have preliminary data with the BML-279 small-molecule inhibitor that suggest vinculin may regulate PL-D1/2 and RAP2 activity to control YAP nuclear accumulation. However, additional studies, such as measurement of PLCγ1 and RAP2 activity within different vinculin mutants, are necessary to confirm this hypothesis.

The improved understanding of vinculin's contributions to FAK localization, Y397 phosphorylation, and YAP nuclear accumulation provided by this work has several implications. First, talin, but not vinculin, is essential for promoting FAK localization and Y397 phosphorylation at FAs. Second, vinculin regulates force-FAK localization and force-FAK Y397 phosphorylation coupling via vinculin-talin binding, and a FAK-talin-vinculin complex is required to linearly couple force-FAK localization and force-FAK Y397 phosphorylation at individual FAs. As such, vinculin likely provides "fine tuning" control required for coordinated processes like cell spreading and FA assembly. Third, talin and vinculin mediate YAP nuclear accumulation, where a full-length vinculin molecule that binds talin via V_H and actin via V_T is required for YAP nuclear accumulation. Finally, force-based regulation of FAK localization and Y397 phosphorylation at FAs provides a mechanism to generate local mechanosensitive responses at FAs, such as force-dependent FA growth [141] and coordinated FA assembly at the cell's leading edge and disassembly at the trailing edge. Collectively, this work provides these important insights into how vinculin's structure and binding partners

interact with actomyosin contractility to promote YAP nuclear accumulation and force coupling with FAK localization and Y397 phosphorylation at individual FAs. Lastly, this research will provide a new framework to understand cell-ECM events, such as FA assembly during cell migration, force-regulated morphogenesis, and stem cell lineage commitment in response to ECM matrix, as well as fundamental principles to design mechanoresponses in cell-biomaterial interactions.

CHAPTER 5. FUTURE CONSIDERATIONS.

Overall, this thesis sheds new light on the relationship between force and FA dynamics and signaling. The relationship between force and FA activity remains complex and is regulated by a myriad of factors, such as substrate stiffness, actomyosin contractility, and FA protein binding partners [181]. In aim 1, we demonstrated that vinculin residence and force are linearly related on stiff substrates, although this relationship is eliminated on soft substrates. Furthermore, we showed that paxillin localization and residence time and FAs is independent of force at single FAs. Lastly, we demonstrated how vinculin and paxillin residence times were relatively insensitive to substrate stiffness and contractility. Interestingly, substrate stiffness and contractility mediated the relationship between vinculin and paxillin residence times at single FAs, where vinculin and paxillin residence times are linearly related on soft substrates or after contractility inhibition, but this linear relationship is eliminated on stiff substrates. Overall, these analyses yield valuable insights on how local forces at FAs and macroscopic force regulators (e.g. substrate stiffness, contractility) can influence FA residence time, which is important in determining processes, such as cell migration and spreading [133]. In aim 1, it would be valuable to consider other FA proteins, such as talin or zyxin, and whether their residence times are related to force at individual FAs. Although others have examined how these proteins influence force transmission [134, 182], it is unclear whether forces influence their residence time at FAs. Furthermore, there is significant attention towards understanding cell mechanobiology in 3D contexts and it would be valuable to assess FA turnover

dynamics within 3D in future work. However, these studies are complicated by the challenge of visualizing FAs and quantifying forces in 3D matrices. However, as 3D imaging and traction force microscopy approaches improve, these valuable studies will become more feasible with time.

In aim 2, we demonstrated that a full-length vinculin that binds talin and actin is required for YAP nuclear accumulation and force-FAK localization and force-FAK Y397 phosphorylation linear coupling while talin is essential for FAK localization and Y397 phosphorylation at FAs. Furthermore, our model suggests that a FAK-talin-vinculin complex is required to couple force-FAK at single FAs, while an integrin-talin-vinculin complex is required to promote YAP nuclear accumulation. Although we've analyzed how FA proteins, such as vinculin and FAK, are related to force, there are many other proteins that localize to FAs. Indeed, reports estimate that there are hundreds of different proteins that are recruited to FA complexes [2]. There are other important force-transducing proteins at FAs, such as zyxin [182], that remain poorly understood. Furthermore, there are multiple signaling proteins at FAs, such as Src, p130Cas, and Lyn, whose relationship to force remain poorly characterized. Waterman and colleagues have performed mass-spectroscopy analyses of FA complexes in the presence and absence of contractility modulators, such as blebbistatin [183]. These analyses have yielded valuable insights on how actomyosin contractility regulate FA composition and which FA components are myosin II responsive [183]. However, these population-level or "averaged" measurements fail to capture local effects of applied force at the individual FA level. Consequently, the process by which local forces can be transduced into multi-variate signaling responses and

composition changes at the individual FA level remain an important question within the mechanobiology field.

Although 2D environments are relevant for certain cell types (e.g. epithelial cells, endothelial cells), many cells in the human body are encapsulated within a 3-dimensional (3D) ECM. Consequently, there is significant interest in performing FA dynamics studies in 3D instead of 2D. Furthermore, there is growing evidence that cells have significantly different adhesive and migration activity in 3D [74]. For instance, cells in 3D are hypothesized to migrate through protrusive extensions and protease activity to degrade ECM proteins [74]. Furthermore, FAs are often significantly harder to image and tend to appear more diffuse in 3D [74]. Interestingly, vinculin has been shown to differentially regulate FAK activity within 2D and 3D [174]. Reinhart-King and colleagues demonstrated that vinculin depletion doesn't affect FAK Y397 phosphorylation in 2D substrates but significantly reduces FAK Y397 phosphorylation levels in 3D [174]. Due to imaging challenges, however, and the low-throughput nature of 3D traction force measurements, many groups have not been able to assess whether force and signaling are coupled at single FAs in 3D culture. However, as imaging technologies improve and 3D traction force measurements become more feasible, there is immense promise for obtaining an improved understanding of cell mechanobiology within 3D contexts. Furthermore, there is a growing interest in mechanomedicine, where researchers seek to analyze how forces play a role in cell disease states [184]. Consequently, understanding how the mechanics of the 3D environment affect cellular drug responses or disease processes will be critical for future

mechanobiology research and efforts to translate mechanobiology discoveries into the clinic.

In aim 2, we found that vinculin is required for YAP nuclear accumulation, where a full-length vinculin molecule that binds talin and actin is necessary to maintain YAP nuclear accumulation. Similarly, FAK kinase activity and actomyosin contractility are required to maintain YAP nuclear accumulation. Although we've demonstrated that vinculin is required for YAP nuclear accumulation, it remains unclear how YAP is localized into the nucleus. Interestingly, vinculin-null cells display large amounts of FAK localization and Y397 phosphorylation at FAs, suggesting that FAK kinase activity by itself is not sufficient to maintain YAP nuclear accumulation but instead requires a full-length vinculin that binds talin and actin to promote YAP nuclear accumulation. We also tested elements of a biophysical model proposed by Roca-Cusachs and colleagues, where forces transmitted at FAs lead to nuclear deformation and elongation to allow transcriptional factors to enter the nucleus [166]. However, we failed to observe any significant differences in nuclear elongation between the different vinculin mutants (WT, T12, null, A50I, V_H) on the mPADs. Furthermore, the differences in nuclear size did not correlate with differences in YAP nuclear accumulation, suggesting that vinculin controls YAP nuclear localization via mechanisms that are independent of nuclear morphology modulation. Other groups have proposed biochemical models, where intracellular signaling decisions regulate YAP nuclear localization [163]. With this model, perhaps the loss of a full-length vinculin molecule leads to aberrant signaling dynamics, which in turn alters YAP nuclear accumulation. However, the molecular mechanisms that drive YAP

nuclear accumulation remain poorly understood. Although it's accepted that the Hippo pathway and Lats 1/2 are important mediators of YAP nuclear localization, it remains unclear how adhesive signals are transduced into eventual changes in YAP nuclear accumulation. Recently, Meng et al proposed an intriguing model, where changes in ECM stiffness are transduced into changes in RAP2 activity, which consequently regulates Lats1/2 activity and YAP nuclear accumulation. In particular, the authors demonstrated that high matrix stiffness leads to reduced RAP2 activity and increased YAP nuclear accumulation. In contrast, cells cultured on softer substrates displayed significantly higher RAP2 activity and reduced YAP nuclear accumulation. Consequently, these data motivate us to analyze whether vinculin regulates RAP2 activity. In particular, it is well-established that stiffness is an important of vinculin recruitment to FAs. Therefore, it is possible that changes in stiffness control vinculin localization to FAs, which in turn regulates RAP2 activity and YAP nuclear localization. Although we intend to explore this question in our future studies by measuring RAP2 activity in MEFs expressing various vinculin constructs (e.g. WT, A50I, vinculin-null), these studies remain challenging to pursue. The biochemical pathways that drive YAP nuclear localization remains poorly characterized and a more comprehensive and systems-focused analysis of the signaling pathways that regulate YAP nuclear dynamics will be critical towards understanding how ECM signals and FA composition changes are transduced into YAP nuclear accumulation changes.

Lastly, although we demonstrate an intriguing relationship between force and FAK recruitment and Y397 phosphorylation in aim 2, it remains unclear whether force-FAK linear coupling at single FAs exists for other cells types and whether vinculin and talin are

critical for maintaining force-FAK coupling in these other cell types. We've begun preliminary studies to assess whether force-FAK are coupled in human mesenchymal stem cells (hMSCs), which have important functions in regenerative medicine applications. Furthermore, there are other cell types where force-signaling coupling at FAs remain an important question. For instance, cancer cells are hypothesized to utilize FAK to increase proliferation and migration. Our model would predict that local forces at FAs generated by talin and vinculin would promote FAK recruitment and Y397 phosphorylation at FAs, to enhance migration speed and cell survival. In all, this thesis paves the way for exciting future studies on how forces are transduced into biochemical signals at the single FA level. In these studies, we dissected the roles of FAK, YAP, and vinculin in cellular mechanosensing. Furthermore, our research has generated new insights into how FAs sense force and how forces at individual FAs are transduced into biochemical and nuclear signals. Moreover, we expect that our analyses will shed new insights and provide a framework for processes, such as cell migration, spreading, and single FA dynamics. Lastly, this research will provide a new framework to understand cell-ECM events, such as FA assembly during cell migration, force-regulated morphogenesis, and stem cell lineage commitment in response to ECM matrix, as well as fundamental principles to design mechanoresponses in cell-biomaterial interactions.

APPENDIX

A. VITA

Dennis W. Zhou

EDUCATION

Ph.D. Georgia Institute of Technology May 2019 (anticipated)

Bioengineering / Biomedical Engineering; GPA: 4.00/4.00

B.S. Cornell University August 2010 - January 2013

Biological Engineering, *Summa Cum Laude*; GPA: 4.09/4.30

JOURNAL PUBLICATIONS

1. Navarro-Requena C, Weaver JD, Clark AY, Clift DA, Pérez-Amodio S, Castaño Ó, Zhou DW, García AJ, Engel E. PEG hydrogel containing calcium-releasing particles and mesenchymal stromal cells promote vessel maturation. Acta Biomater. 2018 Feb;67:53-65. doi: 10.1016/j.actbio.2017.12.009. Epub 2017 Dec 13. PubMed PMID:29246650.
2. Zhou DW, Lee TT, Weng S, Fu J, and Garcia AJ. Effects of Substrate Stiffness and Actomyosin Contractility on Coupling Between Vinculin-Paxillin Recruitment and Force at Single Focal Adhesions. (2017). *Molecular Biology of the Cell. Special Edition: Forces On and Within cells.* 28:1901–1911. doi:10.1091/mbc.E17-02-0116
3. Fernandez I, Martin-Garrido A, Zhou DW, Clempus RE, Seidel-Rogol B, Lassegue B, Garcia AJ, Griendling KK, and San Martin A. (2015). Hic-5 mediates TGF-β-induced adhesion in vascular smooth muscles cells by a Nox4-dependent mechanism. *Arteriosclerosis, Thrombosis, and Vascular Biology (ATVB)* 35(5), pp 1198-206.doi: 10.1161/ATVBAHA.114.305185
4. Kohn JC (*), Zhou DW (*), Bordeleau F, Zhou A, Mason BN, King MR, Reinhart-King CA. (2015). Cooperative Effects of Matrix Stiffness and Fluid Shear Stress on Endothelial Cell Behavior. *Biophysical Journal*. 108(3), pp. 471-8. doi: 10.1016/j.bpj.2014.12.023 (*) denotes equal contribution.

5. Jannie KM, Ellerbroek SM, Zhou DW, Chen S, Crompton DJ, Garcia AJ, and DeMali KA. (2015). Vinculin-dependent actin bundling regulates cell migration and traction forces. *Biochemical Journal*. 465(3), pp. 383-93. doi:10.1042/BJ20140872
6. Zhou DW and Garcia AJ. (2014). Review: Measurement Systems for Cell Adhesive Forces. *Journal of Biomechanical Engineering* 137(2), pp. 020908. doi: 10.1115/1.4029210
7. Werner JJ, Zhou DW, Caporaso JG, Knight R, and Angenent LT. (2012). Comparison of Illumina paired-end and single-direction sequencing for microbial 16S rRNA gene amplicon surveys. *The ISME Journal*, Vol. 6, No. 7, 1273-1276. doi: 10.1038/ismej.2011.186

PRESENTATIONS

1. Zhou DW, Lee TT, Paez J, del Campo A, and Garcia AJ. Force-signaling Coupling at Cell Adhesive Structures. Gordon Research Seminar: Signaling by Adhesion Receptors. Lewiston, ME, June 18, 2016. (oral presentation)
2. Zhou DW, Lee TT, Paez J, Garcia JR, Colasurdo M, del Campo A, and Garcia AJ. Force-signaling Coupling at Cell Adhesive Structures. Hilton Head Regenerative Engineering and Medicine. Hilton Head, SC. March 17, 2016. (rapid fire podium presentation)
3. Zhou DW, Lee TT, del Campo A, and Garcia AJ. Vinculin and paxillin recruitment dynamics to focal adhesions. Gordon Conference: Cell-Matrix Signaling, Waltham, MA, July 7, 2014. (poster)
4. Zhou DW, Lee TT, del Campo A, and Garcia AJ. Vinculin and paxillin recruitment dynamics to focal adhesions. Atlanta Adhesion Authority. Atlanta, GA, March 7, 2014. (oral presentation)
5. Zhou D, Quinodoz M, Woodruff K, and Maerkl S. On-Chip Transformation of Bacteria. EPFL Summer Research Program Symposium, Lausanne, CH. August 22, 2013. (poster)
6. Zhou D, Clarke D, Inman W, Leon L, and Lauffenburger DA. A Computer-Controlled System to Simulate Heat Stroke in vitro. BMES, Atlanta, GA, October 26, 2012. (poster)
7. Zhou D, Slater JH, Culver J, Dickinson M, and West JL. Fabrication of Cell-Derived Biomimetic Pattern Configurations using Image-Guided Laser Scanning Lithography. BioExpo, Ithaca, NY, March 12, 2012. (poster)
8. Zhou D, Slater JH, Culver J, Dickinson M, and West J. Fabrication of Cell-Derived Biomimetic Pattern Configurations using Image-Guided Laser Scanning Lithography. Rice University Summer Research Symposium, 2011, Houston, TX. (poster)

PROFESSIONAL ACTIVITIES

- President, Graduate Intervarsity Christian Fellowship, Georgia Tech (2016-2017)
- Young Professionals Board Member, Cocoa360 (2016-Present)
- Leadership Fellow – serve as leadership coach for undergrads, Georgia Tech (2015-2017)
- Executive Team Member – Bioengineering Graduate Association, Georgia Tech (2015-2017)
- Reviewer – Georgia Tech Presidential Undergraduate Research Award (2014-2016)
- Interviewer, Cornell University Office of Undergraduate Admissions (2014-2017)
- Volunteer Tutor, Cristo Rey High School, Atlanta, GA (2014-2015)
- Co-Instructor, KIDS Club, Georgia Tech Elementary School Outreach, Atlanta, GA (2014-2015)
- Student Advisory Group, Cornell Engineering Leadership Program (2013)
- Section Leader/Co-facilitator, Cornell Engineering Learning Initiatives (2012-2013)
- Executive Board, Institute of Biological Engineering - Cornell Chapter (2011-2012)

AWARDS AND HONORS

2018	US Delegate to 68th Annual Lindau Nobel Laureate Meeting (June 2018)
2016	NSF Hilton Head Conference Travel Award
2015	Georgia Tech Leadership Fellow
2014	BMES Annual Meeting Reviewer's Choice Award
2013	NSF Graduate Research Fellowship
2013	President's Fellowship, Georgia Tech
2013	ThinkSwiss Fellow, School of Life Sciences, EPFL
2013	Merrill Presidential Scholar (top 1% of class of Cornell University)
2013	Churchill Scholarship Finalist
2013	Student Advisory Group, Cornell Engineering Leadership Program
2013	NSF-Noyce Excellence in STEM Teaching Nominee, Cornell University
2012	Tau Beta Pi, Cornell University
2012	NSF BIO REU Travel Award, BMES Annual Meeting, Atlanta, GA

REFERENCES

1. Humphries, J.D., A. Byron, and M.J. Humphries, *Integrin ligands at a glance.* J Cell Sci, 2006. **119**(Pt 19): p. 3901-3.

2. Humphries, J.D., et al., *Proteomic analysis of integrin-associated complexes identifies RCC2 as a dual regulator of Rac1 and Arf6.* Sci Signal, 2009. **2**(87): p. ra51.

3. Dumbauld, D.W., et al., *How vinculin regulates force transmission.* Proc Natl Acad Sci U S A, 2013. **110**(24): p. 9788-93.

4. Xu, W., H. Baribault, and E.D. Adamson, *Vinculin knockout results in heart and brain defects during embryonic development.* Development, 1998. **125**(2): p. 327-37.

5. Shen, M. and T.A. Horbett, *The effects of surface chemistry and adsorbed proteins on monocyte/macrophage adhesion to chemically modified polystyrene surfaces.* J Biomed Mater Res, 2001. **57**(3): p. 336-45.

6. Huynh, J., et al., *Age-related intimal stiffening enhances endothelial permeability and leukocyte transmigration.* Sci Transl Med, 2011. **3**(112): p. 112ra122.

7. McEver, R.P., *Adhesive interactions of leukocytes, platelets, and the vessel wall during hemostasis and inflammation.* Thromb Haemost, 2001. **86**(3): p. 746-56.

8. Kraning-Rush, C.M., J.P. Califano, and C.A. Reinhart-King, *Cellular traction stresses increase with increasing metastatic potential.* PLoS One, 2012. **7**(2): p. e32572.

9. Yang, M.T., et al., *Assaying stem cell mechanobiology on microfabricated elastomeric substrates with geometrically modulated rigidity.* Nat Protoc, 2011. **6**(2): p. 187-213.

10. Cohen, D.M., M.T. Yang, and C.S. Chen, *Measuring cell-cell tugging forces using bowtie-patterned mPADs (microarray post detectors).* Methods Mol Biol, 2013. **1066**: p. 157-68.

11. Heisenberg, C.P. and Y. Bellaiche, *Forces in tissue morphogenesis and patterning.* Cell, 2013. **153**(5): p. 948-62.

12. Gallant, N.D. and A.J. Garcia, *Quantitative analyses of cell adhesion strength.* Methods Mol Biol, 2007. **370**: p. 83-96.

13. Zhou, D.W. and A.J. Garcia, *Measurement systems for cell adhesive forces.* J Biomech Eng, 2015. **137**(2): p. 020908.

14. Garcia, A.J. and N.D. Gallant, *Stick and grip: measurement systems and quantitative analyses of integrin-mediated cell adhesion strength.* Cell Biochem Biophys, 2003. **39**(1): p. 61-73.

15. Coyer, S.R., et al., *Nanopatterning reveals an ECM area threshold for focal adhesion assembly and force transmission that is regulated by integrin activation and cytoskeleton tension.* J Cell Sci, 2012. **125**(Pt 21): p. 5110-23.

16. Gallant, N.D., K.E. Michael, and A.J. Garcia, *Cell adhesion strengthening: contributions of adhesive area, integrin binding, and focal adhesion assembly.* Mol Biol Cell, 2005. **16**(9): p. 4329-40.

17. Amano, M., et al., *Formation of actin stress fibers and focal adhesions enhanced by Rho-kinase.* Science, 1997. **275**(5304): p. 1308-11.

18. Marshall, B.T., et al., *Direct observation of catch bonds involving cell-adhesion molecules.* Nature, 2003. **423**(6936): p. 190-3.

19. Evans, E., et al., *Mechanical switching and coupling between two dissociation pathways in a P-selectin adhesion bond.* Proc Natl Acad Sci U S A, 2004. **101**(31): p. 11281-6.

20. McClay, D.R., G.M. Wessel, and R.B. Marchase, *Intercellular recognition: quantitation of initial binding events.* Proc Natl Acad Sci U S A, 1981. **78**(8): p. 4975-9.

21. Prechtel, K., et al., *Dynamic force spectroscopy to probe adhesion strength of living cells.* Phys Rev Lett, 2002. **89**(2): p. 028101.

22. Tozeren, A., K.L. Sung, and S. Chien, *Theoretical and experimental studies on cross-bridge migration during cell disaggregation.* Biophys J, 1989. **55**(3): p. 479-87.

23. Litvinov, R.I., et al., *Binding strength and activation state of single fibrinogen-integrin pairs on living cells.* Proc Natl Acad Sci U S A, 2002. **99**(11): p. 7426-31.

24. Roca-Cusachs, P., et al., *Clustering of alpha(5)beta(1) integrins determines adhesion strength whereas alpha(v)beta(3) and talin enable mechanotransduction.* Proc Natl Acad Sci U S A, 2009. **106**(38): p. 16245-50.

25. Jiang, G., et al., *Two-piconewton slip bond between fibronectin and the cytoskeleton depends on talin.* Nature, 2003. **424**(6946): p. 334-7.

26. Kong, F., et al., *Cyclic mechanical reinforcement of integrin-ligand interactions.* Mol Cell, 2013. **49**(6): p. 1060-8.

27. Kong, F., et al., *Demonstration of catch bonds between an integrin and its ligand.* J Cell Biol, 2009. **185**(7): p. 1275-84.

28. Reyes, C.D. and A.J. Garcia, *A centrifugation cell adhesion assay for high-throughput screening of biomaterial surfaces.* J Biomed Mater Res A, 2003. **67**(1): p. 328-33.

29. Keselowsky, B.G., D.M. Collard, and A.J. Garcia, *Surface chemistry modulates fibronectin conformation and directs integrin binding and specificity to control cell adhesion.* J Biomed Mater Res A, 2003. **66**(2): p. 247-59.

30. Doroszewski, J., J. Skierski, and L. Przadka, *Interaction of neoplastic cells with glass surface under flow conditions.* Exp Cell Res, 1977. **104**(2): p. 335-43.

31. Truskey, G.A. and J.S. Pirone, *The effect of fluid shear stress upon cell adhesion to fibronectin-treated surfaces.* J Biomed Mater Res, 1990. **24**(10): p. 1333-53.

32. van Kooten, T.G., et al., *Development and use of a parallel-plate flow chamber for studying cellular adhesion to solid surfaces.* J Biomed Mater Res, 1992. **26**(6): p. 725-38.

33. Lawrence, M.B., L.V. McIntire, and S.G. Eskin, *Effect of flow on polymorphonuclear leukocyte/endothelial cell adhesion.* Blood, 1987. **70**(5): p. 1284-90.

34. Cozens-Roberts, C., J.A. Quinn, and D.A. Lauffenberger, *Receptor-mediated adhesion phenomena. Model studies with the Radical-Flow Detachment Assay.* Biophys J, 1990. **58**(1): p. 107-25.

35. Mohandas, N., R.M. Hochmuth, and E.E. Spaeth, *Adhesion of red cells to foreign surfaces in the presence of flow.* J Biomed Mater Res, 1974. **8**(2): p. 119-36.

36. Garcia, A.J., F. Huber, and D. Boettiger, *Force required to break alpha5beta1 integrin-fibronectin bonds in intact adherent cells is sensitive to integrin activation state.* J Biol Chem, 1998. **273**(18): p. 10988-93.

37. Usami, S., et al., *Design and construction of a linear shear stress flow chamber.* Ann Biomed Eng, 1993. **21**(1): p. 77-83.

38. Bundy, K.J., et al., *Measurement of fibroblast and bacterial detachment from biomaterials using jet impingement.* Cell Biol Int, 2001. **25**(4): p. 289-307.

39. Burmeister, J.S., et al., *Effect of fibronectin amount and conformation on the strength of endothelial cell adhesion to HEMA/EMA copolymers.* J Biomed Mater Res, 1996. **30**(1): p. 13-22.

40. Garcia, A.J., P. Ducheyne, and D. Boettiger, *Quantification of cell adhesion using a spinning disc device and application to surface-reactive materials.* Biomaterials, 1997. **18**(16): p. 1091-1098.

41. Michael, K.E. and A.J. García, *Cell Adhesion Strengthening: Measurement and Analysis.* 2007. **83**: p. 329-346.

42. Friedland, J.C., M.H. Lee, and D. Boettiger, *Mechanically activated integrin switch controls alpha5beta1 function.* Science, 2009. **323**(5914): p. 642-4.

43. Engler, A.J., et al., *A novel mode of cell detachment from fibrillar fibronectin matrix under shear.* J Cell Sci, 2009. **122**(Pt 10): p. 1647-53.

44. Singh, A., et al., *Adhesion strength-based, label-free isolation of human pluripotent stem cells.* Nature Methods, 2013. **10**(5): p. 438-+.

45. Dembo, M. and Y.L. Wang, *Stresses at the cell-to-substrate interface during locomotion of fibroblasts.* Biophys J, 1999. **76**(4): p. 2307-16.

46. Harris, A.K., P. Wild, and D. Stopak, *Silicone rubber substrata: a new wrinkle in the study of cell locomotion.* Science, 1980. **208**(4440): p. 177-9.

47. Tan, J.L., et al., *Cells lying on a bed of microneedles: an approach to isolate mechanical force.* Proc Natl Acad Sci U S A, 2003. **100**(4): p. 1484-9.

48. Sabass, B., et al., *High resolution traction force microscopy based on experimental and computational advances.* Biophys J, 2008. **94**(1): p. 207-20.

49. Plotnikov, S.V., et al., *High-resolution traction force microscopy.* Methods Cell Biol, 2014. **123**: p. 367-94.

50. Califano, J.P. and C.A. Reinhart-King, *Substrate Stiffness and Cell Area Predict Cellular Traction Stresses in Single Cells and Cells in Contact.* Cell Mol Bioeng, 2010. **3**(1): p. 68-75.

51. Reinhart-King, C.A., M. Dembo, and D.A. Hammer, *Endothelial cell traction forces on RGD-derivatized polyacrylamide substrata.* Langmuir, 2003. **19**(5): p. 1573-1579.

52. Reinhart-King, C.A., M. Dembo, and D.A. Hammer, *The dynamics and mechanics of endothelial cell spreading.* Biophysical Journal, 2005. **89**(1): p. 676-689.

53. Engler, A.J., et al., *Matrix elasticity directs stem cell lineage specification.* Cell, 2006. **126**(4): p. 677-89.

54. Isenberg, B.C., et al., *Vascular smooth muscle cell durotaxis depends on substrate stiffness gradient strength.* Biophys J, 2009. **97**(5): p. 1313-22.

55. Gilbert, P.M., et al., *Substrate elasticity regulates skeletal muscle stem cell self-renewal in culture.* Science, 2010. **329**(5995): p. 1078-81.

56. Califano, J.P. and C.A. Reinhart-King, *The Effects of Substrate Elasticity on Endothelial Cell Network Formation and Traction Force Generation.* 2009 Annual International Conference of the Ieee Engineering in Medicine and Biology Society, Vols 1-20, 2009: p. 3343-3345.

57. Chowdhury, F., et al., *Material properties of the cell dictate stress-induced spreading and differentiation in embryonic stem cells.* Nat Mater, 2010. **9**(1): p. 82-8.

58. Yeung, T., et al., *Effects of substrate stiffness on cell morphology, cytoskeletal structure, and adhesion.* Cell Motil Cytoskeleton, 2005. **60**(1): p. 24-34.

59. Ng, M.R., et al., *Substrate stiffness regulates cadherin-dependent collective migration through myosin-II contractility.* J Cell Biol, 2012. **199**(3): p. 545-63.

60. Parsons, J.T., A.R. Horwitz, and M.A. Schwartz, *Cell adhesion: integrating cytoskeletal dynamics and cellular tension.* Nat Rev Mol Cell Biol, 2010. **11**(9): p. 633-43.

61. Pelham, R.J., Jr. and Y. Wang, *Cell locomotion and focal adhesions are regulated by substrate flexibility.* Proc Natl Acad Sci U S A, 1997. **94**(25): p. 13661-5.

62. Galbraith, C.G. and M.P. Sheetz, *A micromachined device provides a new bend on fibroblast traction forces.* Proc Natl Acad Sci U S A, 1997. **94**(17): p. 9114-8.

63. Sniadecki, N.J. and C.S. Chen, *Microfabricated silicone elastomeric post arrays for measuring traction forces of adherent cells.* Methods Cell Biol, 2007. **83**: p. 313-28.

64. Fu, J., et al., *Mechanical regulation of cell function with geometrically modulated elastomeric substrates.* Nat Methods, 2010. **7**(9): p. 733-6.

65. Ting, L.H., et al., *Flow mechanotransduction regulates traction forces, intercellular forces, and adherens junctions.* Am J Physiol Heart Circ Physiol, 2012. **302**(11): p. H2220-9.

66. Han, S.J., et al., *Decoupling substrate stiffness, spread area, and micropost density: a close spatial relationship between traction forces and focal adhesions.* Biophys J, 2012. **103**(4): p. 640-8.

67. Sniadecki, N.J., et al., *Micropatterning on micropost arrays.* Methods Cell Biol, 2014. **121**: p. 61-73.

68. Trichet, L., et al., *Evidence of a large-scale mechanosensing mechanism for cellular adaptation to substrate stiffness.* Proc Natl Acad Sci U S A, 2012. **109**(18): p. 6933-8.

69. Liu, Y., et al., *Tension sensing nanoparticles for mechano-imaging at the living/nonliving interface.* J Am Chem Soc, 2013. **135**(14): p. 5320-3.

70. Grashoff, C., et al., *Measuring mechanical tension across vinculin reveals regulation of focal adhesion dynamics.* Nature, 2010. **466**(7303): p. 263-6.

71. Conway, D.E., et al., *Fluid shear stress on endothelial cells modulates mechanical tension across VE-cadherin and PECAM-1.* Curr Biol, 2013. **23**(11): p. 1024-30.

72. Woodfin, A., M.B. Voisin, and S. Nourshargh, *PECAM-1: a multi-functional molecule in inflammation and vascular biology.* Arterioscler Thromb Vasc Biol, 2007. **27**(12): p. 2514-23.

73. Wang, X. and T. Ha, *Defining single molecular forces required to activate integrin and notch signaling.* Science, 2013. **340**(6135): p. 991-4.

74. Fraley, S.I., et al., *A distinctive role for focal adhesion proteins in three-dimensional cell motility.* Nat Cell Biol, 2010. **12**(6): p. 598-604.

75. Schwartz, M.A. and C.S. Chen, *Cell biology. Deconstructing dimensionality.* Science, 2013. **339**(6118): p. 402-4.

76. Baker, B.M. and C.S. Chen, *Deconstructing the third dimension: how 3D culture microenvironments alter cellular cues.* J Cell Sci, 2012. **125**(Pt 13): p. 3015-24.

77. Wu, P.H., et al., *Three-dimensional cell migration does not follow a random walk.* Proc Natl Acad Sci U S A, 2014. **111**(11): p. 3949-54.

78. Koch, T.M., et al., *3D Traction forces in cancer cell invasion.* PLoS One, 2012. **7**(3): p. e33476.

79. Kraning-Rush, C.M., et al., *The role of the cytoskeleton in cellular force generation in 2D and 3D environments.* Phys Biol, 2011. **8**(1): p. 015009.

80. Campas, O., et al., *Quantifying cell-generated mechanical forces within living embryonic tissues.* Nat Methods, 2014. **11**(2): p. 183-9.

81. Legant, W.R., et al., *Measurement of mechanical tractions exerted by cells in three-dimensional matrices.* Nat Methods, 2010. **7**(12): p. 969-71.

82. Legant, W.R., et al., *Multidimensional traction force microscopy reveals out-of-plane rotational moments about focal adhesions.* Proc Natl Acad Sci U S A, 2013. **110**(3): p. 881-6.

83. Fraley, S.I., et al., *Reply: reducing background fluorescence reveals adhesions in 3D matrices.* Nature Cell Biology, 2011. **13**(1): p. 5-U254.

84. Mason, B.N. and C.A. Reinhart-King, *Controlling the mechanical properties of three-dimensional matrices via non-enzymatic collagen glycation.* Organogenesis, 2013. **9**(2): p. 70-5.

85. Mason, B.N., et al., *Tuning three-dimensional collagen matrix stiffness independently of collagen concentration modulates endothelial cell behavior.* Acta Biomater, 2013. **9**(1): p. 4635-44.

86. Salimath, A.S., et al., *Dual delivery of hepatocyte and vascular endothelial growth factors via a protease-degradable hydrogel improves cardiac function in rats.* PLoS One, 2012. **7**(11): p. e50980.

87. Khetan, S., et al., *Degradation-mediated cellular traction directs stem cell fate in covalently crosslinked three-dimensional hydrogels.* Nat Mater, 2013. **12**(5): p. 458-65.

88. Keselowsky, B.G. and A.J. Garcia, *Quantitative methods for analysis of integrin binding and focal adhesion formation on biomaterial surfaces.* Biomaterials, 2005. **26**(4): p. 413-8.

89. Garcia, A.J., M.D. Vega, and D. Boettiger, *Modulation of cell proliferation and differentiation through substrate-dependent changes in fibronectin conformation.* Mol Biol Cell, 1999. **10**(3): p. 785-98.

90. Garcia, A.J., F. Huber, and D. Boettiger, *Force required to break alpha(5)beta(1) integrin-fibronectin bonds in intact adherent cells is sensitive to integrin activation state.* Journal of Biological Chemistry, 1998. **273**(18): p. 10988-10993.

91. Choquet, D., D.P. Felsenfeld, and M.P. Sheetz, *Extracellular matrix rigidity causes strengthening of integrin-cytoskeleton linkages.* Cell, 1997. **88**(1): p. 39-48.

92. Faull, R.J., et al., *Affinity modulation of integrin alpha 5 beta 1: regulation of the functional response by soluble fibronectin.* J Cell Biol, 1993. **121**(1): p. 155-62.

93. Beningo, K.A., et al., *Nascent focal adhesions are responsible for the generation of strong propulsive forces in migrating fibroblasts.* J Cell Biol, 2001. **153**(4): p. 881-8.

94. Case, L.B., et al., *Molecular mechanism of vinculin activation and nanoscale spatial organization in focal adhesions.* Nat Cell Biol, 2015. **17**(7): p. 880-92.

95. Kanchanawong, P., et al., *Nanoscale architecture of integrin-based cell adhesions.* Nature, 2010. **468**(7323): p. 580-4.

96. Wang, H.B., et al., *Focal adhesion kinase is involved in mechanosensing during fibroblast migration.* Proc Natl Acad Sci U S A, 2001. **98**(20): p. 11295-300.

97. Schlaepfer, D.D., C.R. Hauck, and D.J. Sieg, *Signaling through focal adhesion kinase.* Prog Biophys Mol Biol, 1999. **71**(3-4): p. 435-78.

98. Giannone, G., et al., *Periodic lamellipodial contractions correlate with rearward actin waves.* Cell, 2004. **116**(3): p. 431-43.

99. Giannone, G., et al., *Lamellipodial actin mechanically links myosin activity with adhesion-site formation.* Cell, 2007. **128**(3): p. 561-75.

100. Raucher, D. and M.P. Sheetz, *Cell spreading and lamellipodial extension rate is regulated by membrane tension.* J Cell Biol, 2000. **148**(1): p. 127-36.

101. van Hoorn, H., et al., *The nanoscale architecture of force-bearing focal adhesions.* Nano Lett, 2014. **14**(8): p. 4257-62.

102. Humphries, J.D., et al., *Vinculin controls focal adhesion formation by direct interactions with talin and actin.* J Cell Biol, 2007. **179**(5): p. 1043-57.

103. Hu, Y.L., et al., *FAK and paxillin dynamics at focal adhesions in the protrusions of migrating cells.* Sci Rep, 2014. **4**: p. 6024.

104. Lawson, C., et al., *FAK promotes recruitment of talin to nascent adhesions to control cell motility.* J Cell Biol, 2012. **196**(2): p. 223-32.

105. Deramaudt, T.B., et al., *Altering FAK-paxillin interactions reduces adhesion, migration and invasion processes.* PLoS One, 2014. **9**(3): p. e92059.

106. Carisey, A., et al., *Vinculin regulates the recruitment and release of core focal adhesion proteins in a force-dependent manner.* Curr Biol, 2013. **23**(4): p. 271-81.

107. Subauste, M.C., et al., *Vinculin modulation of paxillin-FAK interactions regulates ERK to control survival and motility.* J Cell Biol, 2004. **165**(3): p. 371-81.

108. Scheswohl, D.M., et al., *Multiple paxillin binding sites regulate FAK function.* J Mol Signal, 2008. **3**: p. 1.

109. Lietha, D., et al., *Structural basis for the autoinhibition of focal adhesion kinase.* Cell, 2007. **129**(6): p. 1177-87.

110. Riveline, D., et al., *Focal contacts as mechanosensors: externally applied local mechanical force induces growth of focal contacts by an mDia1-dependent and ROCK-independent mechanism.* J Cell Biol, 2001. **153**(6): p. 1175-86.

111. del Rio, A., et al., *Stretching single talin rod molecules activates vinculin binding.* Science, 2009. **323**(5914): p. 638-41.

112. Balaban, N.Q., et al., *Force and focal adhesion assembly: a close relationship studied using elastic micropatterned substrates.* Nat Cell Biol, 2001. **3**(5): p. 466-72.

113. Sawada, Y., et al., *Force sensing by mechanical extension of the Src family kinase substrate p130Cas.* Cell, 2006. **127**(5): p. 1015-26.

114. Guilluy, C., et al., *The Rho GEFs LARG and GEF-H1 regulate the mechanical response to force on integrins.* Nat Cell Biol, 2011. **13**(6): p. 722-7.

115. Pasapera, A.M., et al., *Myosin II activity regulates vinculin recruitment to focal adhesions through FAK-mediated paxillin phosphorylation.* J Cell Biol, 2010. **188**(6): p. 877-90.

116. Plotnikov, S.V., et al., *Force fluctuations within focal adhesions mediate ECM-rigidity sensing to guide directed cell migration.* Cell, 2012. **151**(7): p. 1513-27.

117. Paszek, M.J., et al., *Tensional homeostasis and the malignant phenotype.* Cancer Cell, 2005. **8**(3): p. 241-54.

118. Huynh, J., et al., *Substrate Stiffness Regulates PDGF-Induced Circular Dorsal Ruffle Formation Through MLCK.* Cell Mol Bioeng, 2013. **6**(2).

119. Schiller, H.B., et al., *beta1- and alphav-class integrins cooperate to regulate myosin II during rigidity sensing of fibronectin-based microenvironments.* Nat Cell Biol, 2013. **15**(6): p. 625-36.

120. Puklin-Faucher, E. and M.P. Sheetz, *The mechanical integrin cycle.* J Cell Sci, 2009. **122**(Pt 2): p. 179-86.

121. Plotnikov, S.V. and C.M. Waterman, *Guiding cell migration by tugging.* Curr Opin Cell Biol, 2013. **25**(5): p. 619-26.

122. Nardone, G., et al., *YAP regulates cell mechanics by controlling focal adhesion assembly.* Nat Commun, 2017. **8**: p. 15321.

123. Totaro, A., T. Panciera, and S. Piccolo, *YAP/TAZ upstream signals and downstream responses.* Nat Cell Biol, 2018. **20**(8): p. 888-899.

124. Varelas, X., *The Hippo pathway effectors TAZ and YAP in development, homeostasis and disease.* Development, 2014. **141**(8): p. 1614-26.

125. Karystinou, A., et al., *Yes-associated protein (YAP) is a negative regulator of chondrogenesis in mesenchymal stem cells.* Arthritis Res Ther, 2015. **17**: p. 147.

126. Ziegler, W.H., R.C. Liddington, and D.R. Critchley, *The structure and regulation of vinculin.* Trends Cell Biol, 2006. **16**(9): p. 453-60.

127. Chen, H., D.M. Choudhury, and S.W. Craig, *Coincidence of actin filaments and talin is required to activate vinculin.* J Biol Chem, 2006. **281**(52): p. 40389-98.

128. Chen, H., et al., *Spatial distribution and functional significance of activated vinculin in living cells.* J Cell Biol, 2005. **169**(3): p. 459-70.

129. Cohen, D.M., et al., *Two distinct head-tail interfaces cooperate to suppress activation of vinculin by talin.* J Biol Chem, 2005. **280**(17): p. 17109-17.

130. Johnson, R.P. and S.W. Craig, *F-actin binding site masked by the intramolecular association of vinculin head and tail domains.* Nature, 1995. **373**(6511): p. 261-4.

131. Yamashita, H., et al., *The role of the interaction of the vinculin proline-rich linker region with vinexin alpha in sensing the stiffness of the extracellular matrix.* J Cell Sci, 2014. **127**(Pt 9): p. 1875-86.

132. Kuroda, M., et al., *Vinculin promotes nuclear localization of TAZ to inhibit ECM stiffness-dependent differentiation into adipocytes.* J Cell Sci, 2017.

133. Wolfenson, H., et al., *Actomyosin-generated tension controls the molecular kinetics of focal adhesions.* J Cell Sci, 2011. **124**(Pt 9): p. 1425-32.

134. Elosegui-Artola, A., et al., *Mechanical regulation of a molecular clutch defines force transmission and transduction in response to matrix rigidity.* Nat Cell Biol, 2016. **18**(5): p. 540-8.

135. Roca-Cusachs, P., et al., *Integrin-dependent force transmission to the extracellular matrix by alpha-actinin triggers adhesion maturation.* Proc Natl Acad Sci U S A, 2013. **110**(15): p. E1361-70.

136. Austen, K., et al., *Extracellular rigidity sensing by talin isoform-specific mechanical linkages.* Nat Cell Biol, 2015. **17**(12): p. 1597-606.

137. Zhou, D.W., et al., *Effects of substrate stiffness and actomyosin contractility on coupling between force transmission and vinculin-paxillin recruitment at single focal adhesions.* Mol Biol Cell, 2017. **28**(14): p. 1901-1911.

138. Mitra, S.K., D.A. Hanson, and D.D. Schlaepfer, *Focal adhesion kinase: in command and control of cell motility.* Nat Rev Mol Cell Biol, 2005. **6**(1): p. 56-68.

139. Provenzano, P.P. and P.J. Keely, *Mechanical signaling through the cytoskeleton regulates cell proliferation by coordinated focal adhesion and Rho GTPase signaling.* J Cell Sci, 2011. **124**(Pt 8): p. 1195-205.

140. Dumbauld, D.W., et al., *Contractility modulates cell adhesion strengthening through focal adhesion kinase and assembly of vinculin-containing focal adhesions.* J Cell Physiol, 2010. **223**(3): p. 746-56.

141. Chrzanowska-Wodnicka, M. and K. Burridge, *Rho-stimulated contractility drives the formation of stress fibers and focal adhesions.* J Cell Biol, 1996. **133**(6): p. 1403-15.

142. Lo, C.M., et al., *Cell movement is guided by the rigidity of the substrate.* Biophys J, 2000. **79**(1): p. 144-52.

143. Liu, Z., et al., *Vinculin head-tail interaction defines multiple early mechanisms for cell substrate rigidity sensing.* Integr Biol (Camb), 2016. **8**(6): p. 693-703.

144. Weng, S., et al., *Mechanosensitive subcellular rheostasis drives emergent single-cell mechanical homeostasis.* Nat Mater, 2016. **15**(9): p. 961-7.

145. Stricker, J., et al., *Spatiotemporal constraints on the force-dependent growth of focal adhesions.* Biophys J, 2011. **100**(12): p. 2883-93.

146. Palmer, S.M., et al., *Lipid binding to the tail domain of vinculin: specificity and the role of the N and C termini.* J Biol Chem, 2009. **284**(11): p. 7223-31.

147. DeMali, K.A., C.A. Barlow, and K. Burridge, *Recruitment of the Arp2/3 complex to vinculin: coupling membrane protrusion to matrix adhesion.* J Cell Biol, 2002. **159**(5): p. 881-91.

148. Deakin, N.O. and C.E. Turner, *Paxillin comes of age.* J Cell Sci, 2008. **121**(Pt 15): p. 2435-44.

149. Cox, T.R. and J.T. Erler, *Remodeling and homeostasis of the extracellular matrix: implications for fibrotic diseases and cancer.* Dis Model Mech, 2011. **4**(2): p. 165-78.

150. Kovacs, M., et al., *Mechanism of blebbistatin inhibition of myosin II.* J Biol Chem, 2004. **279**(34): p. 35557-63.

151. Cohen, D.M., et al., *A conformational switch in vinculin drives formation and dynamics of a talin-vinculin complex at focal adhesions.* J Biol Chem, 2006. **281**(23): p. 16006-15.

152. Oakes, P.W. and M.L. Gardel, *Stressing the limits of focal adhesion mechanosensitivity.* Curr Opin Cell Biol, 2014. **30**: p. 68-73.

153. Webb, D.J., J.T. Parsons, and A.F. Horwitz, *Adhesion assembly, disassembly and turnover in migrating cells -- over and over and over again.* Nat Cell Biol, 2002. **4**(4): p. E97-100.

154. Narumiya, S., T. Ishizaki, and M. Uehata, *Use and properties of ROCK-specific inhibitor Y-27632.* Regulators and Effectors of Small Gtpases, Pt D, 2000. **325**: p. 273-284.

155. Kolega, J., *Phototoxicity and photoinactivation of blebbistatin in UV and visible light.* Biochem Biophys Res Commun, 2004. **320**(3): p. 1020-5.

156. Thompson, P.M., et al., *A Structural Model for Vinculin Insertion into PIP2-Containing Membranes and the Effect of Insertion on Vinculin Activation and Localization.* Structure, 2017. **25**(2): p. 264-275.

157. Huang, D.L., et al., *Vinculin forms a directionally asymmetric catch bond with F-actin.* Science, 2017. **357**(6352): p. 703-706.

158. Lim, S.T., et al., *Knock-in mutation reveals an essential role for focal adhesion kinase activity in blood vessel morphogenesis and cell motility-polarity but not cell proliferation.* J Biol Chem, 2010. **285**(28): p. 21526-36.

159. Kohn, J.C., et al., *Cooperative effects of matrix stiffness and fluid shear stress on endothelial cell behavior.* Biophys J, 2015. **108**(3): p. 471-8.

160. Zhou, J., et al., *Mechanism of Focal Adhesion Kinase Mechanosensing.* PLoS Comput Biol, 2015. **11**(11): p. e1004593.

161. Zhao, B., et al., *The Hippo-YAP pathway in organ size control and tumorigenesis: an updated version.* Genes Dev, 2010. **24**(9): p. 862-74.

162. Zhao, B., et al., *Inactivation of YAP oncoprotein by the Hippo pathway is involved in cell contact inhibition and tissue growth control.* Genes Dev, 2007. **21**(21): p. 2747-61.

163. Meng, Z., et al., *RAP2 mediates mechanoresponses of the Hippo pathway.* Nature, 2018. **560**(7720): p. 655-660.

164. Aragona, M., et al., *A mechanical checkpoint controls multicellular growth through YAP/TAZ regulation by actin-processing factors.* Cell, 2013. **154**(5): p. 1047-1059.

165. Das, A., et al., *YAP Nuclear Localization in the Absence of Cell-Cell Contact Is Mediated by a Filamentous Actin-dependent, Myosin II- and Phospho-YAP-independent Pathway during Extracellular Matrix Mechanosensing.* J Biol Chem, 2016. **291**(12): p. 6096-110.

166. Elosegui-Artola, A., et al., *Force Triggers YAP Nuclear Entry by Regulating Transport across Nuclear Pores.* Cell, 2017. **171**(6): p. 1397-1410 e14.

167. Kuroda, M., et al., *Vinculin promotes nuclear localization of TAZ to inhibit ECM stiffness-dependent differentiation into adipocytes.* J Cell Sci, 2017. **130**(5): p. 989-1002.

168. Seong, J., et al., *Detection of focal adhesion kinase activation at membrane microdomains by fluorescence resonance energy transfer.* Nat Commun, 2011. **2**: p. 406.

169. Fu, J., et al., *Mechanical regulation of cell function with geometrically modulated elastomeric substrates.* Nat Meth, 2010. **7**(9): p. 733-736.

170. Stutchbury, B., et al., *Distinct focal adhesion protein modules control different aspects of mechanotransduction.* J Cell Sci, 2017. **130**(9): p. 1612-1624.

171. Roh, M.E., et al., *Off-targets effects underlie the inhibitory effect of FAK inhibitors on platelet activation: studies using Fak-deficient mice.* J Thromb Haemost, 2013. **11**(9): p. 1776-8.

172. Klapholz, B. and N.H. Brown, *Talin - the master of integrin adhesions.* J Cell Sci, 2017. **130**(15): p. 2435-2446.

173. Zhang, X., et al., *Talin depletion reveals independence of initial cell spreading from integrin activation and traction.* Nat Cell Biol, 2008. **10**(9): p. 1062-8.

174. Rahman, A., et al., *Vinculin Regulates Directionality and Cell Polarity in 2D, 3D Matrix and 3D Microtrack Migration.* Mol Biol Cell, 2016.

175. Michael, K.E., et al., *Focal adhesion kinase modulates cell adhesion strengthening via integrin activation.* Mol Biol Cell, 2009. **20**(9): p. 2508-19.

176. Lim, S.T., et al., *FERM control of FAK function: implications for cancer therapy.* Cell Cycle, 2008. **7**(15): p. 2306-14.

177. Slack-Davis, J.K., et al., *Cellular characterization of a novel focal adhesion kinase inhibitor.* J Biol Chem, 2007. **282**(20): p. 14845-52.

178. Baillat, G., et al., *Early adhesion induces interaction of FAK and Fyn in lipid domains and activates raft-dependent Akt signaling in SW480 colon cancer cells.* Biochim Biophys Acta, 2008. **1783**(12): p. 2323-31.

179. Zhang, X., et al., *Focal adhesion kinase promotes phospholipase C-gamma1 activity.* Proc Natl Acad Sci U S A, 1999. **96**(16): p. 9021-6.

180. Garcia, A.J. and D. Boettiger, *Integrin-fibronectin interactions at the cell-material interface: initial integrin binding and signaling.* Biomaterials, 1999. **20**(23-24): p. 2427-33.

181. Lele, T.P., et al., *Investigating complexity of protein-protein interactions in focal adhesions.* Biochem Biophys Res Commun, 2008. **369**(3): p. 929-34.

182. Smith, M.A., et al., *A zyxin-mediated mechanism for actin stress fiber maintenance and repair.* Dev Cell, 2010. **19**(3): p. 365-76.

183. Kuo, J.C., et al., *Analysis of the myosin-II-responsive focal adhesion proteome reveals a role for beta-Pix in negative regulation of focal adhesion maturation.* Nat Cell Biol, 2011. **13**(4): p. 383-93.

184. Lampi, M.C. and C.A. Reinhart-King, *Targeting extracellular matrix stiffness to attenuate disease: From molecular mechanisms to clinical trials.* Sci Transl Med, 2018. **10**(422).